DEPARTMENT OF PHYSICS
UNIVERSITY OF JYVÄSKYLÄ
RESEARCH REPORT No. 13/2006

DIELECTROPHORESIS AS A TOOL FOR ON-CHIP POSITIONING OF DNA AND ELECTRICAL CHARACTERIZATION OF NANOSCALE DNA

BY
SAMPO TUUKKANEN

Academic Dissertation
for the Degree of
Doctor of Philosophy

To be presented, by permission of the
Faculty of Mathematics and Science
of the University of Jyväskylä,
for public examination in Auditorium FYS-1 of the
University of Jyväskylä on December 21, 2006
at 12 o'clock

Jyväskylä, Finland
December 2006

ISBN 978-951-39-3179-7
URN:ISBN:978-951-39-3179-7

Preface

The work reviewed in this thesis has been carried out during the years 2002-2006 at the Department of Physics in the University of Jyväskylä.

First I wish to thank my supervisor Prof. Päivi Törmä about her guidance and a professional talent to see the overall picture of my research. I'm also grateful to Dr. Vesa Hytönen about his interest in the multidisciplinary research and patient in teaching me the basics about DNA, and PhD. student Anton Kuzyk about his fruitful ideas and dedicated work with the single DNA molecule devices. Special mention is also devoted to Dr. Jussi Toppari who was highly contributing to the analysis and understanding of the experimental results and also about help in maintaining the optimism in our minds and smile on our faces when wandering on the 'lumpy road of molecular electronics'. I wish to thank Mr. Einari Niskanen, Mr. Teemu Ihalainen, Mr. Tommi Hakala, Ms. Heli Lehtivuori, Mr. Marcus Rinkiö, Docent Hannu Häkkinen and Prof. Jorma Virtanen about their valuable contribution on this work. Thank's to my colleagues from nanophysics, nanoelectronics and molecular biology groups about the interesting – sometimes also deeply scientific – conversations. I also wish to thank all the people in the Nanoscience Center about creating an open and pleasant working atmosphere. It has been a pleasure to work with you.

Finally, I wish to thank all my friends, family and relatives about their support and encouragement.

Financial support from the Academy of Finland, the Finnish Cultural foundation, Emil Aaltonen foundation and Ulla Tuominen foundation are gratefully acknowledged.

Jyväskylä, December 2006

Sampo Tuukkanen

Abstract

Tuukkanen, Sampo

Jyväskylä: University of Jyväskylä, 2006, 174 p.
(Research report/Department of Physics, University of Jyväskylä,
ISSN 0075-465X; 12/2006
ISBN 951-39-2669-9
diss.

In this thesis the fabrication and characterization of DNA-based nanodevices is discussed. The main issues are the dielectrophoresis and the electrical properties of DNA.

The dielectrophoresis of different size DNA fragments, varying from 27 bp to 8 kbp, was studied *in situ* under the confocal microscope. The fluorescence data obtained from the experiments combined with the finite-element electric field simulations, revealed information about the frequency and the DNA length dependency of the polarizability of the DNA. In addition to 100 nm length-scale metallic fingertip electrodes, a few nm diameter multi-walled carbon nanotubes were used as a more effective electrodes for dielectrophoresis.

The electrical properties of thiol-anchored about 140 nm long (414 bp) natural DNA bridging the gap between fingertip type gold electrodes were studied in different ambient humidities. In dry air ($\sim$30 %) or in N_2 atmosphere, the I-V (current-voltage) curves showed high resistive behaviour for all measured single molecule devices. However, in high humid air (80-90 %), several samples showed a substantial increase in the conductance beyond the level of humid environment itself. These results suggests the interplay between the humidity and the prevailing conformation of the double-stranded DNA, which determines the level of π-orbital overlap in the base pair stack.

Keywords DNA, dielectrophoresis, conductivity, humidity, immobilization, thiol.

Author's address Sampo Tuukkanen
Department of Physics
NanoScience Center
University of Jyväskylä
Finland

Supervisor Professor Päivi Törmä
Department of Physics
NanoScience Center
University of Jyväskylä
Finland

Reviewers Professor Esko Kauppinen
Laboratory of Physics
Helsinki University of Technology
Finland

Professor Janne Ruokolainen
Materials Physics Laboratory
Helsinki University of Technology
Finland

Opponent Professor Jean-Philippe Bourgoin
Laboratoire d'Electronique Moléculaire
Direction des Sciences de la Matière
Commissariat à l'Energie Atomique
Saclay
France

List of Publications

The main results of this thesis have been reported in the following articles:

A.I TUUKKANEN, S., TOPPARI, J.J., HYTÖNEN, V.P., KUZYK, A., KULOMAA, M.S., AND TÖRMÄ, P., *Dielectrophoresis as a tool for nanoscale DNA manipulation*. Int. J. Nanotechnology **2** (3) (2005) 280–291.

A.II TUUKKANEN, S., KUZYK, A., TOPPARI, J.J., HYTÖNEN, V.P., IHALAINEN, T., AND TÖRMÄ, P., *Dielectrophoresis of nanoscale double-stranded DNA and humidity effects on its electrical conductivity*. Appl. Phys. Lett. **87** (2005) 183102.

A.III TUUKKANEN, S., TOPPARI, J.J., KUZYK, A., HIRVINIEMI, L., HYTÖNEN, V.P., IHALAINEN, T., AND TÖRMÄ, P., *Carbon nanotubes as electrodes for dielectrophoresis of DNA*. Nano Lett. **6** (2006) 1339–43.

A.IV TUUKKANEN, S., KUZYK, A., TOPPARI, J.J., HÄKKINEN, H., HYTÖNEN, V.P., NISKANEN, E., RINKIÖ M. AND TÖRMÄ, P., *Trapping of 27 bp - 8 kbp DNA and immobilization of thiol-modified DNA using dielectrophoresis*. cond-mat/0609414, submitted to Nanotechnology.

Author's contribution

The author of has had a main contribution in writing all the papers A.I - A.IV.

In A.I and A.II the author carried out part of the sample fabrication, the electrical measurements and the analysis of the results. In A.III and A.IV author carried out all the measurements, data analysis and the finite element simulations.

List of Abbreviations

3′ end of ssDNA	phosphate end-group linked to 3^{rd} carbon in the sugar.
5′ end of ssDNA	hydroxyl end-group linked to 5^{th} carbon in the sugar.
A-DNA	double helix in A-form (dried B-form)
AFM	atomic force microscopy
AO	acridine orange (a fluorescence dye)
B-DNA	double helix in B-form
CNT	carbon nanotube
complementary	two ssDNA sequences that can hybridize
CT	charge transfer
DEP	dielectrophoresis
DFT	density functional theory
DNA	deoxyribonucleic Acid
DNAse I	deoxyribonuclease I enzyme
dsDNA	double-stranded DNA
DTPA	dithiol-phosphoramidite
DX	double-crossover junction (similar to two Holliday junctions)
EDEP	electrodeless DEP
EFM	electrostatic force microscopy
ET	electron transfer
FET	field effect transistor
G-quartet	hydrogen-bonded ring formed of four guanines

G-wire	structure formed of adjacent G-quartets
H-DNA	DNA triple helix structure
Hepes	N-2-Hydroxyethylpiperazine-N′-2-ethanesulfonic acid, ($C_8H_{18}N_2O_4S$)
HOMO	highest occupied molecular orbital
hybridization	forming of dsDNA from two complementary ssDNA
I–V	current–voltage
λ-DNA	DNA isolated from bacteriophage lambda
LEEPS	low-energy electron point source
LIPS	laser-induced plasma spectroscopy
LUMO	lowest unoccupied molecular orbital
LPCVD	low-pressure chemical vapour deposition
MWCNT	multi-walled carbon nanotubes
$NaBH_4$	Sodium borohydride
oligonucleotide	short single stranded DNA (order of tens bases)
OTS	octadecyltrichlorosilane
PCR	Polymerase Chain Reaction
PMMA	polymethylmethacrylate
poly(dA)-poly(dT)	dsDNA formed of adenine- and thymine-polynucleotides
poly(dC)-poly(dG)	dsDNA formed of cytosine- and guanine-polynucleotides
RH	relative humidity
RIE	reactive-ion etcher
SEM	scanning electron microscope
SNP	single nucleotide polymorphism
ssDNA	single-stranded DNA
sticky end	overhanging ssDNA sequence in the end of dsDNA
STM	scanning tunneling microscopy

SWCNT	single-walled carbon nanotube
TCEP-HCl	Tris(2-Carboxyethyl) Phosphine and Hydrochloride
TEM	transmission electron microscopy
TIH	thermally induced hopping
TX	DNA triple-crossover junction (three Holliday junctions)
UHV	ultra-high vacuum
XOR	exclusive OR (binary function)
Z-DNA	double helix in left-handed Z-form

Contents

1 Introduction

In microelectronics industry, there is a constant need for smaller size and increased functionality of electronics components [7]. However, the packing density is about to reach the resolution limit of traditional 'top-down' lithography methods. One potential solution is to use 'bottom-up' approach [19], utilizing the self-assembly properties of molecules [141, 258] in the fabrication of electronics components and even build wires, switches, rectifiers and memories out of individual molecules [58, 154]. However, entering into the molecular world brings in new quantum mechanical phenomena and other challenges of molecular electronics [91], e.g., how to compose a complicated circuit from molecular-scale components in a controlled way.

It is very likely that the silicon technology, with its constant progress, will dominate in the foreseeable future. Highly-conductive organic compounds, such as conducting polymers and carbon nanotubes (CNT), are promising molecular candidates to partly replace the silicon. Molecular components such as CNT may well appear in niche applications like sensors even in the near future. Biomolecules, like DNA and proteins, are interesting mainly due to their self-assembly features. The natural environment for the biological molecules is a salty aquatic solution, where they retain their biological functionality. The conformational dynamicity and sensitivity to the environmental conditions makes the use of biomolecules themselves as molecular electronics components extremely challenging. However, the self-assembly of biomolecules can be used to organize more robust nanoscale components, such as CNT, in controlled parallel manner, providing potentially even a serial production.

Due to its exceptional self-assembly properties, DNA can be utilized in building of one-, two- or three-dimensional arrays of other molecules or nanoparticles (e.g. gold particles or quantum dots) and also in fabrication of highly conductive nanowires through chemical metallization [61, 185, 224]. Another feature which makes DNA an interesting material for molecular electronics is its proposed intrinsic electrical conductivity, which has already been demonstrated, e.g., in the study of single-nucleotide polymorphism (SNP) [99]. This could eventually lead to the use of DNA itself as a part of the molecular electronics. However, one has to note that the controversy over the issue of DNA conductivity still remains.

The scientific and technical goals of this Dissertation were the following: 1) To extend the dielectrophoretic trapping and immobilization of DNA, which has been widely applied in the micrometer scale, to the nanometer scale where it is more

challenging and only very few demonstrations exist so far. Specifically, we wanted to develop and optimize a high yield method for a production of single molecule samples. A systematic study of the efficiency of the method as a function of process parameters was performed using *in situ* confocal microscopy. For instance, the effect of the DNA length (varying from a few nm to a few μm) on the efficiency of the dielectrophoretic trapping has not been studied before this work. We were successful in the development of a method for positioning a single 100 nm scale DNA molecule to bridge two metal nanoelectrodes. This was realized using gold nanoelectrodes for the dielectrophoretic trapping and a thiol-based immobilization of the molecules. Additionally, in order to study the contribution of the molecule-electrode contacts on the immobilization and observed electrical properties of the molecules, two different type 5' DNA modifications, i.e., hexanethiol and DTPA (dithiol-phosphoramidite), have been used and compared. 2) To further extend the method to the nanoscale, we studied the dielectrophoretic trapping of DNA using a CNT as one electrode, which has not been reported before this work. We show that indeed the trapping efficiency is better for the CNT if compared with the lithographically fabricated metal electrodes. 3) Electrical characterization of single DNA molecule samples obtained using the methods above. DNA conductivity measurements under different ambient humidities, which have not been carried out on a single molecule level before, were performed and humidity effect on the electrical conductivity of a 140 nm long natural DNA was analyzed. Note that we both imaged the molecule using atomic force microscopy (AFM) and measured the transport. Majority of the previous single molecule measurements of DNA do not include visualization of the molecules. 4) In addition, a more detailed study of dielectrophoresis of DNA molecules revealed information about the polarizability of the DNA. In order to determine the polarizability of DNA finite element method (FEM) simulations were used in conjunction with the data from the trapping experiments. For instance, the dependency of polarizability on the molecule length was obtained here for the first time.

The chapters are organized as follows. Properties of the DNA and applications of DNA-based self-assembly are described in Chapter 2. A principle of DEP and the earlier studies of the DEP of DNA are discussed in Chapter 3. In Chapter 4, I describe the experimental procedures and numerical methods used in this work. The performed DEP studies and the analysis of the results have been discussed in Chapter 5 and the results obtained from the electrical conductivity measurement have been discussed in Chapter 6. The final conclusions and future aspects are given in Chapter 7.

2 Structure and properties of DNA

2.1 DNA structure

2.1.1 Deoxyribonucleic acid

The deoxyribonucleic acid (DNA) is a polymer of deoxyribonucleotides (nucleotides), each of which contains a deoxyribose sugar, a phosphate and an aromatic nitrogenous base attached to the sugar. In DNA, there are four different nucleotides which differ from each other by the base group only. Alternating bases are Thymine (T), Cytosine (C), Adenine (A) and Guanine (G). Thymine and Cytosine are single ring structures called purimidines, and Adenine and Guanine are double ring structures called purines. One can imagine that the phosphate and sugar groups form a backbone of a DNA strand into which the bases attach in the certain order (see Fig. 2.1). This order of the bases carries the genetic information inside the living organism. Each DNA strand has a directionality. So called 5′ and 3′ ends are determined by the carbon atom (5^{th} or 3^{rd}) of the deoxyribose sugar into which the phosphate is attached.

2.1.2 DNA double helix

The secondary structure of DNA is a double helix, where two DNA strands are held together by hydrogen bonding between complementary bases. Bases attach each other in such a way that purine-pyrimidine base pairs (bp), GC or AT, are formed (see Fig. 2.2). In order to form a double helix (by hybridisation), the base sequences of two DNA strands has to be complementary to each other. Two strands are coiled in antiparallel way, which means that one strand goes form 5′ to 3′ and the other from 3′ to 5′.

DNA can adopt several different helical forms. The most stable structure for a random-sequence under physiological conditions is B-DNA (see Fig. 2.3(b)), which is a right handed helix with 10.5 bp per turn and about 3.4 Å distance between adjacent bases. The diameter of a double helix in the B-form is 20 Å. Another right handed form is A-DNA (see Fig. 2.3(a)), which has 11 bp per turn, the helix diameter of 26 Å and about 2.6 Å separation between the bases. One significant difference between these two forms is that in the A-form the pyrimidine and purine planes of paired bases are more tilted respect to the helical axis and thus, not so well stacked

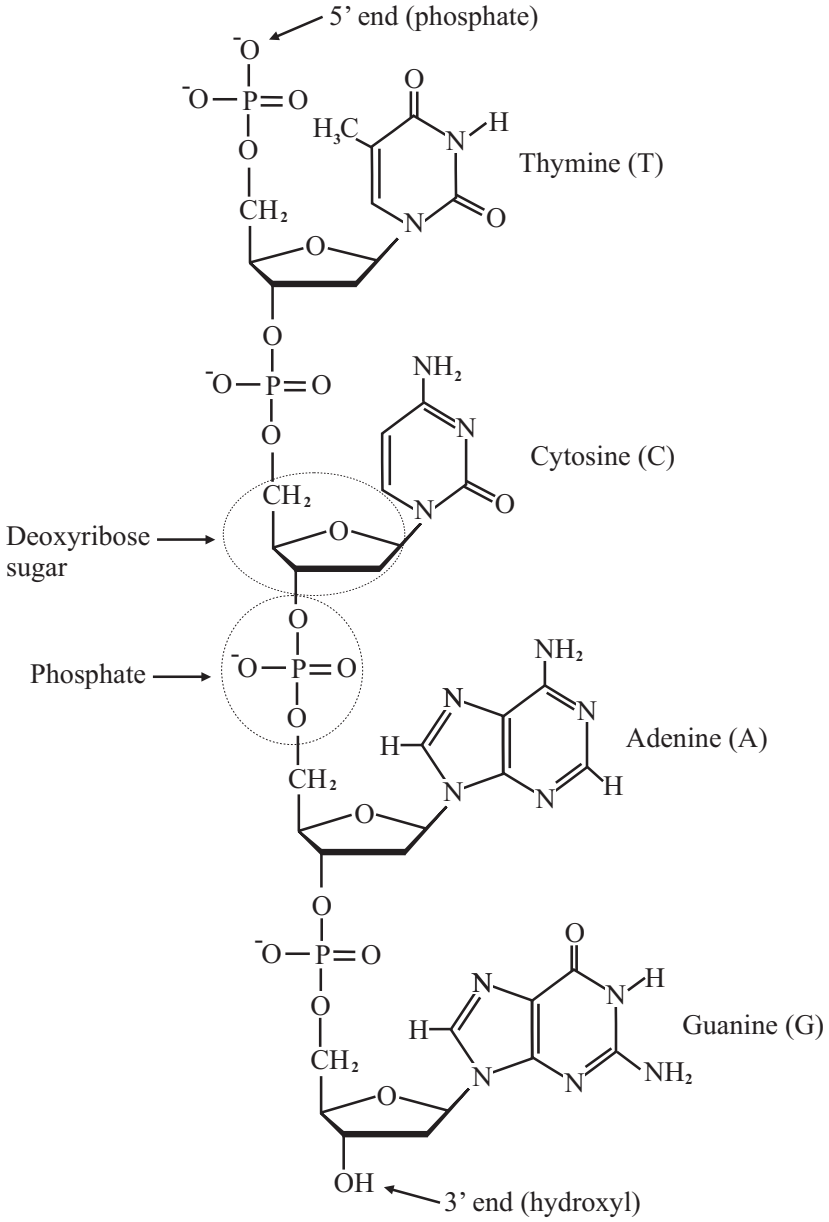

FIGURE 2.1 The structure of a single DNA stand. Bases are attached to the sugar-phosphate backbone.

at the top of each other as in the B-form. This deviation from the perpendicular alignment is $\sim 6^\circ$ for B-DNA vs. $\sim 20^\circ$ for A-DNA, which is a significant difference from the molecular electronics point of view (discussed in Section 2.10).

Different helical forms are favorable in different environmental conditions, e.g., variations in the water content, since at least 13 water molecules per nucleotide are required to stabilize B-form, whereas A-form can be stable having only 5-10 water molecules per nucleotide [250]. One other form is a left handed Z-DNA, which is more tangled, elongated variation from B-DNA.

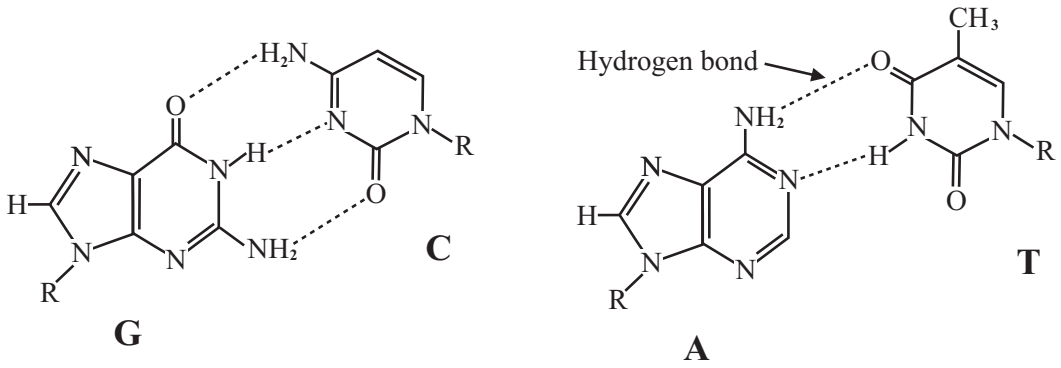

FIGURE 2.2 Forming of Watson-Crick base pairs, GC and AT, by hydrogen bonding between adjacent bases.

2.1.3 More exotic DNA conformations

DNA can also adopt more exotic conformations, like a triple helix structure, so called H-DNA [69, 174, 209], where a third strand binds to a B-form DNA double helix via Hoogsteen-type hydrogen-bonding interactions between the bases [105]. The third strand can attach to the double helix so that A binds to a T-A base pair and G to a C-G pair, forming the plateaus of three nucleotides.

Guanine-rich DNA strands can form in suitable conditions a 'four-stranded' nucleic acid structures called G-quadruplexes, reviewed in [52]. These structures are stabilized by G-quartets formed of four Hoogsteen-bonded guanines. Further, in the precence of some metal ions (e.g. K^+, Na^+ and Mg^{2+}) G-quadruplexes can reorganise themselves to higher molecular weight assemblies called 'G-wires' [164, 165]. G-wires can be more than 1 μm long [133] and their structure is more stable and robust than conventional double helical DNA, which is an advantage when considering molecular candidates for nanotechnological applications, e.g, they can be used as a molecular nanowires [40] (see Sec. 2.10).

2.2 Applications of DNA self-assembly

2.2.1 DNA fabrication

Methods for making specifically designed DNA, with a certain length and base sequence, are very advanced nowadays. The molecular biology offers a numerous collection of the restriction enzymes, which can be used to make DNA fragments of any size by cutting a long DNA molecule from the certain location, which is defined by the binding site of the specific enzyme. On the other hand, by starting from the bottom, short single-stranded DNA molecules, so called oligonucleotides, containing the specified base sequence, can be made using chemical synthesis, where the molecule is constructed from single nucleotides, one by one. Using the chemical synthesis, one can also include chemical modifications, e.g., thiol-group (-SH), in the

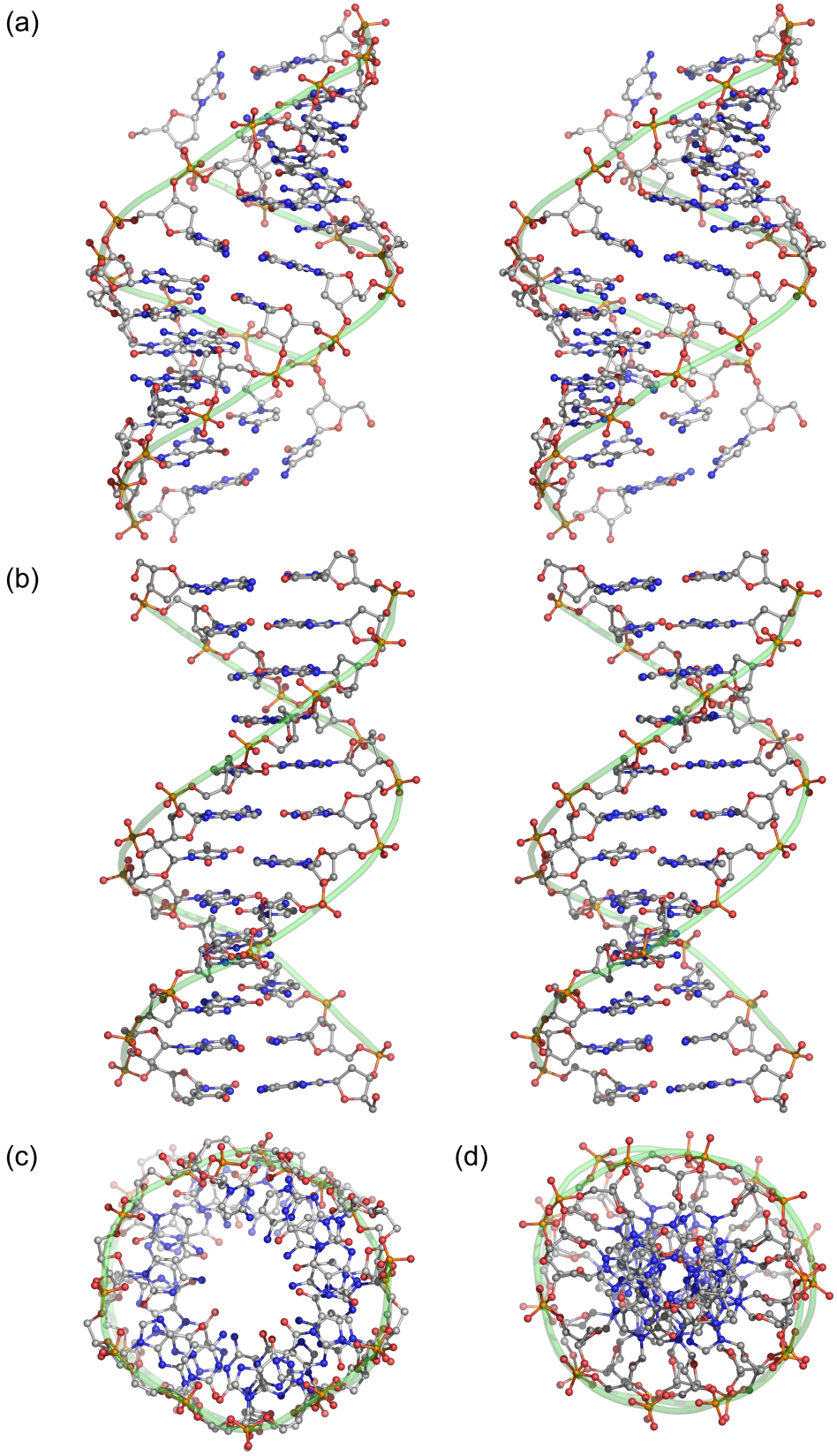

FIGURE 2.3 Stereoscopic images of DNA double helix side view in (a) A- and (b) B-form [5]. Images along the helical axis in (c) A- and (d) B-form. Atoms: carbon (grey), oxygen (red), nitrogen (blue), phosphorus (orange). Hydrogens, counter-ions and hydration water are not presented. The green pipe describes the sugar-phosphate backbone track.

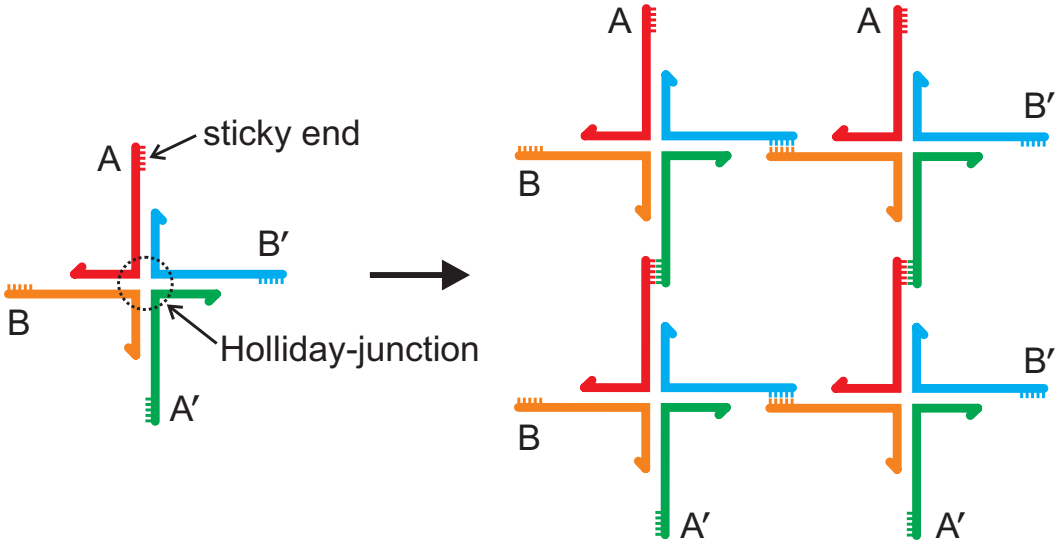

FIGURE 2.4 A single 'branched DNA molecule' (on the left) containing one branched junction formed of four different DNA strands is analogous to Holliday-junction appearing in nature during meiosis. The number of branches, corresponding to the number of DNA strands, can vary from three to eight. The strands coloured red and green have complementary sticky-end overhangs labelled A and A', respectively, whereas those coloured orange and blue have complementary overhangs B and B'. Four branched molecules form a square-like unit (on the right) which contains unpaired sticky ends on the outer edges, so more units could be added to produce a two-dimensional crystal.

end of the oligonucleotide. Chemical modifications can be used as a binding sites to attach some other molecules, particles or surfaces.

Polymerase Chain Reaction (PCR) can be used to fabricate DNA fragments containing a desired sequence from the DNA template, which can be for instance some natural plasmid DNA. In PCR, a polymerase enzyme is used to copy the sequence by using two synthetic oligonucleotides as 'primers', which contain sequences that define the starting and ending points inside the DNA template for the polymerase enzyme. As a result of PCR, large amount of double-stranded DNA containing a desired base sequence is produced.

2.2.2 DNA constructs

The exceptional recognition and self-assembly properties of DNA can be utilized in many ways, e.g., to construct complicated one-, two- and three-dimensional DNA assemblies, for a review see [66, 81, 186, 224].

The first DNA constructs

The principle of constructing DNA-based structures is to use so called 'sticky ends' (see Fig. 2.4), which are overhanging single-stranded regions in the end of double-

stranded DNA region. These sticky ends have a certain base sequence, which can be used as a binding site for another, complementary sticky end. Using simply sticky ends and dsDNA one can obtain one-dimensional chains and rings. To be able to obtain more complicated structures one has to find more sophisticated building blocks. In 1991, Nadrian Seeman and colleagues introduced 'branched DNA molecules' [222], which are formed of three to eight ssDNA molecules linked together through the common crossover point (see Fig. 2.4). The branched junction formed of four DNA strands is analogous to the Holliday-junction intermediate which appears in nature during meiosis. In meiosis, the Holliday-junction can also migrate along the DNA since the sequences are homologous. The branched DNA molecules which contain properly designed sticky ends can be linked together through the hybridization, thus allowing the building of two- or three dimensional constructions.

Seeman and colleagues were the first to construct a polyhedral object, possessing a connectivity of a cube [43], using the branched DNA molecules as building blocks. Finally, the 'nicks', i.e., breaks in DNA backbone formed to the ends of sticky end regions in the branches, were fixed using ligase-enzyme to covalently close the cube. Using similar method, they also fabricated a truncated octahedron in 1994 [278]. However, because of the flexibility of the DNA, these polyhedral objects did not preserve their three-dimensional shape. Later they made also more complex constructs [223], such as specific knots and Borromean rings.

2D DNA lattices

One important goal of the DNA self-assembly is to make two dimensional arrays from DNA. Since individual branched junction as such is very flexible it causes curvature of larger DNA constructs. As a solution, Seeman and colleagues introduced 'double-crossover' (DX) molecules as components for making stiffer DNA constructs [147]. A single DX tile is formed of two parallel dsDNA molecules with two Holliday-junctions between them. It is possible to program DNA tiles to produce a variety of patterned two-dimensional lattices just by controlling their sticky ends. In 1998, Winfree *et al* were first to construct two-dimensional DNA lattices using DX tiles [261]. They used two different design approaches of DX tiles (DAO-E and DAE-O described in Fig. 2.5(a)-(d)), and obtained lattices with different periodicities by using a DNA hairpin incorporated in DX molecule (see Fig. 2.5(e)-(g)).

Later, Thomas LeBean's group used 'triple-crossover' (TX) molecules to make two-dimensional arrays [136], and also build DNA crossbar lattices using slightly different four-arm junction tiles [268]. In 2004, triangular building blocks, as intrinsically rigid objects, were used to construct two-dimensional triangular [151] and pseudohexagonal [56] DNA lattices.

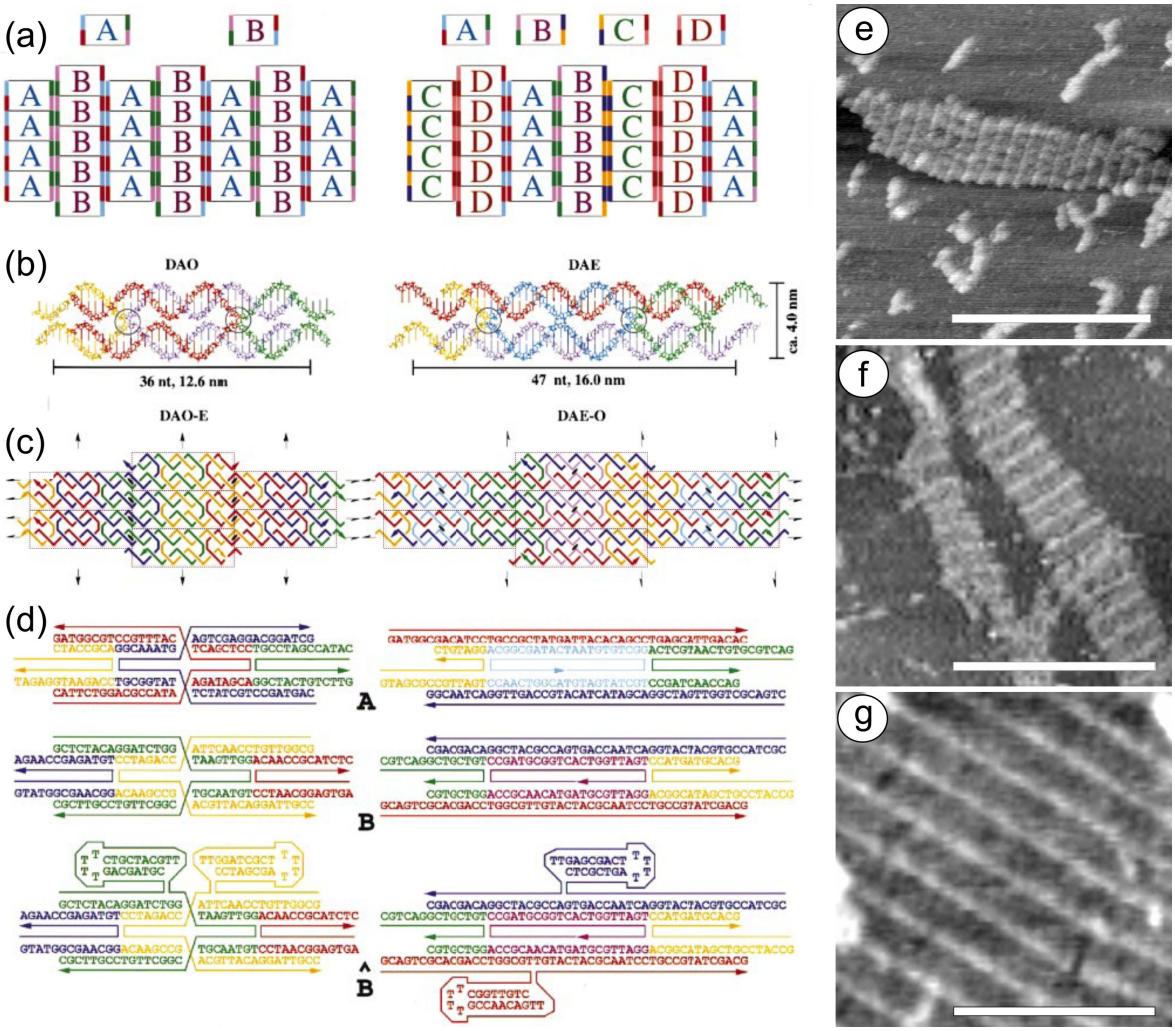

FIGURE 2.5 The design of two type of 'double-crossover' (DX) lattices, DAO-E (on the left) and DAE-O (on the right), is described in figures (a)-(d). (a) The logical arrangement of 2-D lattices consisting of two or four different DX tiles. Each tile contains four colored edge regions (sticky ends) which have to match with the colors of the adjacent tiles. (b) Model structure of a single DAO (double crossover, antiparallel, odd spacing) and DAE (even spacing) type of DX tiles. DAO (DAE) molecules have an odd (even) number of half-turns (3 half-turns equals to 16 bp) between the crossover points. Each strand is shown in a unique colour and strand crossover points are circled. (c) The produced lattice topologies, where each DX unit is highlighted by a rectangle. A unique color is chosen for each different type of strand which would be formed after covalent ligation of assembled tiles. DAO-E design produces four distinct strand types, each continuing infinitely in the vertical direction, whereas DAE-O design contains two small circular strands and four infinite strands, two of which extend horizontally and two of which extend vertically. (d) The actual oligonucleotide sequences used. The figures are not geometrically or topologically truthful because they do not describe the double-helical twisting. The tile $\hat{\mathbf{B}}$ is a version of **B** containing additional DNA hairpin sequences, which serve as topographical labels for AFM imaging, showing increased height. (e)-(g) AFM images of the lattices using the different tiles: (e) DAO-E $\mathbf{A}\hat{\mathbf{B}}$, f) DAE-O $\mathbf{A}\hat{\mathbf{B}}\mathbf{A}\hat{\mathbf{B}}$ and g) DAE-O $\mathbf{ABC}\hat{\mathbf{D}}$. **C** and $\hat{\mathbf{D}}$ tiles are similar to **A** and $\hat{\mathbf{B}}$ but composed of different oligonucleotides. The stripes in the lattices have periodicity of about (e) 25, (f) 33 and (g) 66 nm. Scale-bars are 300 nm.

3D constructs

In addition to planar DNA lattices, DNA tiles have been used to build three-dimensional constructions. Due to the intrinsic property of planar DNA tiles to form curved shapes, so called 'DNA nanotubes' (much stiffer than dsDNA) were made using TX [150] and DX [218] molecules. The walls of the DNA nanotubes are composed of adjacent DNA tiles. Also more stable DNA nanotubes were obtained by means of ligation [195]. As a one strategy for expanding tiling into the third dimension, another types of DNA nanotubes were made using triangular three-helix bundles (3HB) [198] and hexagonal six-helix bundles (6HB) [168], which are composed of parallel helices linked together. However, 3HB do not contain a hollow space inside them as the other tubes.

Individual three-dimensional objects, like a tetrahedron [78, 79] and an octahedron [227] (see Fig. 2.6), were build from the triangular DNA subunits as more rigid tiles. Further, Seeman and co-workers reported a regular, continuous three-dimensional DNA lattice [203]. This rather complex construct consisting of three repeating layers of parallel helices, was composed of numerous copies of only a single 13-base oligonucleotide. The helices in adjacent layers interchange strands in the crossings, thus fixing the two layers together.

2D patterned shapes

One long-term goal of DNA self-assembly is the generation of complex patterns on two-dimensional arrays. In 2004, Rothemund *et al* demonstrated a self-assembly of Sierpinski triangle pattern [219]. Pattern was formed by using tiles whose sticky-ends attach according to association rules of the binary function XOR (see section 2.2.5).

Two-dimensional tiling systems represented so far do not offer control over the overall size of the lattice. In 2006, LeBean's group presented a way to build finite-size DNA crossbar arrays using a set of different specifically designed tiles [199]. Very recently, Rothemund introduced an ingenious method for folding DNA to create two-dimensional nanoscale shapes and patterns, called 'DNA origami' due to the folding method [217]. The method he used was similar to the one used in making an octahedron by Shih *et al* in 2004 [227] (see Fig. 2.6). A desired structure is obtained by raster-filling the aimed shape with long (a few kb) ssDNA scaffold and by using over 200 short oligonucleotides as 'staple strands' to hold the scaffold in place. The resulting DNA structures, e.g., five-pointed stars and disks (see Fig. 2.7(a)-(b)), are roughly 100 nm in diameter. Each staple strand serve as a 6-nm pixel, which defines the spatial resolution. In addition to making a shape itself, staple strands provide a method for decorating shapes with arbitrary patterns or combining shapes together (see Fig. 2.7(c)-(f)).

In addition to using sticky ends, the staple strands can be also labelled us-

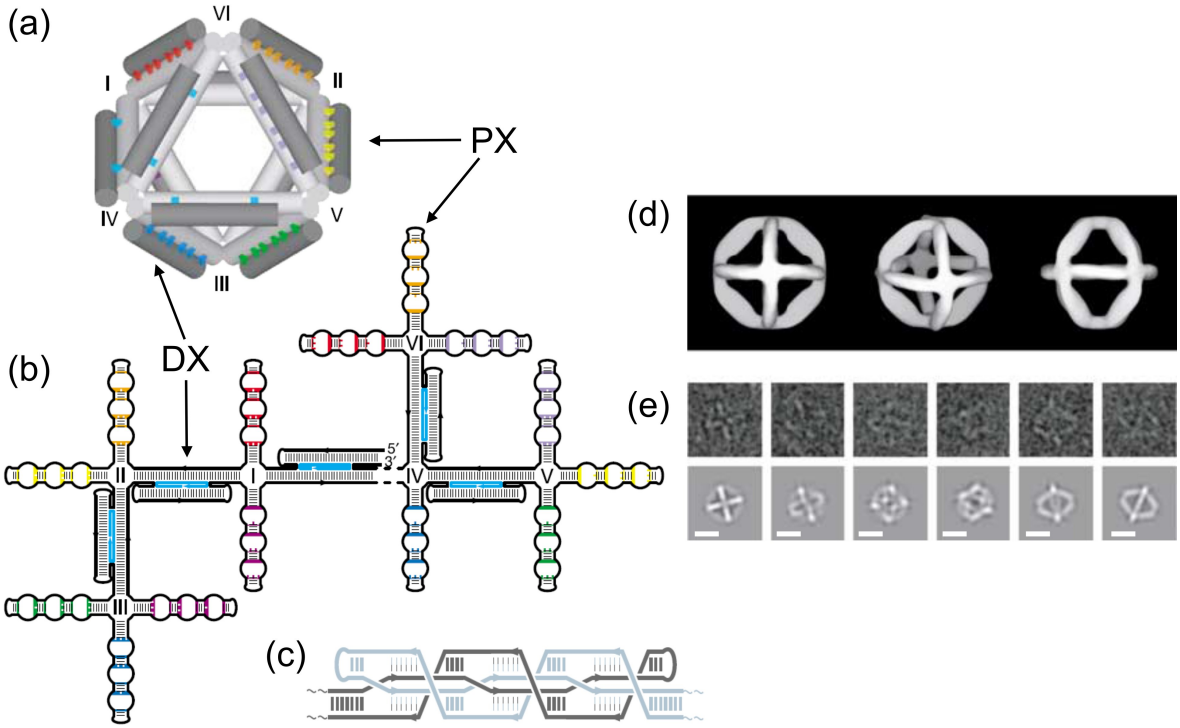

FIGURE 2.6 A 1.7-kilobase ssDNA folded to DNA octahedron using five 40 base staple strands. (a) The final 3D structure contains twelve 'struts' (octahedron edges) connected by six flexible 'joints' (octahedron vertices). Five of the 'struts' are DX motifs (cyan) and seven are PX (paranemic-crossover, see e.g. [269]) motifs (rainbow colours). Folding was performed in two steps (heat denaturation followed by cooling). First, the 1.7 kb strand (black) and five 40 b strands (cyan) were mixed stoichiometrically and to form a branched-tree structure shown in (b). The 'joints' are four-way junctions connected to the double helices of each 'strut'. (c) Schematic of a PX strut. In second step, sequence-specific cross-association of two same colored half-PX motifs generates a 'strut' that serves as an edge of the DNA octahedron. Folding to the 3D structure is complete when all seven PX struts have formed. (d)-(e) Visualization of the DNA octahedron structure by cryo-electron microscopy and single-particle reconstruction techniques. (d) Three views of generated 3D map. (e) Raw images of individual objects and corresponding projections of the 3D map. Scale-bars are 10 nm. Adapted with permission from ref. [227].

ing DNA modifications, e.g., biotin or thiol, which can be used to create a desired pattern of the certain objects in nanoscale using the self-assembly. Patterned DNA origami and the other two- or even three-dimensional DNA structures have obvious applications in nanobiotechnology, since they can be used as scaffolds for making periodic assemblies of biomolecules, e.g., arrays of proteins. Also molecular electronic or plasmonic circuits might be created by attaching nanowires, carbon nanotubes (CNT) or gold nanoparticles to specified locations in these 'DNA circuit boards'. These applications are discussed in more detail in section 2.2.4.

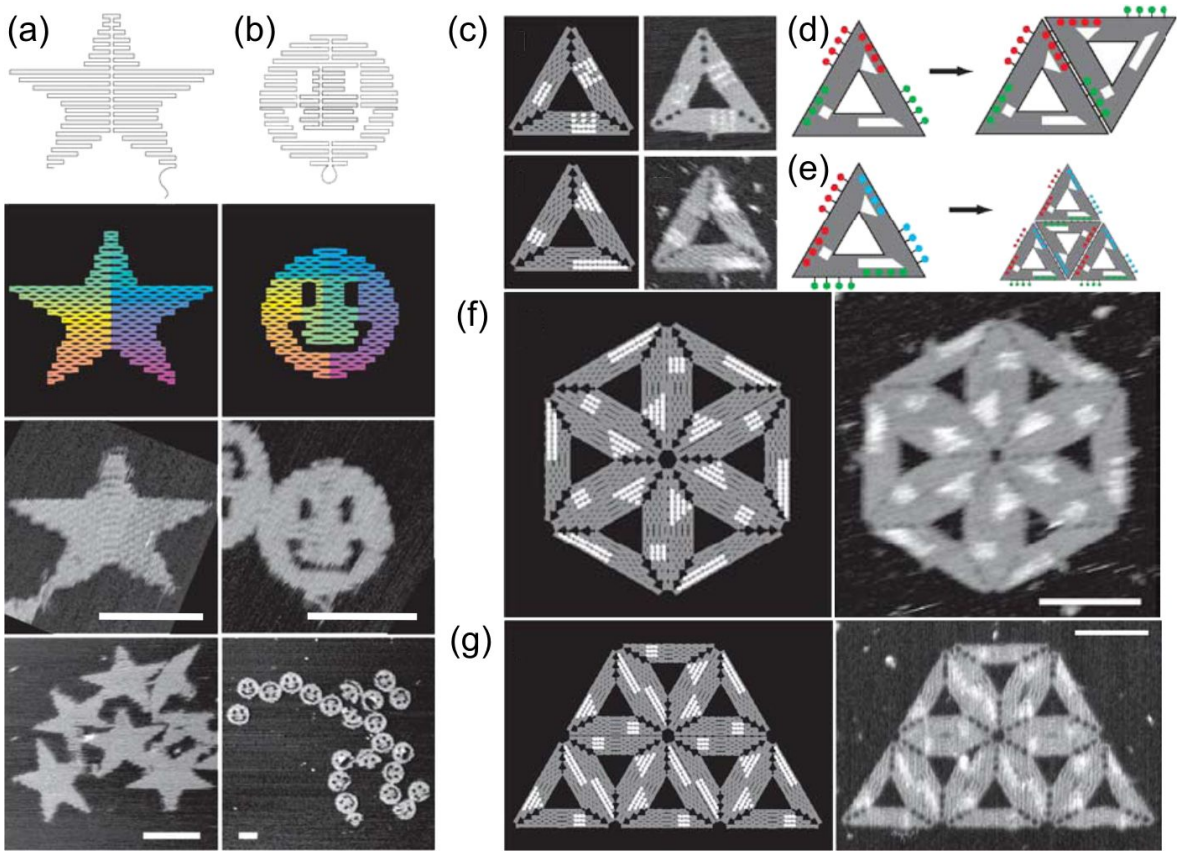

FIGURE 2.7 DNA origami shapes and patterns. (a) A five-point star and (b) a disk with three holes have been made by raster-filling the designed shape by a 7-kilobase ssDNA scaffold and over 200 short oligonucleotides as staple strands. Lower two in (a) and (b) are AFM images. (c) Decoration of triangle shapes with an arbitrary pattern was made using 'dumbbell hairpins' in the end of the certain staple strands. Hairpins contrast 1.5 nm above the unlabelled staple strands in the AFM image (on the right). (d)-(e) Adding of 'extended staples' to the triangle edges in order to combine them to form, e.g., (f)-(d) hexagons (yield was only < 2%) and (g)-(e) lattices. Scale-bars are 100 nm. Adapted with permission from ref. [217].

2.2.3 DNA nanomachines

In addition to constructs and arrays, a number of DNA-based nanomechanical devices have been realized. In 1999, Seeman's group demonstrated a nanomechanical switch [160], containing two rigid DX molecules and a specific shaft which could be converted from the right-handed B-DNA to the left-handed Z-DNA. This conversion leads to the rotation of the protruding DX domains from the same side to the opposite sides of the central helix. The B-Z transition was induced chemically by adding cobalt hexammine ($[Co(NH_3)_6]^{3+}$) to the solution.

DNA devices where the state transition is 'fuelled' by metal ions or protons have also been build. In 2001, Niemeyer *et al* built a device where nanoscale movement as introduced by supercoiling of adjacent DNA helices in the biotin-streptavi-

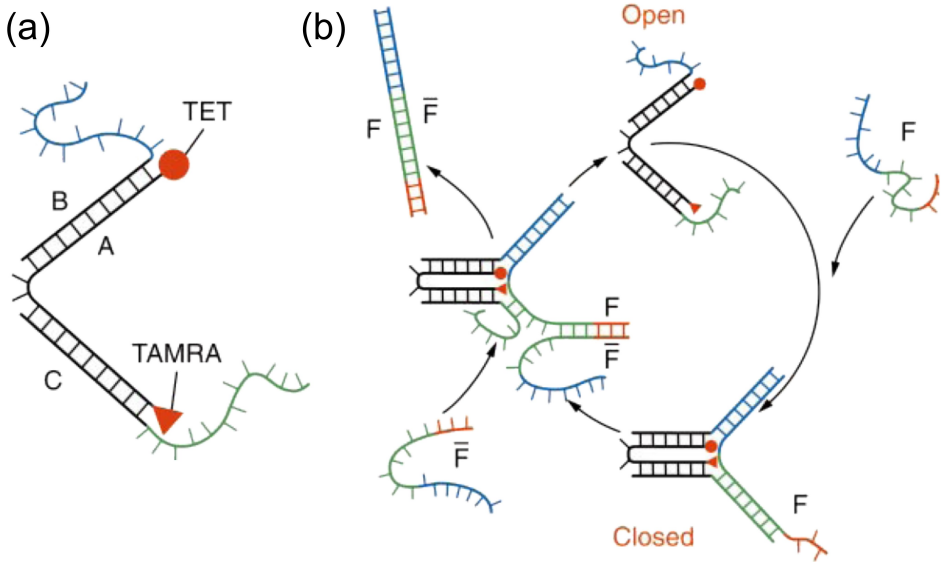

FIGURE 2.8 Construction and operation of the DNA tweezers. (a) Molecular tweezer structure formed by hybridization of oligonucleotide strands **A**, **B** and **C**. (b) Closing and opening of the tweezers. The closing strand **F** hybridizes with the overhanging ends of strands B and C (shown in blue and green) and pulls the tweezers to a closed state. Hybridization with the overhang section of **F** (red) allows $\bar{\mathbf{F}}$ strand (fully complementary to **F**) to detach F from the tweezers, forming a double-stranded waste product $\mathbf{F}\bar{\mathbf{F}}$ and leaving tweezers to an open state. The waste is left to the solution, but it doesn't substantially participate to reactions anymore, so the opening-closing cycle can be started again. Adapted with permission from ref. [274].

din linked DNA network, when the Mg^{2+} ion content was increased [189]. In 2003, Fahlman *et al* demonstrated a 'pinching' of the DNA duplex by Sr^{2+} ion induced formation of G-quartets between two regions rich in G-G mismatches, separated by a short A-T bridge [65]. A proton fuelled DNA machine was made, e.g., by Liu *et al* by using the formation of C-C+ base-pairs from C-rich strands at low pH values [149].

One other way to introduce transition between two states is to use single-stranded DNA for fuelling. In 2000, Bernand Yurke and colleagues built so called 'DNA tweezers' [274], which are composed of three partly hybridized DNA strands (see Fig. 2.8). Its functionality is based on the fact that a system has a tendency to minimize its free energy. Tweezers can be recursively closed and opened by addition of a stoichiometric amount of one of the two fully complementary strands, another of which is partly complementary to the tweezer strands.

Using the similar strategy of 'fuelled' conformational changes, also a more robust nanorobotic device was build by Seeman's group in 2002 [269]. In addition to two state machines, Simmel and Yurke built a device, which has three distinct mechanical states [230].

The first steps towards a DNA-based molecular motor were taken in 2004, by realizing autonomous unidirectional motion using DNA. Yin *et al* fabricated a de-

vice where six nucleotides 'walked' along the double-stranded DNA track equipped with three different branches containing sticky ends for attachment [270]. Three DNA-modifying enzymes were used to cut the formed helix after the each walking step so that six nucleotides could propagate along the track. Also Shin *et al* built a device where a double-stranded DNA walker moved along the track (almost similar to one described before) by the alternating hybridisations of two single-stranded 'feet' of the walker [229].

2.2.4 DNA as a scaffold

A substantial goal of development of DNA constructs and DNA nanomachines (describes in two previous sections) is to use them as 'active scaffolds' in order to build two or three dimensional assemblies of the other components, such as biomolecules, nanoparticles or carbon nanotubes. Some of the different ways of using DNA as a scaffold are described here.

DNA-templated nanowires and chains

The simplest way of using DNA as a scaffold is to chemically modify DNA itself by adding some functional material on it. Natural double-stranded DNA has been successfully used as a template for making nanowires from various metals, including silver [32], gold [33, 128], copper [177], platinum [68] and palladium [213, 214]. Also 'one-dimensional' superconducting nanowires (as thin as 5 to 15 nm in diameter) were made by sputtering $Mo_{21}Ge_{79}$ on individual suspended DNA molecules [106].

Different types of nanoparticles have been assembled using a DNA-template, e.g, magnetic nanowires were made from Fe_3O_4 [192] or Co [85] nanoparticles. Also semiconducting arrays were made using CdS [47] and CuSd [57] nanoparticles.

A DNA scaffold has been used to align molecular wires, e.g., conducting polymer wires were obtained by wrapping polyaniline on a DNA-template [131, 156, 180]. Also carbon nanotubes have been aligned along the DNA scaffold through a covalent amide linkage [259] or by using antibody recognition [127]. In the first case, synthetic PNA (peptide nucleic acid), an uncharged version of intrinsically negatively charged DNA, was used [259].

DNA-functionalized components

Another kind of approach to the DNA-templated arrangement of material is to use DNA oligonucleotide functionalisation of the components. Using this method, a range of different nanoparticles and nanoclusters have been assembled for a variety of purposes. For instance, a DNA-based assembly of metallic nanoparticles can be done in one, two or three dimensions using DNA-functionalised nanoparticles,

reviewed e.g. in [187, 190]. In 1994, Mirkin *et al* and Alivisatos *et al* were first to realize gold nanocrystals using functionalized gold nanoparticles and thiol-modified (-SH group) oligonucleotides [11, 173]. The principle of making these nanocrystals was that two nanoparticles, which are first covered with different kind of oligonucleotides complementary to each other, can be linked together through the double helix formed of the complementary oligonucleotides [173]. In addition to nanoparticles, oligonucleotide-functionalisation has been used to fabricate arrays of other components, e.g., gold nanorods [60], CdSe/ZnS quantum dots [175] or dendrimers [54].

Also carbon nanotubes has been functionalised, e.g., in the work by Li *et al*, where multi-walled carbon nanotubes (MWCNT) were functionalized with amide-linked ssDNA and annealed with gold nanoparticles functionalised with the complementary thiolated ssDNA, resulting in the assemblies where individual MWCNTs were linked to a gold nanoparticle [146]. In another study, the single-walled carbon nanotubes (SWCNT) functionalised similar way were positioned to ssDNA covered gold electrodes by the hybridization of the complementary DNA sequences [90].

A famous biotin-avidin binding has been used to make protein assemblies, e.g., a periodic material was obtained using DNA-functionalized streptavidin (biotin-modified oligonucleotides were linked to streptavidin) and gold nanoparticles as building blocks [201]. Supramolecular nanocycles have been fabricated by mixing streptavidin and double-stranded DNA, which contained a biotin-modification in the both ends [188, 225].

DNA-functionalisation of nanoparticles has been used also in sensor applications, e.g., an electrical DNA array detection method based on functionalized gold nanoparticles was reported [202]. The gold nanoparticles, functionalized with 'probe' oligonucleotides, localize to the electrode gap if the 'target' oligonucleotides are present in the solution, leading to a measurable conductivity change after the subsequent silver deposition. Also a colorimetric sensor, based on red-to-pinkish or red-to-purple color change due to a nanoparticle network formation, resulting from the addition of a single-stranded target oligonucleotides into a solution containing oligonucleotide-functionalized gold nanoparticles, was built [63].

DNA constructs as a scaffold

Particularly, the DNA constructs discussed in Sec. 2.2.2 may be used as more sophisticated scaffolds for building two- and three-dimensional assemblies. The principle in composing this kind of assemblies is that in addition to the sticky ends used to construct the DNA scaffold itself, there are some other binding sites, e.g., free sticky ends or DNA modifications, which are used as a binding sites for a particular component. As well, the arranged component itself must contain the corresponding binding group.

In addition to constructing the first two-dimensional DNA lattices in 1998, Seeman's group also attached rows of streptavidin-nanogold, i.e., 1.4 nm gold particles covered with streptavidin protein, to the DNA tile lattice by labelling one of the DX tiles with biotin [261]. Also, Thomas LeBean's group fabricated two dimensional protein arrays using crossbar lattice made of four-arm junction DNA tiles [268]. Later, two self-assembled periodic DNA structures, two-dimendional nanogrids and one-dimensional nanotracks, were used to make streptavidin arrays with controlled density [200]. Recently, they were able to construct fully addressable, finite-sized arrays with a variety of programmed streptavidin patterns using a set of different specifically designed DNA tiles [199].

The overall control of the lattice conformation was obtained by incorporation of a bacterial recombination protein, RuvA, as an intrinsic component of a DNA nanostructure [157]. Two crystals built from the same four oligonucleotides resulted completely different lattice symmetry and connectivity, i.e., square lattice was formed in the presence of protein, whereas in absence of the protein a pseudo-hexagonal lattice was formed.

LeBean's group has reported the fabrication of silver nanowires by metallization of different type of DNA constructs, i.e., crossbar lattice made of four-arm junction tiles [268], DNA nanotubes made of TX tiles (wire width and height were 40 nm) [150] and the three-helix bundles (wire width 20 nm) [198]. Even if the silver nanowires made using DNA constructs have height and width of 20-40 nm, which is more than in the case of wires made by metallization of individual dsDNA molecules, they are much smoother and more conducting.

Two-dimensional DNA lattice was used to pattern 5 nm gold particles into precisely spaced rows [138]. This was done by using the gold nanoparticles functionalized with T_{15} oligonucleotides, which attached to a DX tile array containing A_{15} sticky-ends in certain tiles. Using a similar method, also two-dimensional arrays containing alternating rows of 5 and 10 nm nanoparticles attached to different type of tiles were obtained [205]. Recently, two-dimensional crystal of 5 and 10 nm nanoparticles with precise spacing in both directions was obtained using 3D-DX triangle tiles [280].

DNA-templated carbon nanotube transistor

An ingenious example of using DNA as a scaffold for device fabrication was reported in 2003, when Keren *et al* built a carbon nanotube field effect transistor (CNT-FET) by using DNA-templated assembly of a single walled carbon nanotube and metallic nanowires contacting the nanotube (see Fig. 2.9) [127]. The functionality of the field-effect transistor operating at room temperature was verified using the substrate as a back-gate.

The ability to organize electrically active species such as gold nanoparticles and carbon nanotubes using DNA scaffolds, and further, to use chemical methods

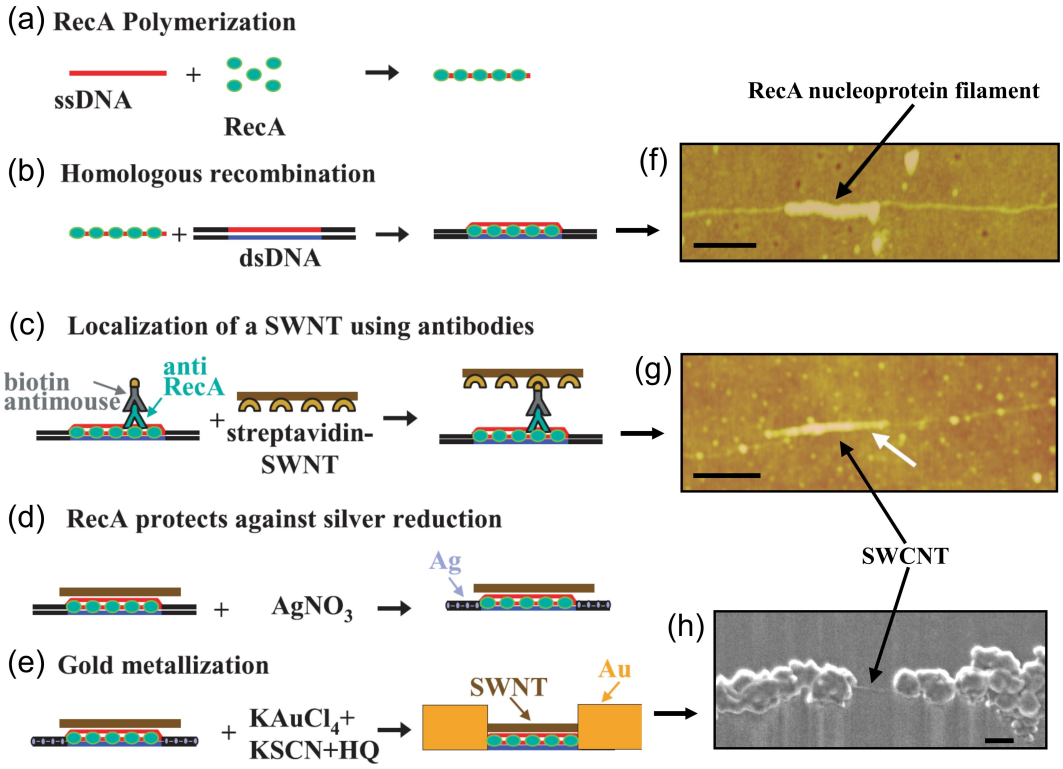

FIGURE 2.9 Assembly of a DNA-templated carbon nanotube field effect transistor (CNT-FET) and wires connected to it. Fabrication steps are as follows: (a) RecA protein monomers polymerize on a ssDNA molecule to form a nucleoprotein filament. (b) A three-strand homologous recombination reaction leads to a binding of the nucleoprotein filament at the desired address on an aldehyde-derivatized scaffold dsDNA molecule. (c) The DNA-bound RecA is used to localize a streptavidin-functionalized SWCNT, utilizing a primary antibody to RecA and a biotin-conjugated secondary antibody. (d) Incubation in an $AgNO_3$ solution leads to the formation of silver clusters on the segments that are unprotected by RecA (RecA works as a sequence-specific resist). (e) Electroless gold deposition, using the silver clusters as nucleation centers, results in the formation of two DNA-templated gold wires contacting the SWCNT bound at the gap. (f) An AFM image after the step (b). A 500-base-long (250 nm) RecA nucleoprotein filament (black arrow) localized at a homologous sequence on a DNA scaffold molecule. Scale-bar is 200 nm. (g) An AFM image after the step (c). A streptavidin-coated SWCNT bound to a nucleoprotein filament. Scale-bar is 300 nm. (h) An SEM image after the step (e). A SWCNT contacted by self-assembled DNA-templated gold wires. Scale-bar is 100 nm. Adapted with permission from ref. [127].

to make conducting nanowires by DNA metallization, points the way toward the templating of complex devices and circuits for nanoelectronics applications.

2.2.5 DNA computing

In 1994, Adleman demonstrated experimentally that DNA can be used to computationally solve a small example of a standard problem in computer science, i.e.,

the Travelling Salesman Problem [9]. Since then, several different approaches have been demonstrated to exploit the parallel hybridisation of complementary ssDNA sequences for highly parallel computing. For a review see e.g. [72]. In 2000, Liu *et al* reported a DNA computation method using a 'DNA chip' readout system, where an array of surface bound ssDNA probes are hybridized with the ssDNA target and the amount of attached target is detected by measuring the fluorescence from each DNA spot [152].

Seeman and colleagues proposed that complete computations can be executed using the self-assembly of the TX tiles, due to their similarity to Wang tiles, which is a mathematical model of two-dimensional geometric shapes which are arranged by their 'colored edges'. In 2000, Mao *et al* demonstrated the one-dimensional self-assembly of the TX tiles according to four steps of a logical (cumulative XOR) operation [159]. A two-dimensional arithmetic self-assembly of DNA tiles was demonstrated in 2004, when Rothemund *et al* built so called Sierpinski triangle using the self-assembly of the DX tiles according to the association rules of binary function XOR [219]. One substantial challenge in the DNA based computation is its relatively high error level.

2.3 Charge migration in DNA

2.3.1 Why should DNA conduct?

Another aspect of utilizing DNA in molecular electronics is related to its electrical properties. In 1962, soon after the discovery of the DNA double helix by Watson and Crick in 1953 [257], Eley and Spivey first proposed that DNA may act as an electrical conductor due to the overlapping π-orbitals of the base pair stack [62]. This originates from the fact that the DNA bases are aromatic entities containing planar, unsaturated, benzene-type ring structures, whose atomic p_z orbitals perpendicular to the plane of the base (see horisontal planes in Fig. 2.3b) can form rather delocalised π bonding and π^* antibonding orbitals (energy gap between π and π^* is about 4 eV). If the electronic coupling between the π orbitals of the adjacent bases is strong enough, it can lead to formation of extended states along the helical axis, reducing the size of the energy gap, due to the energy level broadening. If the energy gap totally vanishes, it leads to an ohmic behavior of DNA, or even if the gap substantially diminishes, conductivity can be obtained by doping the DNA (like in the case of conventional semiconductors).

The alignment and the distance between the bases (3.4 Å) in a B-form DNA is similar to stacked aromatic crystals such as Bechgaard salts, $(TMTSF)_2PF_6$ where TMTSF is tetramethyltetraselenafulvalene, which behave like metals [216]. Their most significant difference is that the biological DNA is not a periodic system, and thus the electronic coupling between the highest occupied (HOMO) or the lowest

unoccupied (LUMO) molecular orbitals of the neighboring base pairs varies along the DNA sequence. However, it has been suggested that a biological DNA sequence is not truly random but it contains long-range correlations [41].

When considering the electronic properties of DNA, one must also take into account the hydration water molecules, which are needed to stabilize the helix, and the positive counter-ions in the vicinity of the backbone, compensating the negative charge of the phosphates, which highly affects to the electronic structure of the π-stack. Due to the backbone flexibility and the hydrogen bonded reversible pairing, DNA is a dynamic molecule and the molecular vibrations are an order of magnitude higher than in the aromatic crystals, which further complicates its electronic structure. These issues make theoretical considerations quite complicated in the case of electronic properties of the DNA.

The nature of the electron transfer (ET) along the DNA has received intensive attention in biology and chemistry, due to its close relation to the repairing mechanism of the oxidative damages in DNA. One vision is that guanine-rich telomeric overhanging regions at the termini of chromosomes act as a "cathodic protectors" reducing the oxidative stress of DNA, so that a radiation induced hole could migrate from genetic region to the telomeric regions [95]. In another proposed biological mechanism the DNA charge transfer chemistry would be used by enzymes, which detect mismatches and other local perturbations by scanning the genome and then "marking" the damaged spots for a repair [210].

In physics and electronics, the interest towards electrical properties of DNA are due to its possible use as a one-dimensional conductor. The electrical properties of DNA have been studied widely using both chemical (charge transfer) (For a review see e.g. [31]) and physical (electron transport) approaches (For a review see e.g. [53, 64, 208, 239]). The experimental results are briefly summarized in the following sections. The charge transfer (CT) studies are discussed in Sec. 2.3.2. The direct conductivity measurements are chronologically listed in Sec. 2.3.3 and later, in Sec. 2.3.4 discussed more with focus on observed phenomena and conclusions.

2.3.2 Charge transfer

In a chemical approach the charge transfer (CT) along the DNA is studied experimentally by injecting a charge to a donor, usually a hole to a guanine (doping of DNA), which has the lowest oxidation potential, and looking the charge migrating along the DNA until it is absorbed by an acceptor. The simplest model for CT only involves tunneling through a one-dimensional energy barrier. In this case the rate of CT, k_{CT}, decays exponentially as

$$k_{CT} = k_0 e^{-\beta R}, \tag{2.1}$$

where k_0 is the rate of CT when donor and acceptor are in close contact, R is the donor-acceptor distance and β is a constant describing how fast tunneling rate falls off as a function of the distance [24]. In more detailed considerations, there are two competing mechanisms how a charge can travel from the donor to the acceptor through the intermediate base pair bridge [25, 27, 28]. The first one is a tunneling in which the excited donor and the acceptor has lower energy than the bridge. The tunneling may be either a coherent uni-step tunneling process, so-called superexchange, or an incoherent sequential tunneling process, where the charge is transfered through the intermediate sites by diffusion type random walk. Another process is a thermally activated hopping between the sites. A long-range CT in DNA is most likely a combination of these processes.

In the pioneering photoexcitation studies [12, 179], Barton and colleagues used the metallointercalators, ruthenium(II) as donors and rhodium(III) as an acceptor, attached covalently to different ends of the DNA duplex. When two complementary oligonucleotides, one linked to ruthenium(II) and another to rhodium(III), where hybridized, the ruthenium(II) steady-state luminescence was completely quenched by the rhodium(III) intercalator positioned to the opposite end of the over 40 Å long double helix. This suggests that the charge induced to the donor travels along the helix and is absorbed by the acceptor. They also demonstrated the detection of a photoinduced oxidation damage of the guanine site within 100 ps time window by using rhodium metallointercalator attached to the DNA over 40 Å away from the guanine site [87]. These very high rates of CT found in these studies correspond to values $\beta \leq 0.2$ Å^{-1}, which suggest wire-like behavior. It must be noticed that the definition of "wire" in this context means that injected charges undergo a long-range transport (tens of ånströms) on fast time scale (in picoseconds). This is different from the definition of solid-state wire, where conductivity is related to the electronic structure of the whole system under applied external potentials.

The low β values found by Barton's group were different from the theoretical predictions [24, 75, 118, 161] and the experimentally obtained values by the other groups [36, 70, 144, 169]. For instance, a protein-like rate of CT (β value from 0.8 to 1.4 Å^{-1} [12]) was obtained by Brun and Harriman using DNA-intercalated organic donors and acceptors [36] and by Meade *et al* using covalently attached ruthenium complexes in the both ends of a 21 Å long dublex. Values of $\beta \sim$0.7 Å^{-1} were observed by Lewis *et al*, by measuring photoinduced electron transfer between the stilbene acceptor and a guanine donor in the synthetic DNA hairpins [144, 145], and Giese *et al*, by generating a guanine radical cation ($G^{+\bullet}$) and measuring its migration through dA:dT stacks to GGG site [76, 170, 171]. The controversy over the experimental results stimulated a lot of significant research activity to further investigate the mechanism of CT in DNA.

In futher studies by Barton's group they pointed out that the rate of CT can range from insulator- to wire-like (β varies from 0.1 to 1.0 Å^{-1}) depending on the

charge injection system (reactant energetics, i.e, the energy gap between donor (or acceptor) orbitals and base pair stack orbitals), the donor-acceptor distance, the intervening base sequence and the structural integrity of the base stack [51, 123, 125, 248, 249, 260]. They also demonstrated the electrochemical detection of a single Cytosine-Adenine mismatch based on the CT through the DNA monolayer on gold surfaces [124, 126]. Since the rate of CT is highly sensitive to base stacking, it can be utilized widely in sensor applications, e.g., in a DNA recognition sensor, where the sequence of a single-stranded 'target' could be checked by electrically monitoring the hybridization of the 'target' DNA with the known 'probe' sequence.

It seems that contradicting results were mostly due to the CT being highly sensitive to the coupling of a donor and an acceptor to the DNA [123]. This coupling can be compared to the importance of the electrode-molecule contacts in the case of solid-state conductivity measurements, discussed later in Sec. 2.3.4.

It has been estimated that a long-range CT in DNA can occur over 300 ångströms, falling off exponentially with distance [25, 28, 31]. There starts to be a consensus that guanines, which have the lowest oxidation energy, have a major role in hole transfer along the DNA [31]. As mentioned above, a hole can be transferred from a donor to an acceptor by the coherent uni-step tunneling mechanism (superexchange) [28] (see Fig. 2.10a) or by multi-step processes. In the superexchange process a charge which is localised to the G site tunnels through the intervening dA-dT stack and is localized to the next G-site. The multi-step process may be either incoherent sequential tunneling [145] or thermally induced hopping (TIH) [144]. Sequential tunneling contains several consecutive superexchange steps, in which a travelling hole uses G-sites as 'stepping stones' within the migration step. In the thermally induced hopping (see Fig. 2.10b), a hole is thermally excited so that it can be localized to an A-T pair and it can migrate through bridge by hopping between the A-T pairs until it is localised to a G site and relaxed. In addition to single G sites, hole can be localized to $(G)_m$ domains (containing m adjacent guanines), which has even lower oxidation potential than a single G [76]. Whether the tunneling or thermal hopping is the dominant process, depends on the distances of the G sites in the sequence. The uni-step superexchange mediated tunneling dominates in the case of 'short' A-T bridge, whereas in the case of 'long' bridges (> 3-4 A-T pairs) the tunneling is prohibited and thermal hopping is the dominant mechanism [28].

Also some more complicated mechanisms have been proposed. Polaron, which is formed by the polarisation of adjacent base pairs or surrounding medium, causes spreading of the charge over several bases and may result in a much faster charge migration through the DNA [49, 96]. Solitons, meaning the localized excitations propagating along the system, have also been proposed to participate to the charge transfer in DNA [97].

As a conclusion, in the case of long DNA molecules, which usually contain too large A-T bridges for a pure tunneling mechanism, efficiency of CT can not be

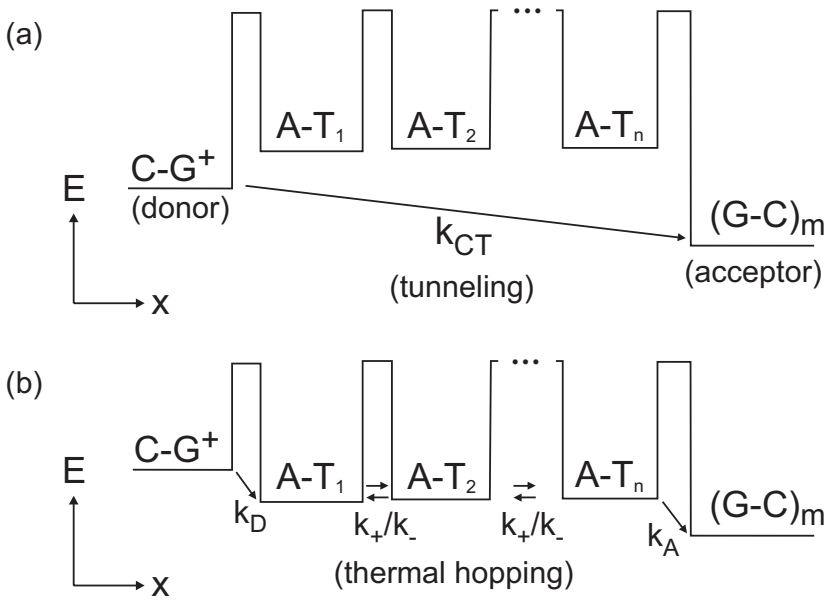

FIGURE 2.10 A schematic representation of the proposed charge transfer (CT) mechanisms. Arrows indicate the CT processes. (a) The uni-step coherent tunneling from a donor to an acceptor (superexchange). (b) Thermally induced hopping (TIH), where charge migrates through intermediate A-T sites by diffusion type of random walk. Mechanism (a) dominates when the A-T bridge is 'short' enough for tunneling to occur (n < 3-4). The real mechanism is a parallel combination of the mechanisms (a) and (b). The figure is a modified version from Ref. [28]

described by the parameter β anymore. In addition, the charge transfer mechanisms described here occurs only in the presence of excited states, where electron-hole pair is formed by high-energy injection. This does not correspond to the case of usual DC electron transport, where energies associated to single migration steps are low. Thus, the charge transfer results can not be as such utilized to determine electron transport in the long DNA molecules.

2.3.3 Conductivity

In the preliminary direct conductivity measurements carried out in 1960's using bulk samples (dry fibers and solid gels of DNA), it was found that DNA has semiconductor-like behaviour, with energy gap E_g of around 1.8-2.4 eV and room temperature resistivity of order of 10^7-10^{11} Ωcm [59, 62, 148, 155, 232]. The presence of water moisture was observed to decrease the E_g value [62, 148]. In AC measurements, it was observed that the AC conductivity increased sharply with the frequency, which suggests that the conductivity has an electronic origin (e.g. proton-tunneling as discussed in [155]) and thus not simple due to ionic conduction.

DNA films and networks

In 1998, Okahata *et al* observed anisotropic conductivity in the aligned DNA cast films [193, 194]. It was observed that if the film was aligned so that long DNA molecules (from Salmon) in the film were aligned perpendicular to the two electrodes (thus bridging the electrodes) relatively high current was observed, whereas in the case of molecules aligned in parallel to the electrodes very small current was observed. This suggests that the current is mediated by the DNA. In the later work by the same authors, they observed temperature dependence of the conductivity of the DNA films and also found lower conductivity for the film which contained DNA molecules shorter than the separation between the electrodes [182].

In 2000, de Pablo *et al* spread λ-DNA on a mica surface and deposited a gold electrode to cover parts of the molecules lying on the surface [197]. A conductive AFM tip was used as another electrode to contact the uncovered parts of the molecules. They did not observe any conductivity.

Cai *et al* also used the conductive AFM to determine the conductivity of networks made of poly(dA)-poly(dT) or poly(dG)-poly(dC) DNA [39]. The better conductivity was found in the case of poly(dG)-poly(dC) and suggested that it could be used as a semiconducting nanowire. These results clearly contradicted with the observations of Pablo *et al*.

Single molecules or bundles

Since the bulk DNA measurements do not exactly probe the conductivity along a single double helix, the measurements using individual DNA molecules were desired. In took until late 1990's, beyond the development of fine processing techniques like electron-beam lithography and probe microscopies such as scanning tunneling microscopy (STM) and atomic force microscopy (AFM), before the conductivity measurement on single molecule level could be realized.

In 1998, Braun *et al* were the first to measure a conductivity of individual DNA molecules by using 16 μm long λ-DNA stretched on the glass surface and connected to two 12 μm separated gold electrodes using the thiol-groups (in 5'-ends of different strands) [32]. They found no significant conductivity of DNA.

In 1999, Fink and Schönenberger bridged a hole in a gold coated carbon foil with a bundle of few λ-DNA molecules and measured the conductivity between the foil and a tungsten micro-manipulation tip attaching DNA in vacuum [67]. They observed that DNA was a good conductor. However, all the measurements were performed during the low-energy electron point source (LEEPS) imaging, which can induce a carbon hydride contamination layer around the DNA leading to a similar I-V characteristics [197].

In 2000, Porath *et al* trapped a 30 bp poly(dG)-poly(dC) dsDNA between suspended 8 nm separated metal nanoelectrodes using a DC dielectrohoresis (see Ch.

5) and observed semiconducting behaviour [207]. The contact resistance between the metal electrodes and the DNA containing no specific attachment group is not known, which can also cause semiconducting characteristics of the obtained I-V curve.

In 2001, Storm *et al* [234] performed an intensive study using two different DNA, i.e., a sequence from λ-DNA and a homogeneous poly(dG)-poly(dC), and various substrates and electrode separations, i.e., 40-500 nm. In contradiction with the earlier work by the same group [207], no conductivity was observed in any of the samples. However, here the DNA was lying on the substrate.

Ratikin *et al* measured bundles of λ-DNA using suspended electrodes and found semiconducting behaviour of B-DNA with a few hundred meV band gap at room temperature and an ohmic behaviour of M-DNA (see 'Doping of DNA' in Sec. 2.3.4) [211].

The most controversial results were obtained by Kasumov *et al*, who observed that λ-DNA, extended between 0.5 μm separated rhenium/carbon (Re/C) electrodes, was a conductor and observed a proximity induced superconductivity below the superconducting transition temperature of Re/C film ($\sim$1 K) [121].

Yoo *et al* used a method similar to Porath *et al* to trap poly(dA)-poly(dT) or poly(dG)-poly(dC) DNA between nanoelectrodes with 20 nm separation [272]. They found, using field-effect doping, that poly(dA)-poly(dT) exhibits n-type semiconducting behaviour, while poly(dG)-poly(dC) act as a p-type. In a later work by the group of Tomoji Kawai, the doping of DNA films was intensively studied. They showed using poly(dA)-poly(dT) or poly(dG)-poly(dC) DNA films that the electrical conduction in DNA can be enhanced using oxygen hole doping [139]. One other possible way to increase the DNA conductivity is so-called 'photo-doping', which means the transfer of photo-excited electrons [83, 84].

Watanabe *et al* used a three probe AFM to measure a single salmon DNA molecules deposited on a glass surface [256]. Two MWCNTs were used as a drain and source electrodes for DNA and a third electrode, acting as a gate, was a SWCNT attached to the AFM tip. They found semiconducting behaviour with the voltage gap of about 2 V, which was significantly reduced when the gate voltage was applied. In later studies by Shigematsu *et al*, the same technique was used to measure the electric properties of DNA with injected carriers applied by a field effect transistor (FET) arrangement and a chemical doping [226]. They observed that charge injection into the DNA increases its conductivity.

In 2002, Zhang *et al* used fluid flow to stretch the λ-DNA, which contained thiol-modified bases for attachment, between 4 or 8 μm separated gold electrodes [277]. They did not observe significant conductivity.

Hwang *et al* observed nearly linear I-V characteristics in experiments where 60 bp poly(dG)-poly(dC) DNA was deposited in 20 nm nanogap [110, 111, 112, 113].

Heim *et al* used conducting AFM and SiO_2 surfaces chemically treated using various silanization agents. They observed the λ-DNA to exhibit different thickness

depending on the surface treatment, but did not observe conductivity in either case [93].

Very recently, Legrand *et al* observed insulating behaviour of a single DNA in aqueous environment placed between gold nanoelectrodes with 70 nm separation using optical traps and submicrometer beads linked to both ends of the DNA [140].

The conductivity of individual DNA molecules thiol-anchored between gold nanoelectrodes has been characterized also in this Dissertation (see Ch. 6) [2].

Humidity effects

In 2002, the group of Tomoji Kawai observed that the resistance of poly(dG)-poly(dC) films decreases dramatically with the increase of relative humidity of the environment [83, 196]. They also showed by using impedance spectroscopy (AC measurements) that the dominant conduction mechanism is not due to an electron transport but to an ionic conduction through water layers under atmospheric conditions [240].

Ha *et al* observed the exponential dependence of a conductance of DNA assemblies on the relative humidity in and explained it in terms of the ionic conduction through the hydration layers around DNA. They also observed that a poly(dG)-poly(dC) specimen was more sensitivity to the relative humidity giving smaller activation energy for the ionic conduction than the poly(dA)-poly(dT) specimen. Kleine *et al* observed a strong humidity dependence in the conductivity in the sample containing individual λ-DNA molecules and attributed it to the capillary condensation of water to the DNA molecules causing ionic conduction [129].

Recently, Kleine-Ostmann *et al* used herring DNA spotted to a 100 nm nanogap and found exponential increase of the conductivity with increasing humidity, identical for single- and double-stranded DNA [130]. The results was explained by water molecules accumulating to the phosphate backbone.

The effect of humid environment on the conductivity of individual DNA molecules has also been studied in this Dissertation (see Ch. 6) [2].

Single-stranded vs. double-stranded DNA

In 2003, Hartzell and colleagues used AC DEP to capture λ-DNA between 8 μm spaced gold electrodes [88, 89, 233]. The double-stranded DNA was modified with thiol-groups either at the both ends of the same strand (5′ and 3′ ends) or at 5′ ends of the opposite stands of the dublex [89]. They did not observe difference in the conductivity between these configurations, which suggests that the charge transfer is not due to the DNA backbone. The resistance of the samples was of the order of GΩ. They also studied nicked and repaired λ-DNA and observed close-to-linear I-V characteristics in the case of repaired DNA and semiconducting type of characteristics in the case of the nicked DNA, with an energy gap of $\sim$3 eV [88]. To further

evaluate the influence of the double helical structure, they measured the I-V characteristics of dsDNA versus ssDNA molecules and observed about 50 times smaller current in the case of the ssDNA which suggests conductivity being sensitive to the base stacking [233].

The electrical properties of single- and double-stranded DNA has been compared also by using microwave resonators [34, 35]. These experiments showed that dsDNA is conducting better than ssDNA, which suggests that the current is indeed transferred via 'π-way', through the base stack. In contrast to the previous results, Kleine-Ostmann *et al* did not observe difference in the conductivity of single- and double-stranded DNA [130]. In this context, to be able to truly determine the electrical properties of the dsDNA, it is critical to preserve its perfect double-helical structure, since even small deformations deteriorates the π-orbital overlap between the bases.

Temperature dependence

In 2005, Iqpal *et al* used a 18 bp thiol-modified dsDNA covalently attached to a gold nanogap break-junction and observed a dramatic decrease in the conductance when temperature was raised from 300 to 400 K, possibly related to complete or partial denaturing of the dsDNA. They also observed that the dc resistance of dry DNA strands of the same length decreases with increasing G-C pair content in the sequence. The observed values ranged from 10 MΩ to 2 GΩ [116].

Recently, Yun *et al* studied the humidity and temperature effect on the conductance of DNA-linked Au nanoparticle aggregates [273]. They observed anomalous temperature dependence in the conductivity, which is probably related to the denaturation of the DNA-linkages.

Scanning tunneling microscope measurements

A reproducible scanning tunneling microscope (STM) measurement technique was first described by Cui *et al* in 2001 [50], when the conductivity of alkane-thiol molecules was measured. Measurement setup contains a gold surface covered with the molecules containing the thiol-linker group in the both ends. The gold surface is used as one and the gold STM tip as another electrode. In each single measurement, the gold STM tip is brought into contact with the surface, so that the molecules can attach to the tip, and then slowly taken up while simultaneously measuring the conductance. The histogram of the numerous repeated conductance measurements reveals peaks at an integer multiples of the fundamental conductance value, which is interpreted as the conductance of a single molecule. Xu *et al* used the same method to study the conductivity of short thiol-modified dublexes in aqueous solution [265]. They used two series of DNA sequences, a 5'-$(GC)_n$-3'-$(CH_2)_3$-SH with n = 4, 5, 6 and 7 (8-14 bp) and a 5'-CGCG$(AT)_m$CGCG-3'-$(CH_2)_3$-SH with m = 0, 1, and 2 (8-12 bp).

The obtained conductance depended on the sequence and the length. For the $(GC)_n$ sequence, the conductance was inversely proportional to the length, whereas in the case of adding AT base pairs (m) in between the CG-domains, the conductance was exponentially decreased.

Hihath *et al* used the same technique to study a single-nucleotide polymorphisms (SNP), i.e., the recognition of the occurrence of mutations in the base-stack [99]. 11 and 12 bp dsDNA were used to investigate the change in the conductance in the cases of a single base, or two separate bases in the stack, being modified. They showed that a single base mutation in dsDNA can cause a significant change in the conductance and thus the method may be used for SNP analysis.

Nogues *et al* used STM and gold nanoparticles to study the conductivity of a short dsDNA [48, 191]. In this method, a ssDNA was adsorbed onto a flat gold surface while the complementary strand was chemisorbed onto the gold nanoparticle. The final structure is formed through the hybridization of the complementary strands. The adsorption of a ssDNA monolayer at each gold interface eliminates non-specific interactions of the dsDNA with the surface, allowing the bridge formation only by hybridization. They found that DNA is a wide band gap semiconductor and passes significant current outside the voltage gap.

Xu *et al* used ultra high vacuum scanning tunneling microscopy/spectroscopy (UHV-STM/STS) to measure 12 bp thiolated poly(dG)-poly(dC) DNA molecules and observed wide band gap semiconducting behaviour also [266].

Indirect measurements

Various indirect methods have also been used to investigate the DNA conductivity. In microwave frequency resonator studies λ-DNA was found to be a good ionic conductor at low temperatures [34, 35, 242]. The insulating behaviour was found in the electrostatic force microscopy (EFM) [29, 77, 143] and in the point-contact current imaging AFM (PCI-AFM) [241].

Nakamae *et al* observed in the magnetization studies that λ-DNA in the B-form exhibits a paramagnetic behaviour below 20 K whereas, in the A-form, it remains diamagnetic down to 2 K [181]. Due to this interplay between the molecular structure and the magnetic properties of DNA they proposed that the paramagnetism of the B-DNA originates from the overlapping π-orbitals. A finite magnetic dipole moment may be induced by intra- and interstrand (across the hydrogen bonds) transfer of π-electrons on bases, which suggests the existence of a long range coherent transport in B-DNA at low temperatures.

2.3.4 Remarks on conductivity measurements

The results obtained from the DNA conductivity studies (described in Sec. 2.3.3) varies from insulating [29, 32, 77, 86, 93, 129, 139, 140, 143, 196, 197, 234, 240, 241, 266,

277] via wide-bandgap semiconducting [48, 83, 84, 182, 191, 193, 194, 207, 226, 256] to ohmic (or nearly ohmic with small activation gap) [39, 67, 88, 89, 99, 110, 111, 112, 113, 116, 211, 233, 242, 265, 272, 273] or even to truly metallic behaviour [121]. This is the case, since it is very difficult to obtain reproducible and reliable results from the experiments with nanoscale molecules, which can be easily damaged. Also, there are numerous experimental variables such as the measurement method, the environmental conditions, the buffer used, the molecule-electrode contact and the DNA length, sequence and conformation. Since the importance of the most of these parameters have been realized only in later experiments and also due to the fact that most of the results are reported in the short format letter-type journals, the publications do not often contain sufficiently experimental details to be able to reliably evaluate and compare the results.

Humidity induced conductivity

Since the results of the DNA conductivity measurements have remained controversial, the mechanism of the conductivity (observed in some cases) is still unclear. It has been observed that the relative humidity of the environment highly affects to the observable conductivity of DNA samples [34, 35, 83, 86, 129, 130, 196, 240, 241], which may explain some of the controversy, since the used environmental conditions vary from a vacuum to a high humidity. Also in the case of DNA films [83, 182, 193, 194, 196, 240], which can contain some hydrated water around the DNA, the ionic conduction may take place. The impedance spectroscopy can be used to distinguish the electronic conductivity from a simple ionic conduction, i.e., the contribution of water and ions.

Even if the increase in the conductivity with the increase of humidity observed in the recent experiments was related to ionic conduction, it does not exclude the contribution of DNA, which may function, e.g., as a water gathering substrate due to formation of the hydration layer. It has been proposed that the ac conductivity of DNA originates from dissipation due to the collective motion of water dipoles in the surrounding water layer around DNA [34, 35]. One other option is, that deformed helical structure (diminished π-stacking) of dried DNA can be recovered when relative humidity of the environment is increased (shown by STM-imaging of DNA in different humidities [275]), which can increase the DNA conductivity.

Interactions with the substrate

In most of the cases where DNA was found totally insulating, the molecules were in contact with the untreated substrate, which causes deformations to the helical structure deteriorating the possible conductivity [32, 77, 86, 129, 140, 197, 234, 241, 277].

In the later studies by Kasumov *et al* [120], it was argued that the interactions between the molecules and the substrate can strongly deform the double-helical structure of the DNA, which can cause the insulating behaviour observed in several experiments. They observed that single DNA molecules deposited on a mica surface, which was treated with pentylamine vapour (containing NH_3^+ molecules), maintain their nominal thickness of about 2.4 nm, whereas on the untreated substrate the thickness of the DNA shrinks down to about 1 nm (this has been observed also in this Dissertation work). Heim *et al* studied the thickness of DNA molecules deposited on SiO_2 surfaces treated with silanization agents containing different terminal-groups [93]. They found the highest thickness of about 1.6 nm when using a hydrophobic methyl-terminated octadecyltrichlorosilane (OTS) treated surface.

Heim *et al* also suggested that the interplay between charge localization/delocalization and different deposition techniques may explain the reported transport results ranging from insulating to conductive [94]. In the electrostatic force microscopy (EFM) studies they observed that a presence of spermidine during the deposition leads to relaxed DNA molecules exhibiting a charge delocalization over micrometers. It was suggested that the spermidine protects the helical conformation of the DNA, by reducing the molecule-surface interactions.

DNA structure

There is a large variety of lengths and base sequences of DNA used in the experiments, which may have a crucial effect on the results. For instance, it was observed that the rate of the charge transfer decreases exponentially with the length of the molecule (see Sec. 2.3.2). Biological sequences like λ-DNA have no clear periodicity, which leads to a disorder along the one-dimensional molecule and diminishing of its conductance. Homogenous sequences such as poly(dG)-poly(dC) and poly(dA)-poly(dT) provide the best condition when considering the π-orbital overlap, but their hybridisation is not specific since the sequence is regular. Also the supramolecular stucture of the molecules, e.g., a DNA bundle vs. a single molecule, may affect the conductivity.

In addition to the charge transfer studies, it has been observed also in the conductivity measurements, that the structural integrity of the dublex has a significant effect on the electrical properties of the DNA [88, 89, 233]. It was shown in the STM studies, that even a single base pair mismatch highly decreases the electrical conductivity of a short dsDNA ($\sim$10 bp) [99, 266].

Also the sample treatment is important, since DNA can be easily harmed, e.g., when the DNA is deposited on the substrate and dried using N_2 flow, it looses most of its hydration water layer and becomes completely deformed [250]. Zareie *et al* have shown by the atomic resolution STM studies that the conformation of a B-DNA on a surface changes along the environmental humidity [275].

Doping of DNA

It has been demonstrated in some cases that DNA conductivity can be enhanced with doping, e.g., using oxygen [139], photon [83, 84, 193, 194] or field-effect doping [256, 272]. Also the use of different type of counter-ions may affect to the conductivity of the DNA, e.g., it has been proposed that Mg^{2+} ions may dope unoccupied π^* states, leading to the possibility of the electron doping of DNA [64]. The water and the counter-ions may also create impurity states to the main π-π^* energy gap, thus doping the DNA [64]. Also the contribution of the positive counterions to the electrical conductivity via gating effect has been suggested [18].

One interesting approach to increase DNA conductivity is a so-called M-DNA, which is formed from a B-DNA by replacement of the amino protons of Guanine and Thymine by the divalent metal ions, e.g., Zn^{2+}, Co^{2+} or Ni^{2+}, at the high pH environment [10]. Ratikin *et al* demonstrated that a semiconducting B-DNA can be changed to an ohmic M-DNA [211]. The fact that the M-DNA is better conducting than the native B-DNA has also been shown using electrochemical impedance spectroscopy [153].

The molecule–electrode contacts

Obtaining of an electrical contact between the molecules and the metallic electrodes is one of the challenges of molecular electronics, and it is suggested to be a major reason for the wide variation of the reported DNA conductivities [100]. In ideal case, the contact between molecule and the metal electrode should be ohmic, so that its non-linearities do not affect to the observed I-V characteristics, and also the resistance should be as low as possible to ensure that the contact is not limiting the electron transport through the molecule. In the case of molecules, whose electronic structure is different from the metals, a simple physical contact, such as a DNA molecule is lying on the electrode surface, do not offer an adequate electrical contact.

An electrical contact may be obtained by using a chemical bonding between the molecule and the electrodes, which is usually done by using sulphur (thiol) or selenium bonding with gold, silver or platinum [100]. As mentioned above, Cui *et al* demonstrated a reliable and repeatable conductance measurement of the single octanedithiol molecules by using the STM 'dipping' technique and the chemical (almost covalent) sulphur-gold bonding in molecule-electrode contacts.

Very recently, a novel metal-carbon bonding has been utilized in the fabrication of monolayer-protected metal (Au or Pt) nanoparticles [172]. It was observed that metal-carbon bond is stronger than metal-sulfur or metal-nitrogen bond and providing an enhanced chemical stability. Also, the formation of a covalent bond between an individual pentacene molecule and a gold atom has been demonstrated using STM [212].

In the case of DNA, the thiol-modification can be used for chemical bonding

[92]. However, commercially available DNA-modifications contain an alkane-chain spacer between the thiol-group (i.e. -SH) and the DNA backbone [6]. The shortest linkers for 5′ end contain C6 (alkane chain with six carbons) and for 3′ end C3 chain, which are both highly resistive [23, 264]. In addition, the linkers are connected to the sugar-phosphate backbone, which is also supposed to have high resistance [34, 233]. An optimal linker for the DNA conductivity measurements would be (1) conducting, e.g., composed of conjugated polymers, and (2) directly connected to the π-stack (to the base nearest to the electrode). For instance, Zhang *et al* used thiol-groups attached directly to the Thymine bases in 5′ ends of the λ-DNA [277]. They observed insulating behaviour of DNA, which may however be due to the use of very long ($\sim$16 μm) molecules or the deterioration of conductivity of the molecules by the interactions with the quartz substrate. Also the thiol-modified Thymine was directly linked to the gold surface (without spacer in between), which may harm the B-helical conformation of the nearest part of the DNA.

It has been shown that the sulphur-gold bonds are present in both physi- and chemisorbed states [247]. Due to this, before immobilization of DNA to electrodes one has to take care that thiol-linkers in the end of the DNA are in such condition that they can chemically attach to the gold surface, and not only physically adsorb to the surface. For instance, some thiol-modifications contain a protection group [6], which must be removed using a reduction agent, e.g., TCEP-HCl (Tris(2-Carboxyethyl) Phosphine and Hydrochloride) [38, 191], prior to immobilization. Another possibility is that the DNA molecules containing thiol-groups in both ends form multimers by bonding to each other via S-S bridge formation. This can also be prevented by using a reduction agent. Also the gold surface must be cleaned from any organic residues before the immobilization of DNA, e.g., using a piranha solution [191] or oxygen plasma cleaning.

When using the thiol-linkers in electrical measurements, relatively low bias voltages ($\leq$0.7 V) should be used. This is because the sulphur may be electrostatically released from the gold by reduction reaction within aquatic solution [237, 247]. The release of the thiols may be avoided by using a solution without water, that is, however, not convenient in the case of DNA.

Even the charge migration in DNA has been widely studied using the DNA molecules of different length and sequence, and by applying numerous different methods the consensus has not been found. However, based on these experiments, significant remarks have been made concerning, e.g., the fragility of the helical conformation of DNA under variant environmental conditions and the significance of the molecule-electrode contacts. In this Dissertation (see Ch. 6), we tend to further clarify these ambiguous areas of the DNA conductivity research.

3 Dielectrophoresis

3.1 Theory of dielectrophoresis

3.1.1 What is dielectrophoresis?

Dielectrophoresis (DEP) means the translational motion of matter caused by the polarization effect in an inhomogeneous electric field [206]. DEP phenomenon results from the electric field gradient which induces a force on any polarizable particle, neutral or charged. The principle of DEP is represented in Fig. 3.1.

An external electric field induces surface charges on the polarizable object, yielding a positive charge on one side and the negative (of the same magnitude) on the opposite side. The Coulomb interactions between the surface charges and the electric field induces forces, acting on the opposite directions on the different sides of the object. In an uniform electric field these forces averages to zero and no translational effect occurs in the case of neutral object, as shown in Fig. 3.1(a). However, in the case of an inhomogeneous electric field, as shown in 3.1(b), the field density is higher on the right side of the object, yielding a net force towards the field gradient acting on an object. In the case of a charged object, in addition to the dielectrophoretic force, there is also an electrophoretic force, which exists both in the case of homogeneous and inhomogeneous electric field, originating simply from the Coulomb interactions.

In the simplified picture of DEP described above, the effect of a surrounding

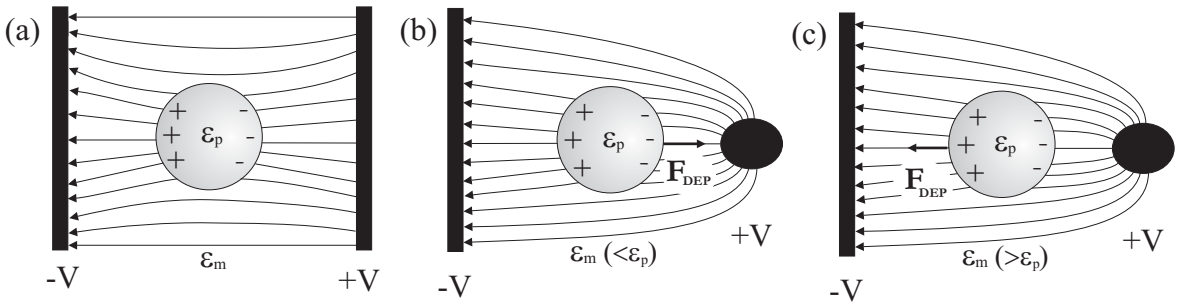

FIGURE 3.1 The principle of a dielectrophoresis (DEP). (a) No net force is acting on a neutral polarizable particle in a homogeneous electric field. In the positive DEP (b), the particle, polarized by the inhomogeneous electric field, feels the force towards the field maximum, and in the negative DEP (c) towards the field mimimum.

medium was neglected. In the general case the polarization of the medium should also be considered. According to an effect of the surroundings, DEP can be divided into two classes: positive and negative DEP. In the positive DEP, the object itself has a higher polarizability than the surrounding medium and it is pushed towards the higher electric field, as shown in Fig. 3.1(b). Whereas, if the medium has a higher polarizability than the object, the object is pushed towards the decreasing field strength, resulting in a phenomenon called negative DEP, which is shown in Fig. 3.1(c).

3.1.2 Dielectrophoretic force

A dielectric particle and its surrounding medium in the electric field $\vec{E}$ can be considered as an effective dipole which has an induced dipole moment $\vec{p}$, that is proportional to the electric field [107, 117], i.e.,

$$\vec{p} = \alpha \vec{E}. \tag{3.1}$$

The constant $\alpha = \alpha(\omega, r_{\mathrm{p}})$ is the effective polarizability of the object, which depends on the angular frequency of the electric field ω, the diameter of the particle r_{p} and the electrical properties of both the particle itself and the surrounding medium. Polarizability of a particle of volume V with a permittivity ϵ_p is

$$\alpha = 3V\epsilon_m Re[K], \tag{3.2}$$

where Re denotes real part, and K is so-called Clausius-Mossotti factor, which depends on both the particle and the medium, and is described by [281]

$$K = \frac{1}{3}\frac{\epsilon_p^\star - \epsilon_m^\star}{\epsilon_m^\star + A(\epsilon_p^\star - \epsilon_m^\star)}. \tag{3.3}$$

In Eq. 3.3, A is a geometrical factor, which varies so that, e.g., $A = \frac{1}{3}$ for a sphere and $A \approx 0$ for a rod-shaped object. The complex permittivities of the particle and medium, $\epsilon_p^\star$ and $\epsilon_m^\star$ respectively, are described by

$$\epsilon_p^\star = \epsilon_p - i\frac{\sigma_p}{\omega} \tag{3.4}$$

and

$$\epsilon_m^\star = \epsilon_m - i\frac{\sigma_m}{\omega}. \tag{3.5}$$

In these equations, ω is the angular frequency of the applied field, ϵ_p and ϵ_m are the real parts of the permittivities, and σ_p and σ_m are the conductivities of the particle and the medium, respectively.

In the presence of a non-uniform electric field, the force acting on the particle

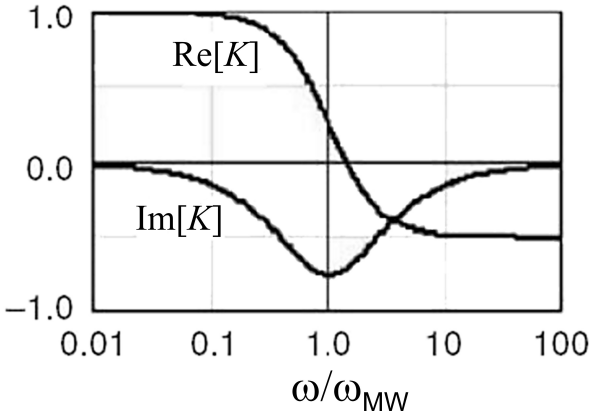

FIGURE 3.2 Frequency dependence of Clausius-Mossotti factor for a spherical particle ($A = \frac{1}{3}$) exhibiting a single dielectric dispersion (from positive to negative DEP) at frequency $\omega_{MW} = (\epsilon_p + 2\epsilon_m)/(\sigma_p + 2\sigma_m)$. $K(\omega = 0) = 1$ and $K(\omega = \infty) = -0.5$.

is termed as a dielectrophoretic force $\vec{F}_{\mathrm{DEP}}$ and is given by

$$\vec{F}_{\mathrm{DEP}} = (\vec{p}\cdot\vec{\nabla})\vec{E} = \frac{\alpha}{2}\vec{\nabla}(E^2). \tag{3.6}$$

For instance for an isotropic homogeneous spherical particle with radius r_{p}, the time-averaged dielectrophoretic force is

$$\vec{F}_{\mathrm{DEP}} = 2\pi\epsilon_m r_{\mathrm{p}}^3 Re\left[\frac{\epsilon_p^\star - \epsilon_m^\star}{\epsilon_p^\star + 2\epsilon_m^\star}\right]\vec{\nabla}(E^2), \tag{3.7}$$

where $E = E_{\mathrm{RMS}}$ is a root-mean-square value of the electric field (assuming a sinusoidal time dependence).

As seen from the Eq. 3.3 Clausius-Mossotti factor K is a frequency dependent variable, with real part varying from -0.5 to +1. When $Re[K] > 0$, the particle experiences the positive DEP, whereas, when $Re[K] < 0$, the particle experiences the negative DEP. The imaginary part $Im[K]$ varies from -0.5 to 0, which is an important factor in an electrorotation where a polarizable object tends to orient with respect to the field lines [37, 107]. A linear analogue to the electrorotation is so-called traveling-wave DEP (TWD), where a motion of the particle in an inhomogeneous ac electric field arises not only from a non-uniformity of the field magnitude ($\vec{\nabla}(E^2_{\mathrm{RMS}})$) but also from a non-uniformity of the field phase [37, 107]. An example of a frequency dependence of the Clausius-Mossotti factor is shown in Fig. 3.2.

Several notifications about the Eq. 3.7 should be made.

- By changing the frequency of the electric field, the Clausius-Mossotti factor can change from positive to negative, which causes the DEP force on the particle to change its direction accordingly. This unique property of Clausius-Mossotti factor of the particle under a specified suspending medium can be utilized to manipulation of particles.

- The DEP force is proportional to the size of the particle, which possess a challenge for the manipulation of nanoscale particles. However, the equation is derived using classical description of permittivity and conductivity, which are derived as bulk values, and may thus not be exactly valid in the case of nanoparticles or macromolecules, where a significant fraction of the atoms of the object reside on the surfaces. Moreover, charged objects can contain so-called counter-ion cloud formed around the object, e.g., in the case of DNA, which can have a significantly affect to the DEP. Thus, the applicability of this model to single molecules may not be quantitatively valid.

- Consequently, the direction of the DEP force does not depend on the direction of the electric field, since the field gradient causes the force on the particle, not the field itself. In the case of ac field, the particle experiences time-varying force, but the direction of the force is always the same, even though the direction the electric field vector is changing in time. Thus, it is sufficient to consider only a time-averaged values as done in Eq. 3.7. Consequently, even the equation represents the DEP force in the case of an ac electric field, it is valid also for a dc electric field.

- Sometimes the dipole approximation is not accurate enough and higher order multipoles have to be considered. However, the general solution for multipoles has also been obtained [251].

To be able to trap particles using DEP, the DEP force must overcome the Brownian motion, which can be treated as a random force, i.e., so-called drag force, whose maximum value is given roughly by [206]

$$F_{thermal} = \frac{k_B T}{2 r_{\mathrm{p}}}, \tag{3.8}$$

where k_B is the Boltzmann constant, T is the temperature, and r_{p} is the diameter of the spherical particle (assumed). This sets the minimum particle size that can be manipulated using certain DEP force. Since the thermal drag force ingreases with decreasing particle size, a higher DEP force is needed in order to manipulate nanoscale particles. The higher field gradients, which are needed to create a higher DEP force, can be generated by reducing the electrode dimensions or increasing the voltages applied to the electrodes. However, due to the practical reasons, e.g., use of aquatic solution or rigidity of the electrode structure, the applied voltage cannot be increased too much.

There are also several other forces acting on the particle originating from the motion of the solvent under the high electric field [42]. For instance, the Joule heating in the solvent can cause electrothermal forces. Also, the geometry of the electrodes produces a tangential electric field at the electrode-electrolyte double layer

inducing a steady motion of the solvent, which is termed as electro-osmosis. These forces may also limit the manipulation of the particles using DEP.

3.1.3 Dielectrophoretic potential

One can also define the DEP potential energy for polarizable uncharged molecules in an applied electric field $\vec{E}(\vec{r})$ as

$$U_{\mathrm{DEP}}(\vec{r},\omega) = -\frac{1}{2}\alpha(\omega, r_{\mathrm{p}})[E(\vec{r})]^2. \tag{3.9}$$

On the other hand, since each degree of freedom gives a contribution $k_BT/2$ to the thermal energy, total Brownian motion is associated with the thermal energy

$$U_{\mathrm{thermal}} = \frac{3}{2}k_BT. \tag{3.10}$$

In the case of neutral particles we obtain for the total potential energy

$$U_{\mathrm{tot}} = U_{\mathrm{thermal}} + U_{\mathrm{DEP}} = \frac{3}{2}k_BT - \frac{1}{2}\alpha[E(\vec{r})]^2, \tag{3.11}$$

which has a minimum at the point of the highest electric field, towards which the particles are driven. In the case of an ac field, the Eq. 3.11 applies also for charged particles, e.g., DNA, since the ac field averaged the electrophoretic forces to zero.

When $U_{\mathrm{tot}} = 0$ in the point of maximum electric field, the trapping begins, which can be used to experimentally determine the polarizability α by determining the minimum electric field needed to trap a certain particle (see Ch. 5).

3.2 Earlier DEP studies

In a pioneering DEP study, Batchelder demonstrated the manipulation of 600 μm steel balls and 1-mm water droplets in heptane [21]. Since then DEP has been successfully applied in many different fields, reviewed e.g. in [37, 107].

3.2.1 DEP of micronscale objects

In the micrometer scale, DEP has been widely used as an active, non-destructive manipulation method for trapping biological objects like eukaryotic [22, 166, 167, 255] and prokaryotic (i.e. bacterial) cells [162, 163], and DNA of different lengths [103], yet, mostly 16 μm DNA of the bacteriophage lambda (λ-DNA) [13, 14, 55, 73, 74, 88, 89, 183, 243, 246, 252, 262, 281].

Since long, thin objects have an enhanced polarizability (as can be seen from Eq. 3.3 when $A \approx 0$), they can be easily manipulated using DEP. Even if the diameter

of a double-stranded DNA is only $\sim$2 nm, long DNA molecules can be considered as micron-scale objects due to the longitudinal polarization of the molecules. This applies also for the DEP of carbon nanotubes [44, 134, 267] and nanowires [37]. One interesting phenomenon resulting from the electrorotation is the tendency of elongated objects to align along the field lines, which can be utilized, e.g., in the case of DNA and carbon nanotubes.

An important application for DEP is the separation of particles by their different polarizabilities. This has been used, e.g., for the separation of metallic carbon nanotubes from semiconducting ones [134].

3.2.2 DEP of nanoscale objects

For fully nanometer-scale objects, in which all dimensions are in nanoscale, the Brownian motion poses a challenge. In nanoscale, DEP has been demonstrated, e.g., for latex beads [82, 108, 176, 178], viruses [82, 109, 178, 221], nanoparticles [26] and proteins [104, 122, 254, 281].

In 1999, Morgan *et al* used DEP to separate a mixture of Herpes Simplex and Tobacco Mosaic viruses into two distinct populations. They also managed to separate the latex spheres of different sizes or of the similar size but a different surface treatment applied on the particles [178].

3.2.3 DEP of DNA

Washizu and co-workers

In 1990, Washizu and Kurosawa showed for the first time that DEP can be used to manipulate DNA [252]. By using a field strength of $\sim 10^6$ V/m and frequencies from 40 kHz to 2 MHz applied to two parallel 60 μm-spaced aluminium electrodes they observed, that individual λ-DNA molecules were trapped and also elongated along the electric field. DNA was chemically bound to the Al electrode (only in one end) and stayed attached, even after the electric field was switched off.

In 1995, the group of Washizu described possible applications of an electrostatic stretching and positioning of DNA [253]. They showed that by measuring the fluorescence intensity of a stretched and positioned DNA as a function of a displacement from the electrode edge it is possible to determine the size-distribution of the DNA sample. Also the nuclease activity, determining how fast the DNA digests, can be measured a similar way. The immobilization of DNA bridge between electrodes where obtained using a floating potential (capacitively coupled) electrode geometry. The use of the floating electrodes was necessary for immobilization of the both ends of the molecule. The reason for that is not known, but it is most likely due to the drag of the molecules induced by the electrohydrodynamic convectional flows being too high near the electrically connected electrodes. The authors also developed

a method to immobilize a stretched DNA molecule to the substrate using biotin-avidin complexes in the both ends of the molecule. Since the avidin contains four binding sites for the biotin, there was a vacant site left for attachment to the biotin-modified substrate. Since the immobilized DNA was still biochemically active, it could be used to study the interactions of the stretched DNA with RNA molecules [119] and proteins [228]. This offers a powerful tool for the biochemical research, in particular to study the regulation and control of a gene expression.

In 1998, the group of Washizu performed a quantitative study of DNA orientation under a stationary ac field by using pUC18 (2.7 kbp plasmid DNA). They measured the dependence of the polarization of the observed fluorescence on the frequency and intensity of the applied electric field, and on the pH and conductivity of the buffer solution, revealing information about elongation and orientation of DNA under an ac electric field. Surprisingly, the obtained polarizability was found several orders of magnitude larger than in the case of a conducting ellipsoid with the same dimension. This observation was explained so that an electrical equivalent diameter of a DNA is $\sim$20 nm, which is comparable to the Debye length, i.e., the thickness of a counterion cloud. They also observed that if the pH increases, an increase in the fluorescence anisotropy was also observed, which is most likely related to the increased dissociation of the phosphate groups, further increasing the amount of counter-ions. These results suggest that the DNA polarization during DEP is related to the counter-ion polarization (alternating distribution of counter-ion along the DNA).

The group of Washizu convincingly showed that the micrometer scale DNA molecules can be elongated along the field lines and immobilized to a desired location using DEP and still the molecules remain biochemically active. The method they described has obvious applications in the future biochemistry and nanotechnology. The work of Washizu's group inspired several other groups to further study the DEP of DNA, e.g., as a function of DNA length and applied signal frequency, as described in the following sections.

DNA DEP in micronscale

In 1998, Asbury and co-workers observed the positive DEP of λ-DNA by using the audio frequency of 30 Hz [14]. The DEP force acting on DNA was estimated to be in femtonewtons range. In contrast to Washizu's group, they did not observe any stretching of DNA, which was suggested to be related to the use of low frequencies. In 2002, the group made a simple microfluidic device in order to study the DEP efficiency. The trapping efficiency was found to decrease with increasing frequency from 5 Hz to 2 kHz [13].

In 1998, Bakewell and co-workers demonstrated the application of DEP to the manipulation of an avidin protein and pTA250 DNA (12 kbp plasmid) [17]. Using frequency of 20 MHz, they reported for the first time an observation of the negative

DEP in the case of DNA. In later work, they studied properties of pTA250 using dielectric spectroscopy with frequencies ranging from 200 kHz to 3 GHz [15]. From the dielectric decrement and the relaxation frequencies they determined the frequency dependent polarizability of a DNA molecule. Very recently, they studied the time dependency of the dielectrophoresis of pTA250 DNA, quantifying especially two parameters: the initial DEP collection rate and the initial to steady-state DEP collection transition (the amount of collected DNA) [16]. The values of the parameters exhibited a clear decrease as the frequency increased from 100 kHz to 20 MHz.

In 2000, Porath and co-workers used the dc DEP to trap a 10 nm long poly(dG)-poly(dC) DNA between 8 nm spaced nanoelectrodes in order to measure electrical properties of the DNA [207]. By using such a small gap, small voltages can be utilized to create a strong enough field gradient to realize the trapping without causing the electrolysis in the solvent. A similar technique was used by Yoo *et al*, who trapped about 1 μm long supercoiled poly(dG)-poly(dC) or poly(dA)-poly(dT) DNA into a 20 nm gap [272].

In 2001, Tsukahara and co-workers observed by using a quadrupole electrode geometry and the field strength of $\sim 10^4$ V/m, that DNA (about 40 kbp) underwent the positive DEP for frequencies between 1 kHz and 500 kHz, and negative DEP between 500 kHz and 1 MHz [243]. They did not observe any stretching of DNA.

In 2002, Namasivayam and co-workers used 1 MHz frequency combined with $3 \cdot 10^5$ V/m field strength applied to gold electrodes in order to trap and immobilize λ-DNA containing a 3'-thiol-modification (-SH) in one end (for attachment to gold) [183]. They studied the DEP induced stretching of the molecules as a function of a polyacrylamide (PA) concentration. Already in 1997, Ueda and co-workers had first observed PA assisted DNA stretching (but no trapping) using the field strength as low as 10^4 V/m and frequencies from 0.1 to 100 Hz [246]. After the immobilization of the one end Namasivayam *et al* were able to stretch DNA bridging two 20 μm spaced electrodes. Even the natural contour length of λ-DNA (48 kbp) is $\sim$16 μm, its fully extended length is reported to be as long as $\sim$21 μm, when it is labelled with intercalating dyes such as YOYO-I [204].

Dewarrat and co-workers trapped λ-DNA using an electric field of 10^6 V/m applied to saw-tooth type electrodes containing an underetched gap [55]. They found the most efficient trapping using the positive DEP with the frequencies between 100 kHz and 1 MHz, and observed also partial orientation of the molecules across the electrodes.

In 2003, Germishuizen and co-workers studied the DEP induced stretching of λ-DNA molecules, which were attached to a gold electrode from the other end, as a function of the frequency (from 100 kHz to 1 MHz) of the applied electric field [74]. At the frequencies around 300-500 kHz they observed a maximal elongation of λ-DNA to $\sim$15 μm. In their later work, different size λ-DNA fragments (15, 25, 35 and 48 kb) were used [73]. The maximum elongation, e.g., to $\sim$20 μm in the case

of the 48 kb λ-DNA, was observed between 200 and 300 kHz for all the fragments. They also found that elongation of DNA was only possible in electric fields higher than 0.06 MV/m.

In 2004, Hartzell and co-workers [88, 89] used 1 MHz frequency and $\sim 10^6$ V/m field strength to trap and immobilize (using thiol-groups) λ-DNA between gold electrodes with 8 μm spacing. The success of the trapping was proven by fluorescent confocal microscopy before the subsequent DNA conductivity measurements.

The group of P. J. Burke studied DEP of λ-DNA using quadrupole electrodes with a spacing ranging from 3 μm to 100 μm and applying a field strength of $\sim 10^6$ V/m [281]. The positive DEP was observed for a range of frequencies from 100 kHz to 30 Mhz, whereas below 100 kHz no effect was observed. They also demonstrated the use of a simultaneous low frequency (13 Hz) conductance measurement while applying the high frequency ac signal for DEP (also utilized in this Dissertation work).

So far, there exists two reported observations of the negative DEP in the case of DNA, both performed using the quadrupole electrodes with frequencies from 500 kHz to 1 MHz [243] or 20 MHz [17]. In these experiments, it was possible to observe the negative DEP since the quadrupole electrodes generate a local field minimum in the center, whereas, e.g., in the case of the fingertip electrodes there exist no local minimum. In addition, there may be other experimental details to be tracked, e.g., the solvent used, which might explain the observation of the negative DEP. It has been estimated, by calculating the effective Clausius-Mossotti factor using an ellipsoidal model applied for λ-DNA, that a crossover frequency, where DEP turns from the positive to negative DEP, would be $\sim$6 MHz [281].

In the case of long DNA molecules, i.e., substantially longer than the persistence length of DNA ($\sim$150 bp) [215], their native state in a solution is to be packed to a randomly coiled globular ball. It has been observed in several studies [74, 183, 252, 253], that under high enough frequency and electric field strength (particularly when the electrode separation is larger than the contour length of the molecule) DNA has a tendency to elongate (or stretch) near to its contour length. However, a detailed understanding of the orientation and elongation of DNA as a result of the dielectrophoretic force and torque, has not yet been established.

DNA DEP in nanoscale

In spite of all studies of the DEP of DNA there is only a few successful demonstrations for trapping nanoscale DNA molecules. In 2002, Chou and co-workers used electrodeless traps for the DEP of different size DNA fragments using the field strength of 10^5 V/m and frequencies between 50 Hz and 1 kHz [45]. The microfabricated insulating posts, with constrictions of 1 μm wide and 1.25 μm deep, and external electric field were used in their device to achieve an electrodeless DEP (EDEP). The experiments were done using a single-stranded, i.e., 137-base-long ($\sim$76

nm), and double-stranded, i.e., 368 (∼125 nm), 1137 (∼390 nm), 4361, and 49936 bp, DNA. They found that the DEP force, which was calculated to be ∼1 fN, increased with increasing frequency, which is in contrast to the work by Asbury *et al* [13]. Also a strong increase in the DEP force with the increase of the length of the DNA was found. In this work, the DNA was apparently not stretched at all, most likely because of the constricted geometry and/or the low frequencies used. Later, they proposed that EDEP could be utilized in the Lab-On-a-Chip applications to build 'micro total analysis systems' (μTAS) [46].

In 2004, Ying and co-workers used another type of electrodeless DEP setup for trapping 40-base-long (∼22 nm) and 1-kilo-base-long (∼560 nm) ssDNA, 40 bp (∼14 nm) dsDNA and a single-nucleotide triphosphate (dCTP) inside a nanopipette using frequencies from 0.1 Hz to 10 kHz [271]. The tapered tip of the nanopipette of 100 nm inner diameter was coated with a 5 nm thick gold layer to be used as an electrode for the electrodeless DEP.

Even if the detailed mechanism of the DNA DEP and the dependence on a frequency, an electric field strength, DNA concentration, or pH and conductivity of the solvent are not systematically and quantitatively explained, it has been shown that DNA in an aquatic solution is highly polarizable, which is most likely due to the polarization of the positively charged counter-ion cloud [15, 235, 246]. The DNA DEP has proven to be useful in applications of biochemistry and nanotechnology, e.g., it has been proposed that a pulsed electric field DEP may be used for the size separation of short DNA fragments [184].

The dielectrophoretic trapping of DNA fragments of different size, varying from 27 bp to 8 kbp, has also been studied in this Dissertation (see Ch. 5) [3, 4].

4 Materials and methods

4.1 Nanoelectrode samples

4.1.1 Fingertip nanoelectrode fabrication

Fingertip type nanoelectrodes were composed of two opposing ∼100 nm wide wires with about 100 nm constriction between them. They were fabricated on a thermally oxidized (∼200 nm thick SiO_2) slightly boron-doped (100)-silicon substrate. Polymethylmethacrylate (Microchem C2 PMMA) resist was spin-coated with 2500 rpm and baked for 5 min on a hot plate (160 °C). Patterning was done using an electron beam writer (Raith eLine, equipped with Elphy Quantum 4.0 -lithography software, or LEO 1430+ SEM, equipped with Raith Elphy Plus -lithography software). The resist was developed by immersion to a mixed (1:3) solution of methyl-iso-butylketon (MIBK) and isopropyl alcohol (IPA) for about 30 seconds at room temperature (22 °C). After that the sample was rinsed with IPA and dried with N_2 flow. The evaporation of metals took place in an ultra-high vacuum (UHV) chamber, under the pressure of the order of 10^{-8} mbar during the evaporation. The thickness of the evaporated gold layer was 15 nm, under which 2-5 nm of titanium was used to improve the adhesion of gold.

The fingertip electrode samples were cleaned using short flash of oxygen plasma in a reactive ion etcher Oxford Plasmalab 80 Plus RIE (parameters: 100 sccm O2-flow, 50 W RF power and 1 min time) before the DNA immobilization in order to clean the gold from any organic contaminants which would prevent sulphur to chemically bond with the gold surface. The treatment also changed the originally hydrophobic SiO_2 surface to a more suitable hydrophilic form.

4.1.2 Carbon nanotube electrode fabrication

A diameter of a single-walled carbon nanotube (SWCNT) can be as small as 1 nm, which is about two orders of magnitude smaller than the width of a lithographically fabricated metal electrode (i.e. ∼100 nm). Due to this, CNT may be used as an electrode instead of metal ones to achieve higher electric field gradients, which are needed in dielectrophoretic trapping of very small particles (see Ch. 5), as suggested, e.g., by P. J. Burke [37, 282]. In this work, we have used multiwalled carbon

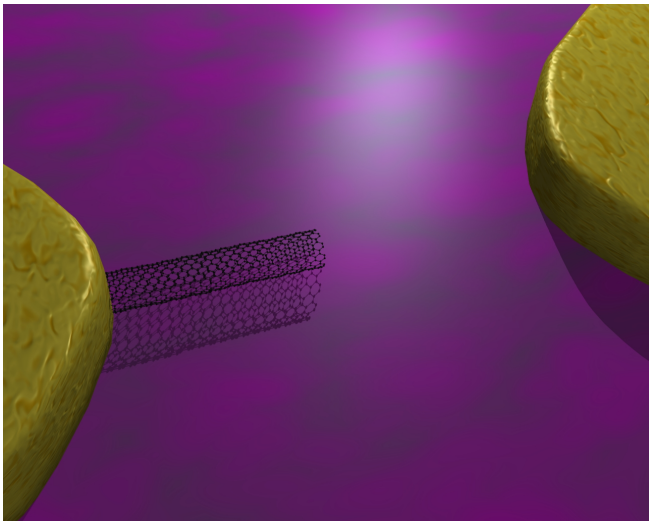

FIGURE 4.1 Schematic view of a single carbon nanotube (CNT) used as an electrode for the dielectrophoresis of DNA [Image by Tommi Hakala].

nanotubes (MWCNTs), which have a diameter of few nanometers, still much less than in the case of metallic electodes.

The nanostructure containing gold electrode as a one and a MWCNT as another electrode (see Fig. 4.1) was obtained by using two-step e-beam lithography with nanoscale pattern alignment and atomic force microscope (AFM) imaging in between [101]. In the first e-beam lithography step, a metallic mark grid was patterned (LEO) on the substrate, i.e., 300 μm thick silicon wafer containing 700 nm thick low-pressure chemical vapor deposition (LPCVD) grown Si_3N_4 on both sides. The grid was fabricated using two layer PMMA resist, i.e., 11 % PMMA in Ethyl Lactate was spinned using 6000 rpm and baked for 2 minutes, and on top of it 2 % PMMA in Anisole was spinned using 3000 rpm and baked for 2 minutes. The resist was developed for 30 seconds in MIKB:IPA (1:2) and 30 seconds in methyl glycol:methanol (1:2), then flushed with IPA and finally He dried. Metallization (5 nm Ti and 15 nm Au) was done as in Sec. 6.1.

A mixture of MWCNTs in powder form, obtained from the research group of S. Iijima [132], was dissolved in 1,2-dichloroethane by diluting and sonicating several times to unravel the intrinsically formed nanotube clumps until the solution was homogeneous. 5-10 drops of the CNT-solution were spun on the substrate using 3000 rpm and imaged using AFM and/or scanning electron microscope (LEO). AFM (Veeco Dimension 3100) was operated in tapping-mode using silicon probes (Veeco MPP-11100), which have the resonance frequency of 300 kHz and the spring constant of 40 N/m.

In the second lithography step, the prefabricated mark grid was used for the stage alignment to make electrical contacts to the nanotubes located by AFM imaging. Metallization was done as above.

4.2 DNA specimens

4.2.1 Fabrication of DNA fragments

For dielectrophoresis experiments, DNA fragments of lengths varying from 27 bp to 8 kbp were fabricated using three different methods: 1) 27 bp fragments – by annealing of synthetic oligonucleotides. 2) 145 and 444 bp fragments – using PCR (Polymerase Chain Reaction). 3) 1065, 5141 and 8461 bp (from now on called as 1, 5 and 8 kbp) fragments – using a restriction enzyme digestion of plasmids multiplied in bacteria. The obtained concentrations were measured spectrophotometrically. All fragments (except 27 bp fragment) were eluted to Hepes/NaOH buffer, i.e., 3 mM Hepes (N-2-Hydroxyethylpiperazine-N'-2-ethanesulfonic acid) and 1 mM NaOH, and stored in a refrigerator in small aliquots.

27 bp fragments were made by mixing stoichiometric amounts of complementary oligonucleotides (TAGC, Copenhagen, Denmark) *Primer1* and *Primer2* (see Table 4.1) in 6.5 mM Hepes buffer (pH 7.0 adjusted with NaOH) and heating the solution to 70 °C for 5 minutes and then cooling it at room temperature. 145 and 444 bp DNA fragments were produced by PCR reaction using TAQ polymerase (Fermentas) with oligonucleotides *Primer3* and *Primer4* or *Primer4* and *Primer5*, respectively, as primers in PCR reaction. The PCR product was subjected to 1 % agarose gel electrophoresis and extracted with GFX^{TM} PCR, DNA and Gel Band Purification Kit (Amersham Biosciences). Chicken avidin complementary DNA in pFastBac1-plasmid (Invitrogen) was used as a template in the PCR reaction [80].

1 kbp DNA fragment were generated by digesting the pBVboostFG plasmid [137] using BglI and SpeI restriction enzymes. 5 kbp fragments were produced by linearizing pFASTBAC1 plasmid (Invitrogen) containing chimeric avidin expression construct [115] using HindIII enzyme. 8 kbp fragments were generated by linearizing pBVboostFG containing modified avidin expression construct [114] using ApaI enzyme. The restriction enzymes were from Promega. Fragments were purified as explained above in the case of PCR products. Plasmids were produced by culti-

TABLE 4.1 The oligonucleotides used as a primers for PCR.

Name	Base sequence
Primer1	5'-GGT GAA TTC GCC GGC ACC TAC ATC ACA-3'
Primer2	5'-TGT GAT GTA GGT GCC GGC GAA TTC ACC-3'
Primer3	5'-CCC GAT GGT CAT GTT GGC GCC CAG ATC GTT GGT-3'
Primer4	5'-CTG CTA GAT CTA TGG TGC ACG CAA CCT CCC C-3'
Primer5	5'-GAG TGA AGA TGA TGA TGC CGA CC-3'
Primer6	5'-HS-$(CH_2)_6$-GCC AGA AAG TGC TCG CTG AC-3'
Primer7	5'-HS-$(CH_2)_6$-TTC TCG ACA AGC TTT GCG GG-3'
Primer8	5'-DTPA-GCC AGA AAG TGC TCG CTG ACT G-3'
Primer9	5'-DTPA-CTT CTC GAC AAG CTT TGC GGG-3'

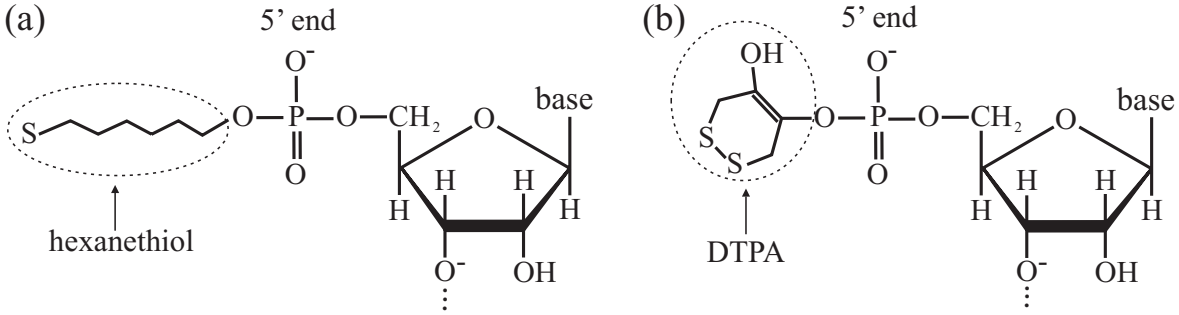

FIGURE 4.2 (a) Hexanethiol- and (b) DTPA-modification in the 5′ end of the oligonucleotide.

vating transformed *E. coli* JM109 cell line (Stratagene) at 37 °C in suspension and isolating the plasmids from overnight cultures by using plasmid purification kit (Macherey-Nagel, Düren, Germany).

4.2.2 Fabrication of thiol-modified DNA

Chemically bonded contacts between DNA molecules and gold electrodes can be achieved by utilizing gold-sulphur bonding [92, 100, 245]. In the DNA immobilization studies two different type of chemical DNA-modifications, i.e., hexanethiol (HS-$(CH_2)_6$) and DTPA (dithiol-phosphoramidite), were used (see Fig. 4.2). Double-stranded DNA containing a modification group in the both ends of the molecule was obtained by using 5′-modified oligonucleotides as primers in PCR (see Table 4.1). Oligonucleotide *Primer6* (purchased from Synthegen, Houston, Texas) was used as a forward primer and *Primer7* as a reverse primer for hexanethiol-modified 414 bp DNA (from now on called C6-DNA). Oligonucleotide *Primer8* (purchased from TAG Copenhagen A/S) was used as a forward primer and *Primer9* as a reverse primer for DTPA-modified 415 bp DNA (from now on called DTPA-DNA). The PCR was done as above in Sec. 4.2.1.

4.3 DEP of DNA *in situ* under confocal microscope

4.3.1 DNA solution for DEP studies

Prior to a labelling and use in DEP studies, the DNA fragments were diluted into Hepes/NaOH buffer, which have pH 6.9 and conductivity 20 μS/cm (conductivity meter, model CDM3, Radiometer, Copenhagen). Low conductivity buffer was necessary to prevent an excess Joule heating of the buffer [42], to reduce the oxidation-reduction reactions at the electrode-solution interface, and to obtain high polarisation of DNA relative to the polarisation of the buffer (lower conductivity induces lower polarisation of the buffer and also the thickening of the Debye layer around

DNA, i.e., counter-ion cloud) [235]. High polarisation is desired, because it increases the dielectrophoretic force as discussed in Sec. 3.1.2.

Unmodified DNA

For confocal microscopy, the DNA was labelled with double-stranded DNA specific fluorescent label PicoGreen (Molecular Probes, Eugene, USA). PicoGreen stock solution was first diluted 1:100 into Hepes/NaOH buffer and then mixed 1:1 with the DNA solution to obtain the final solution, i.e., 1:200 diluted PicoGreen into Hepes/NaOH buffer. The final concentrations of the fragments were chosen so that the concentration of the nucleotides (bases) remains the same in all cases (see Table 4.2). The fluorescent dye molecules attach approximately uniformly along the double helix [283], which ideally results in the same amount of fluorescence in the solutions of DNA molecules of different length. The final concentration of PicoGreen was 1.6 μM yielding a dye to base pair ratio of 1:5 [231].

Thiol-modified DNA

For DNA immobilization experiments performed *in situ* under confocal microscope, 10 nM solutions of C6-DNA and DTPA-DNA diluted into Hepes/NaOH buffer were used. Unlike in the case of unmodified DNA fragments, for thiol-modified DNA the reduction agents were used (in some cases) to break sulphur-sulphur bonds formed between separate DNA molecules and to make thiol-groups more reactive. The reduction agent, either TCEP-HCl (Tris(2-Carboxyethyl)Phosphine and Hydrochloride) or $NaHB_4$ (Sodium Borohydride), was first added to Hepes/NaOH buffer in which the DNA solution was then diluted to and kept about 1 h before the DEP experiment for the reduction to take place. Also, some experiments were performed without using a reductive agent at all. Prior to the experiments 1.6 μM PicoGreen was added as above.

TABLE 4.2 DNA fragments for DEP experiments.

Length (bp)	Modification	c (nM)
8461 (8 kbp)	-	1,0
5141 (5 kbp)	-	1,6
1065 (1 kbp)	-	7,9
414	C6-SH	10,0
415	DTPA	10,0
444	-	19,1
145	-	58,3
27	-	313,4

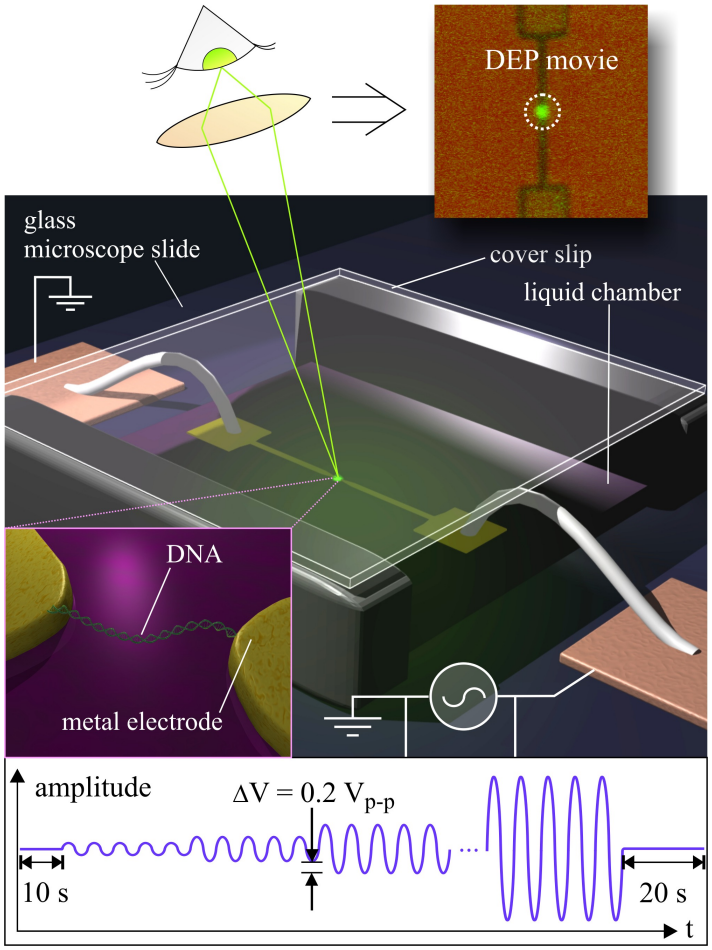

FIGURE 4.3 Schematic view of the experimental setup used in the DEP of DNA fragments *in situ* under the confocal microscope [Schematic 3D images by Tommi Hakala].

4.3.2 Experimental setup for confocal microscope

The DEP studies were performed *in situ* under the confocal microscope (Zeiss Axiovert LSM 510) equipped with an oil objective (Zeiss "Fluar" h 40x/1.3 Oil objective) by (fluorescent) imaging a square area (a 10 x 10 μm^2) around the DEP trap simultaneously with applying of an ac signal (Agilent 33120A waveform generator) to the electrodes used for trapping. The experimental setup is represented in Fig. 4.3. Prior to the DEP experiment, the DNA solution is placed into the liquid chamber between the nanoelectrode sample (described in Sec. 4.1) and the glass cover slip. Argon laser (488 nm) with power of 0.45 mW was used for imaging. Before the actual DEP studies the bleaching tests were performed to confirm that the laser excitation does not cause too much bleaching of the fluorescent dye (see beaching tests in [4]).

Fluorescence data was collected simultaneously using two channels: (1) *fluorescence channel* (containing 505 nm high pass), which corresponds to the amount of

DNA, and (2) *reflection channel* (containing 475-525 nm band pass), which shows the location of the gap between the electrodes since the laser reflects differently from the substrate and the gold electrodes.

To optimize the measurement for obtaining accurate information about the voltage and frequency dependence of the trapping process, especially to exactly determine the minimum voltage for which the trapping of DNA begins (discussed in Sec. 5.2), the detector sensitivity was maximized by fine-tuning the detector gain and the amplification offset according to the fluorescence background of each sample. The background fluorescence level varied quite a lot between the samples most likely because of the variations in the thickness of the DNA solution layer in the liquid chamber, which mostly affects on the *fluorescence channel*, and a possible tilting of the substrate and variations in the SiO_2 layer thickness between the used substrates (pieces of silicon wafers), which mostly affect on the *reflection channel*. This makes the absolute fluorescence values (in arbitrary units) not exactly comparable between the samples, but it was needed to be able to distinguish from the background the very small changes in the fluorescence due to a trapped DNA.

The DEP movies were obtained by capturing two 128 x 128 pixel frames per second (image refresh rate 2 Hz). In the beginning of each DEP movie, the voltage was kept OFF for 10 s, after which the sinusoidal AC signal is turned ON (to a certain starting voltage value). The voltage was raised in ΔV = 0.2 V_{p-p} (0.07 V_{rms}) steps after each 20 s capturing period until the final voltage value was reached (see Fig. 4.3). The final voltage value was chosen while capturing in such a way that when the amount of fluorescence in the 'DEP trap' is so high that the pixels in there start to saturate the voltage is not raised anymore. After reaching the final value, the voltage was turned OFF but the data collection was still continued for 20 seconds to see how DNA diffuses away from the gap.

The amount of the fluorescence which does not diffuse away from the 'DEP trap' after the voltage is turned OFF is interpreted as immobilised DNA, either through the specific chemical sulphur-gold binding in the case of thiol-modified DNA or by non-specific interactions between (unmodified) DNA and the surface, e.g., Coulomb interactions between surface charges on the gold and the negatively charged phosphate groups in the DNA.

4.4 Electrical measurement methods

4.4.1 DNA solution for single molecule immobilization

In order to study electrical properties of the DNA itself, measurements must be done for an individual DNA molecules instead of films or bundles. Here we use DEP to trap and attach thiol-modified DNA, i.e., C6-DNA or DTPA-DNA, bridging the fingertip electrodes. In contrast to the DNA solution made for the DEP studies in

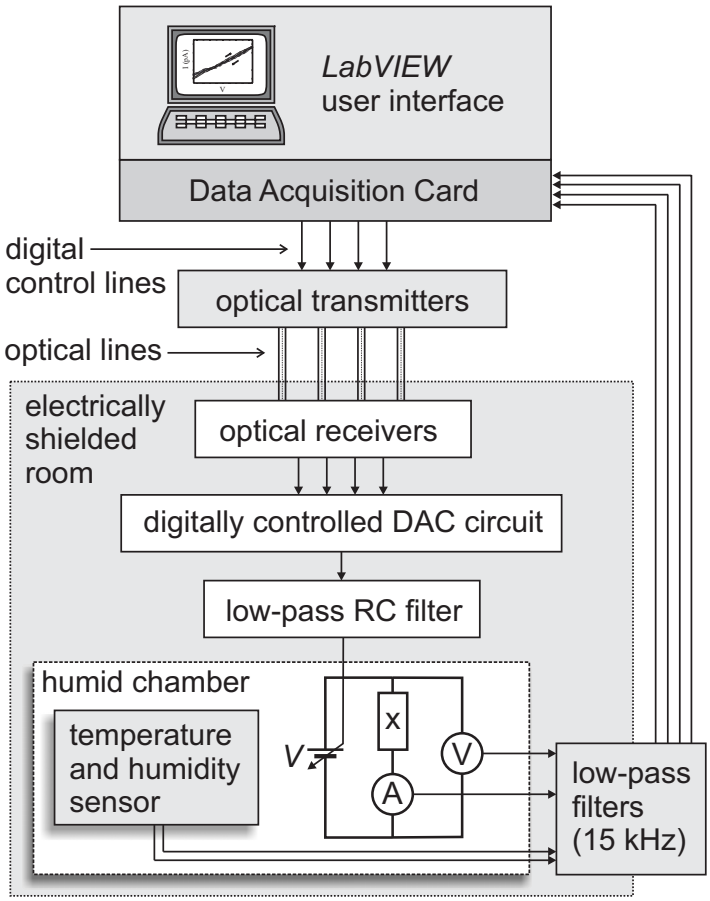

FIGURE 4.4 Schematic view of the measurement setup used to obtain I-V curves from the DNA sample (marked with "x" in the circuit).

Sec. 4.3.1, more dilute DNA concentrations were used in this case to obtain samples containing a single or a few molecules only. DNA was diluted to 6 mM Hepes and 2 mM $NaBH_4$ buffer, which had pH 7 and conductivity 25 μS/cm, so that the final DNA concentration was 1 nM (containing about 1 molecule per cubic micrometer). The DNA solution was exposed to the reduction agent for about 1 hour before the trapping and immobilization using DEP. Also the $NaBH_4$ was added to Hepes buffer just before diluting of DNA to it, so that the reduction agent do not lose its reducing power due to formation of hydrogen gas.

4.4.2 I-V measurement setup

The electrical conductivity measurements were performed inside the electrically shielded room, equipped with highly filtered ($\sim$15 kHz low-pass) feed-through lines for the data acquisition (see Fig. 4.4). The measurement computer outside the shielded room was equipped with a data acquisition card (National Instruments PXI-6251) and LabVIEW 7.1 software (National Instruments) as a user interface.

Current-voltage (I-V) characteristics of the sample were obtained by measur-

ing a number of individual dc current-voltage points. An tunable dc voltage bias was obtained from the battery powered DAC (digital-to-analog converter) circuit (The BNC-output of the RF circuit reported in [244]), which was digitally controlled through the optical lines. A low-pass RC filter (R = 100 Ω and C = 47 μF) was used between the voltage source and the sample to prevent damaging of the molecule or the nanoelectrodes by the high frequency transients. The current (DL Instruments Model 1211) and voltage (DL Instruments Model 1201) low noise preamplifiers were used to amplify the measured signals from the sample, and also to function as a buffer between the sample and the measurement card. The data acquisition and the control of the DAC circuit were done using a purpose-built LabVIEW-program [244].

The humidity chamber was a small metallic box (for electrical shielding also), which included a water container at the bottom in order to increase the humidity inside the box after being closed. Temperature and the relative humidity (RH) inside the chamber were monitored during the measurement using the Honeywell Humidity sensor (HIH-3602-A).

The I-V curves were measured by changing the dc bias voltage inside a certain voltage range in finite steps, which varied from 1 to 10 mV. There was a few second (depending on the sample and the humidity) settling time between a voltage adjustment and the subsequent current measurement. Used voltage ranges varied from $\pm$0.1 to $\pm$1.0 V. The most reliable results were obtained using the $\pm$0.1 V range, which is due to the minimization of the undesired effects such as electrolysis and collecting of contaminant particles from the air. The measurements were performed in room temperature ($\sim$23 °C) and in the relative humidities between $\sim$5 % and $\sim$90 %. Since the normal room humidity is about 30 %, the box was purged with dry N_2 to obtain very low humidity.

4.4.3 DEP Monitoring setup

The desirable way to confirm an attachment of only a single molecule between the fingertip electrodes would be the *in situ* observation of the attachment on single molecule level during the trapping process. In the case of trapping highly conducting molecules or metal particles with DEP, one can monitor the high frequency current flowing through the trapping electrodes and observe an increase in the current when a particle or a molecule is bridging the electrodes. In the case of ac frequencies as high as 1 MHz, the leak currents through the stray capacitances are so large that one cannot reliably observe the attachment of single molecules, especially since they usually have quite high resistance. However, one may use additional low frequency signal and the lock-in technique to distinguish from the high frequency signal at the measurement (used, e.g, by Zheng *et al* [281]).

We have used the lock-in amplifier (Lock-in amplifier SRS-830) to monitor the current through the nanoelectrodes during the dielectrophoretic trapping using the

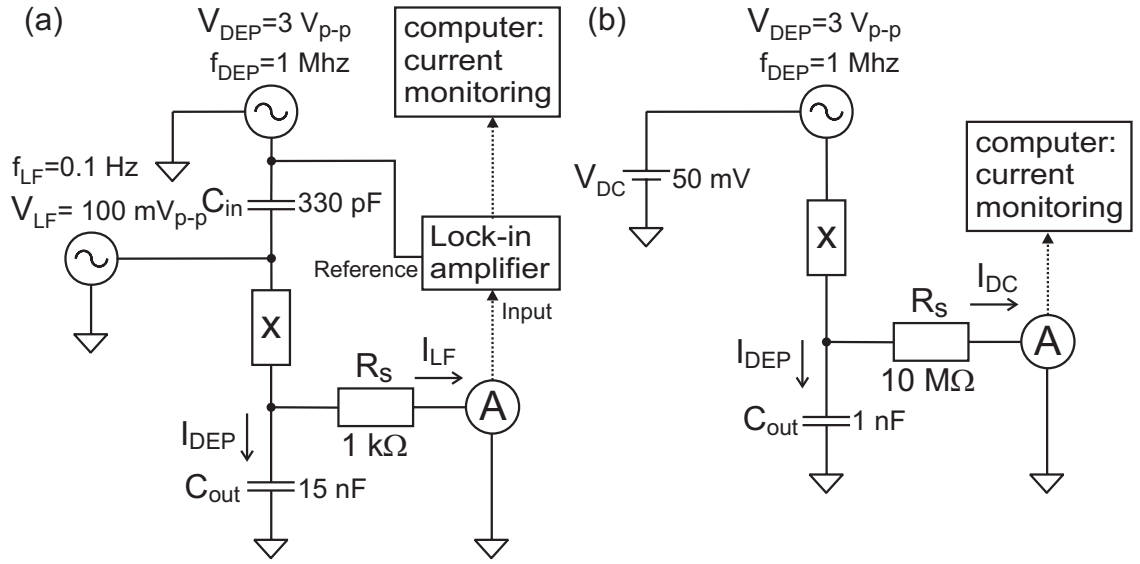

FIGURE 4.5 Schematic view of the DEP monitoring setup. The current between the fingertip nanoelectrodes is measured simultaneously with DEP trapping by using (a) a low-frequency ac signal or (b) dc offset added to the high frequency DEP signal.

measurement setup shown in Fig. 4.5(a). Since the virtual ground of the current amplifier (DL Instruments Model 1211) cannot follow the frequencies higher than ∼10 kHz and causes inconsistent results if the higher frequencies are connected to the current amplifier input, we added the low-pass filter to the circuit before the current meter to separately ground the high frequency signal used in the DEP.

Another possibility is to use a small dc offset added to the high frequency ac signal and filter out (by grounding) the ac signal before measuring the contribution of the dc current using a setup shown in Fig. 4.5(b). It has been observed in DEP studies under confocal microscope that the dc offset of less than ∼1 V added to the DEP signal do not have an observable effect to the DEP process (data not shown here). These two methods has been used in Ch. 6.

4.5 Modeling techniques

4.5.1 Electric field simulations

The finite element method simulations (COMSOL Multiphysics 3.2a) were accomplished to determine the electric field in three dimensions around the used nanoelectrode stuctures. The results obtained from the simulations were utilized in the data analysis in Ch. 5 to determine a polarizability of DNA. To correspond to the real electrodes (described in Sec. 6.1 and 4.1.2) two different electrode configurations were used in the simulations: (1) two fingertip type electrodes or (2) one fingertip type electrode and one CNT-electrode (A schematic view shown in Fig. 4.1). The separation between the electrodes was varied between 100 nm and 1 μm. The fingertip

electrodes were 20 nm high and 100 nm wide and they were lying on top of the substrate. At the simulations the electrode edges were rounded, which corresponds well to the real lithographic results, and the CNT was buried 0.2 nm in the substrate to prevent high transients in the calculations. The diameter of the CNT was chosen to be 2 nm in the simulations, which is an approximation of the diameter of the MWCNTs used in the real samples.

For the 1 μm buffer layer above the substrate, we used the permittivity of water, ϵ_r = 80, which is a good approximation for the dilute Hepes/NaOH buffer which was used in the experiments. Two real electrode configurations were fabricated on the different substrates which are described in the simulations as follows: in the case of the electrode configuration (1), a 200 nm layer of SiO_2 (ϵ_r = 3.6) under which a 800 nm layer of silicon (ϵ_r = 11.8) (see Sec. 6.1), and in the case of electrode configuration (2), a 700 nm layer of Si_3N_4 (ϵ_r = 6.0) under which a 300 nm layer of silicon (see Sec. 4.1.2). The values for the relative permittivities were chosen to correspond to the situation of using a 1 MHz electric field [236]. To find out the contribution of the substrate, the simulations were performed using both of the substrates for each electrode configuration. Because of the much higher ϵ_r of the buffer, the contribution of the substrate material (as long as it is insulating) was very minimal and the electric field above the substrate, which we are really interested in, remains essentially the same.

Since the simulations did not include time-dependency, dc voltage (varying from 0.4 to 4 V, with 0.4 V steps) was applied to the electrodes, which corresponds to the root mean square (RMS) value of the ac voltage used in the experiments. Thus, the simulated electric field is a root mean square value of the electric field ($E = E_{\mathrm{rms}}$) if one assumes a sinusoidal time dependence of the ac signal.

DEP force

From the simulation results one can calculate the gradient of the electric field square, $\nabla(E^2)$, which is plotted in Fig. 4.6 for different electrode configurations. Since the DEP force is proportional to the gradient of the electric field square ($F_{\mathrm{DEP}} = \frac{\alpha}{2}\nabla(E^2)$, see Sec. 3.1.2) one can obtain the DEP force from $\nabla(E^2)$ by multiplying it with the effective polarizability of the molecule divided by two ($\alpha/2$).

The use of the fingertip and CNT electrode has been compared in the Fig. 4.6. By comparing the $\nabla(E^2)$ values near the fingertip electrode and near the CNT-electrode in the Fig. 4.6(a)-(d) one can observe substantially higher values near the CNT. This suggests that a higher DEP force can be obtained by using CNT as an electrode by using the same voltage applied to electrodes. Also, in the case of CNT electrode high gradients are obtained even if the gap size is as large as 1 μm, which can be seen by comparing Fig. 4.6(b) and (c) with Fig. 4.6(d). The DEP force dependence on the small changes in the gap size in the case of fingertip electrodes can be seen from Fig. 4.6(f)-(g).

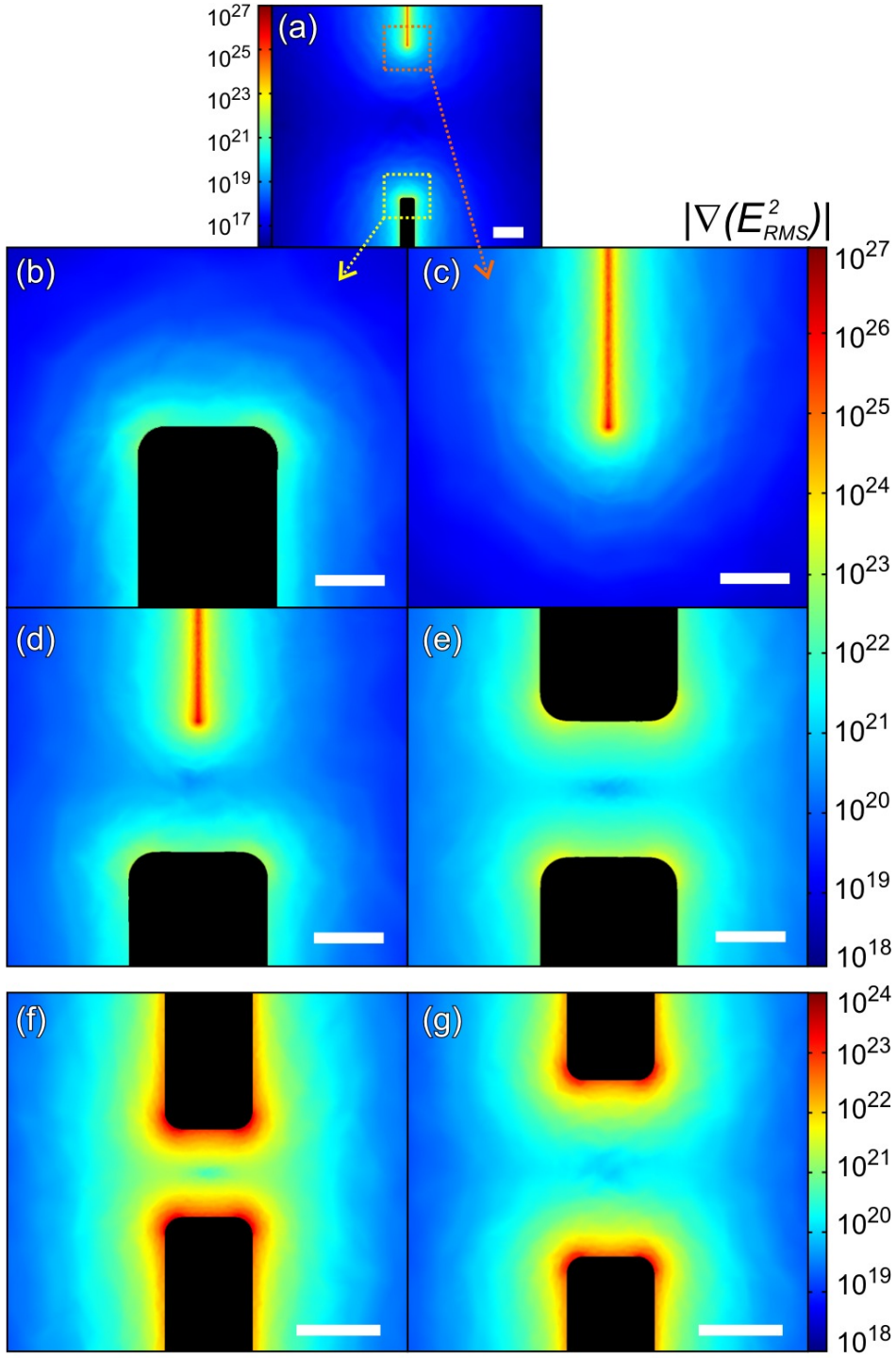

FIGURE 4.6 The gradient of an electric field square $\nabla(E^2)$ in the case of different electrode configurations, i.e., (a)-(d) one fingertip electrode and one CNT-electrode are used and (e)-(g) two fingertip type electrodes. The gap size in (a), and its close-ups (b)-(c), is 1 μm, in (d)-(f) 100 nm and in (g) 200 nm. Contour plots are taken in the plane 2 nm above the substrate, i.e., 0.2 nm above the CNT (diameter of 2 nm) in (a)-(d). The DEP force has the maximum value in the very end of the CNT. The dc voltage applied to the electrodes is 1.6 V. The scale bars are (a) 200, (b)-(e) 50 and (e)-(f) 100 nm.

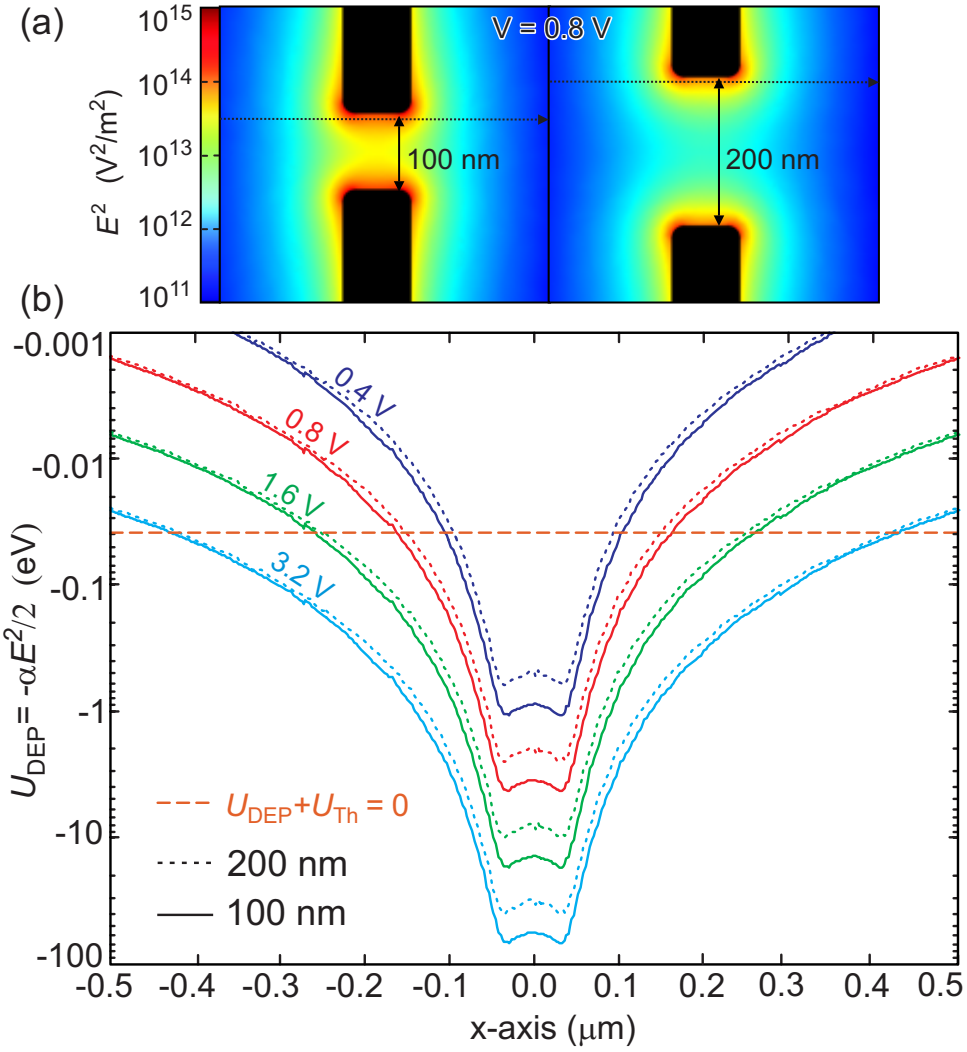

FIGURE 4.7 (a) Contour plot of the electric field square E^2 in the fingertip electrodes with a 100 and 200 nm gap for the 0.8 V voltage applied to the electrodes. (b) DEP potential energy, $U_{\mathrm{DEP}} = -\frac{1}{2}\alpha E^2$, calculated from the simulation results. x-axis is a dotted line shown in (a), which is on 5 nm distance from the electrode end (to avoid the equipotential surface of the electrode). The polarizability α = 10^{-32} Fm^2 (typical value in literature, see text) was used to calculate DEP potential energy. The results are given for the fingertip electrode separations of 100 and 200 nm and for the dc voltages 0.4, 0.8, 1.6 and 3.2 V. The horizontal dotted line represents the level where the thermal energy at T = 300 K cancels the DEP potential energy ($U_{\mathrm{Th}} + U_{\mathrm{DEP}} = \frac{3}{2}k_BT - \frac{1}{2}\alpha E^2$ = 0 at the crossings).

DEP potential

The 'DEP potential energy', defined as $U_{\mathrm{DEP}} = -\frac{1}{2}\alpha E^2$ (see Sec. 3.1.3), is plotted in Fig. 4.7(b) as a function of the perpendicular distance from the gap (between electrodes, 5 nm apart from the electrode end), for different applied voltages (0.4, 0.8, 1.6 and 3.2 V) and gap sizes (100 and 200 nm). To calculate the DEP potential energy from the electric field shown in Fig. 4.7(a), we used the polarizability of 100 bp DNA

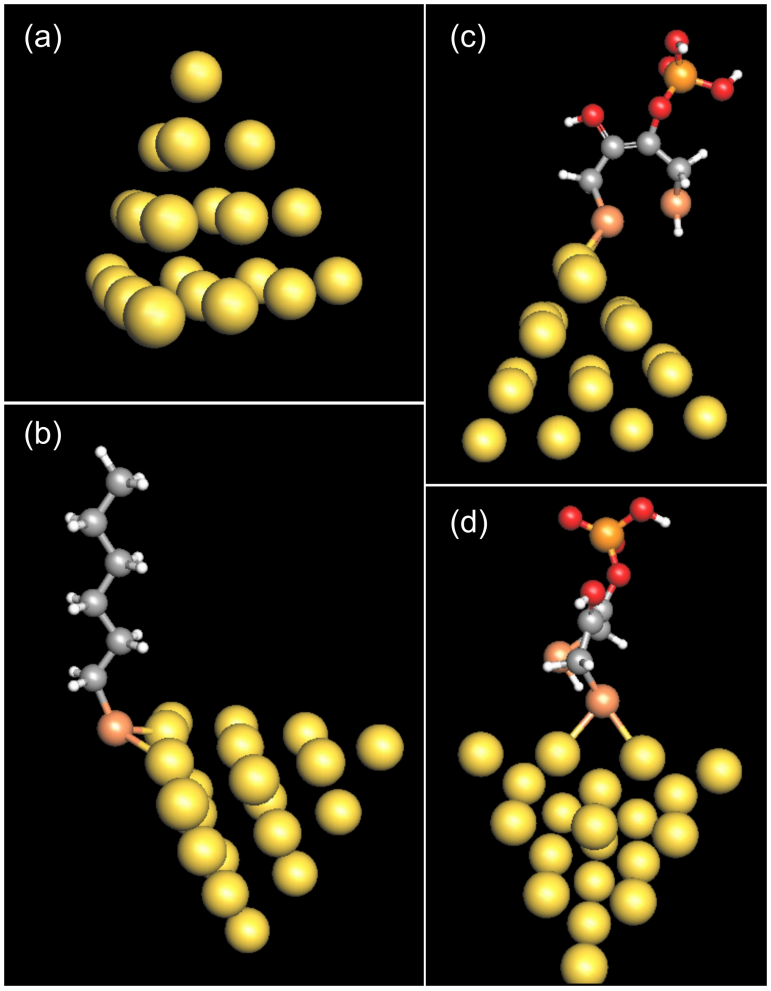

FIGURE 4.8 (a) The tetrahedral 20-atom gold cluster used for modelling of binding of the DNA linkers to gold, by the density functional theory calculations. Optimal binding configurations for (b) hexanethiol and (c)-(d) DTPA linkers on the cluster. (c) and (d) are two different views of the same configuration. The S-Au distances are: (b) 2.44 Å and 2.45 Å; (c) 2.45 Å and 2.51 Å. The S-S distance is 3.34 Å in (c).

(as an example), α = 10^{-34} Fm^2/bp $\cdot$ 100 bp = 10^{-32} Fm^2, calculated using a typical value found from the literature [15, 16, 235] and also observed in this Dissertation [3, 4]. The horizontal line, where the thermal energy, $U_{\mathrm{Th}} = \frac{3}{2}k_{\mathrm{B}}T$ cancels the DEP potential energy, i.e., $U_{tot} = U_{\mathrm{Th}} + U_{\mathrm{DEP}} = 0$ at the crossings, is drawn to the same plot to visualize the 'DEP potential well', which is the area below the line of the thermal energy and above the DEP potential energy.

4.5.2 Density functional calculations

The bonding of the hexanethiol and DTPA linkers on gold were studied by density functional theory (DFT) calculations by Hannu Häkkinen (NanoScience Center, University of Jyväskylä). A plane-wave pseudopotential density functional total energy

method was used in the calculations. For the details of calculating Au-S interaction, see e.g. Häkkinen *et al* [102]. The gold electrode was modelled as a tetrahedral twenty-atom gold cluster (see figure 4.8(a)).

Vertex, edge and face-centered atoms in the cluster have three, six and nine nearest-neighbours, respectively, and provide convenient models for adsorption sites with various local chemical properties. In DFT calculations it was found that the optimal binding site for a hexanethiolate is a bridging position at the edge of the cluster (see figure 4.8b), with a binding energy of 1.8 eV. In the case of DTPA linker, a stable adsorption site on the cluster was not found if the S-S bond in the DTPA molecule was left intact. Partial hydration of the S-S bond resulted in binding of the linker at the bridging edge position by 1.2 eV (see figure 4.8c and d). These calculations do not include effects from the environment and are not directly comparable with the experiments. However, these results can be used as a suggestive reference in the interpretation of the results from the immobilization experiments (see Ch. 5) and the electrical measurements (see Ch. 6).

5 DNA DEP studies

In this chapter, the results of the DNA DEP experiments performed *in situ* under the confocal microscope are presented and discussed. Two types of nanoelectrode configurations, i.e., two fingertip-type gold electrodes or one fingertip and one carbon nanotube (CNT) electrode, have been used to generate the electric field for DEP. The numerical methods, i.e., the finite element method (FEM) electric field simulations and density functional theory (DFT) calculations, have been used in conjunction with the analysis of the experimental data. The DEP experiments performed using different size DNA fragments, length varying from 9 nm to 2.8 μm, reveal information about the efficiency of DEP for small molecules and the polarizability of the DNA molecules. The immobilization of two different thiol-modified DNA, namely hexanethiol- and DTPA-modified, to the fingertip electrodes using DEP provides information about the molecule-electrode binding.

5.1 DEP of the DNA fragments

5.1.1 Analysis of the fluorescence data

For a quantitative analysis of the fluorescence data (see Sec. 4.3), the collected amount of DNA in the gap was obtained from the DEP movies by determining the mean fluorescence intensity inside the circle shaped (diameter of 1.6 μm, see upper right inset in Fig. 4.3) area in the gap between the fingertip electrodes (or in the end of the CNT electrode) subtracted by the mean intensity of the background fluorescence, which was measured from the circle shaped area on the substrate a few μm away from the DEP trap. The data analysis of the fluorescence movies was done using the confocal microscope software (LSM 510), Matlab 6.1 and Origin 7.5.

As discussed in Sec. 4.3.2 the absolute fluorescence values are not exactly comparable between the samples due to the fine-tuning of the detector sensitivity. However, since the fine-tuning has only a minor effect on the obtained fluorescence values, they can be still be qualitatively compared, e.g., when comparing the trapped amounts of the different size fragments in Fig. 5.1(a). In some cases, the obtained fluorescence curves were normalized by setting the maximum fluorescence intensity observed for each sample to unity, e.g., in Fig. 5.1(b). In any case, the results obtained from the fluorescence data are based on the voltage and frequency depen-

dence of the trapping process and thus not affected by the small variations on the absolute fluorescence values.

5.1.2 DEP using the fingertip electrodes

Trapping efficiency vs. DNA length

The fingertip electrodes were used to study the DEP of different size DNA fragments (from 27 bp to 8 kbp) as a function of the voltage using different frequencies (0.2, 0.5, 1, 2, 5 and 10 MHz). Observed fluorescence intensity in the DEP trap, i.e., in the ends of the fingertip electrodes, as a function of the trapping voltage for the different fragments, using 1 MHz frequency (as an example), is represented in Fig. 5.1. The fluorescence intensity corresponds to the amount of trapped nucleotides, since the dyes are supposed to attach uniformly along the DNA helix [283]. From the fluorescence curves in Fig. 5.1(a) one can easily see that when the contour length of the molecule is short, more voltage is needed for the trapping to begin. This is due to two issues; first of all, for a smaller molecule the Brownian motion is higher and secondly, the polarization of the molecule is smaller resulting in the smaller DEP force. However, it was observed that the trapping works also in the case of very short DNA fragments, having contour length less than $\sim$50 bp. This is due to the polarization of DNA being mainly caused by the counter-ion cloud, which has a certain minimum thickness, i.e., the Debye layer which is $\sim$10 nm in the case of NaOH/Hepes buffer used (Debye layer thickness was estimated using Eq. (9) in ref. [45]). For instance, in the case of 27 bp fragment, which is about 9 nm long rod-like object, the counter-ion cloud makes its effective length substantially longer, enhancing its polarizability and thus increasing the DEP force.

Here we used an average electric field, i.e., the voltage divided by the electrode separation, between 10^7 and $9 \cdot 10^7$ V_{rms}/m. In earlier studies, where electrode separations of 1 - 10 μm and DNA molecules larger than 10 kbp were used, the field strength from 10^5 to 10^6 V_{rms}/m was enough for trapping [15, 45, 73, 74, 235, 262]. To realize the trapping in the case of smaller DNA fragments, the field strength higher than 10^6 V_{rms}/m have been used [45, 103, 235]. However, when the size of the electrode separation is suppressed to a nanoscale even higher electric field strengths have been used, e.g., in the DEP of a protein of about the same mass as 400 bp DNA by using the gap of 500 nm, the electric field of $\sim 2 \cdot 10^7$ V_{rms}/m has been used [104]. We have used even slightly higher field strengths because the electrode separation in our fingertip electrode structure is only $\sim$100 nm.

Trapping efficiency vs. gap size

It was observed experimentally (see Fig. 6 in ref. [4]) that the trapping of DNA starts at the same voltage with no correspondence to the difference in the fingertip electrode separation between 80 and 130 nm. This suggests that the absolute voltage

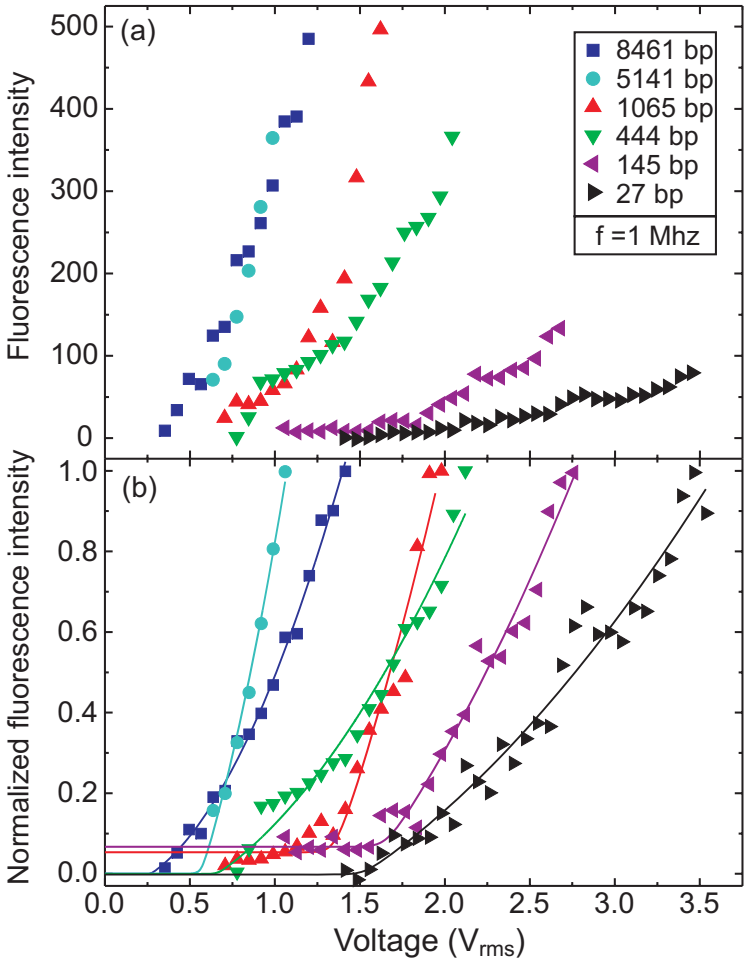

FIGURE 5.1 The trapped amounts of DNA fragments as a function of the trapping voltage using 1 MHz frequency [4]. (a) The relative fluorescence amounts (in arbitrary units) are nearly comparable to each other, because almost the same capturing settings have been used. (Some high fluorescence data points are cut off from the plot) (b) The normalized fluorescence curves (maximum fluorescence point in each curve is set to unity) and fits to the function shown in Eq. 5.2 [4].

had more influence to the trapped amount of DNA than the (calculated) average electric field, which contradicts the description of the DEP force. However, this can be explained by means of the electric field simulations.

When using the narrow (∼100 nm wide) fingertip electrodes, the points of the highest electric field (and electric field gradients) are located near the end of the electrodes as observed from Fig. 4.7(a). In the region of the maximum field strength (in the point $x = 0$ in Fig. 4.7(b)), the DEP potential (and also the trapping efficiency) depends highly on the gap size, whereas relatively far (a few hundreds of nanometers) from the electrode edge the DEP potential depends mostly on the absolute voltage applied to the electrodes (the gap size dependence is small).

The minimum size of the fluorescence spot that could be reliably observed in our experiments was as large as ~ 1 μm due to, e.g., spreading of the DNA by

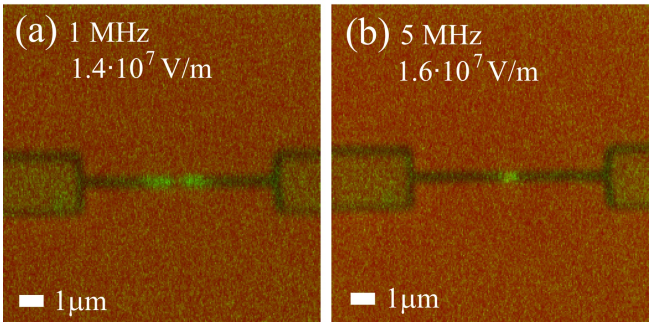

FIGURE 5.2 Confocal microscope images captured during the DEP of C6-DNA when frequency of the applied signal is (a) 1 MHz or (b) 5 MHz [2]. When higher frequency is used, the DNA spot is smaller because of the decreased electrophoretic effects.

the electrophoretic effects [45] and the resolution limitations, e.g., in the trapping voltage (raise in 0.2 V_{rms} steps). This makes the 'trapping region', i.e., the volume around the gap where DEP potential exceeds the thermal energy of the molecules and the trapping occurs, large ($\sim$1 μm spot) compared to the size of the gap ($\sim$100 nm).

The issues described above explain why the effect of a small (less than 100 nm) change in the gap size could not be resolved in our experiments. This also proves that our trapping region is really larger than the gap size and the observed $\sim$1 μm fluorescence spot is not optically limited (estimated lateral resolution of confocal microscope $\sim$200 nm). Note that larger changes in the gap size, i.e., change comparable or larger than the trapping region $\sim$1 μm, would be observable in the fluorescence intensity curves and thus interpreted as a change in the trapping efficiency (see Sec. 5.1.3).

Effects of the frequency on the trapping

It was observed that by using higher frequencies the DNA was more efficiently localized to the areas of the highest field gradient, while for lower frequencies DNA was spread around the electrodes, as can be observed from the images in Fig. 5.2. This can be explained by the decreased spreading of the DNA spot due to the electrophoretic effects in the case of higher frequencies [45].

It was also observed for all used DNA fragments that when the higher frequencies are used the higher voltages must be applied to realize the trapping. This can be explained by the time-scale of the polarization. When the trapping frequency is higher the molecule has less time to polarize and the achieved maximum polarization is lower (see Sec. 5.2), yielding a lower DEP force. For the frequencies higher than 10 MHz the trapped amounts of DNA were too low to be distinguished from the fluorescence background. This may be due to either the actual frequency dependence of the DNA DEP or to the signal losses in the narrow ($\sim$100 nm) electrodes, which are not optimized for the high frequency signals.

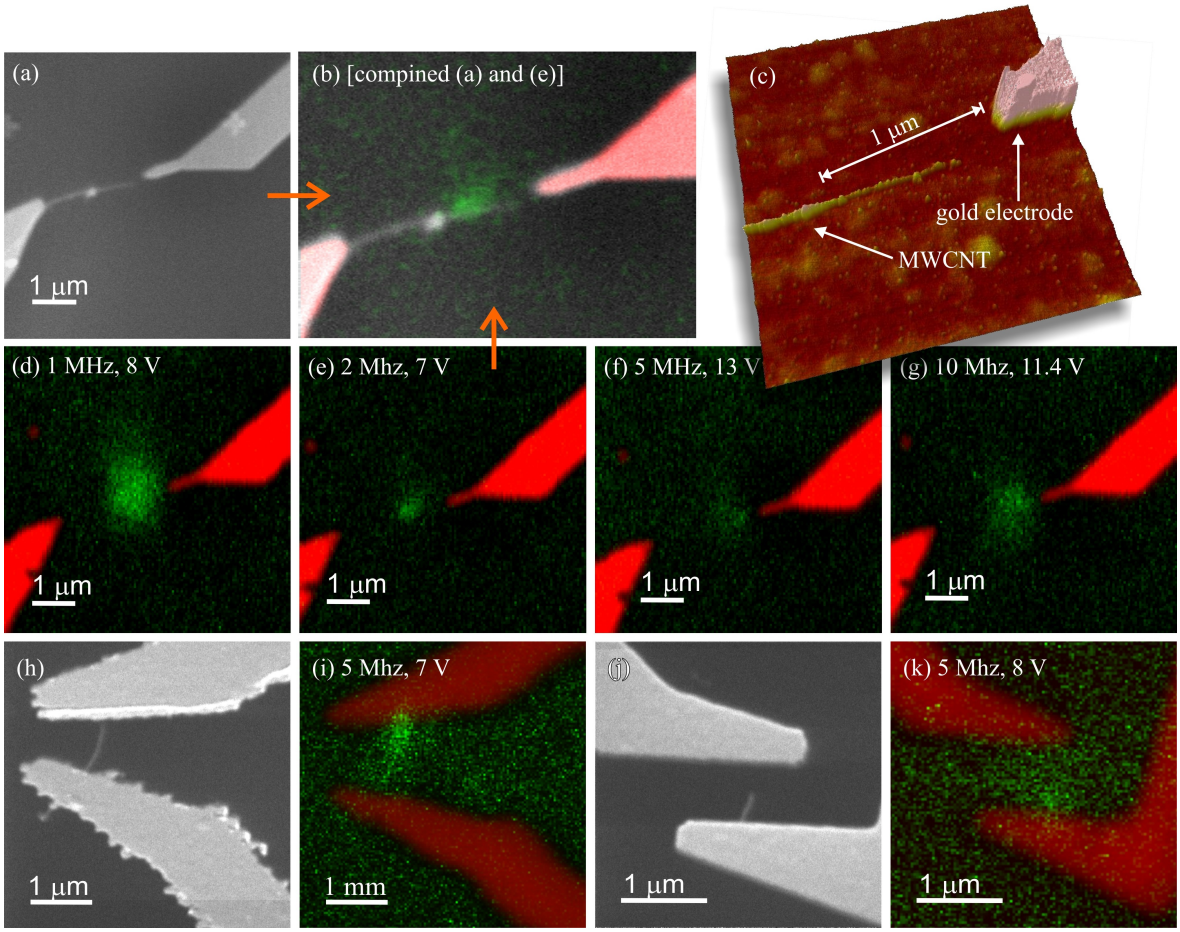

FIGURE 5.3 DEP of (a)-(g) 1065 bp and (h)-(k) 145 bp DNA using a multi-walled carbon nanotube (MWCNT) as another electrode. (a) SEM and (c) AFM images of the multiwalled CNT electrode sample before the confocal experiment. (d)-(g) Fluorescence images of gathered 1 kbp DNA when a given frequency and voltage were applied to the electrodes (using the same sample). (b) Compined SEM and confocal microscope image, (a) and (e), showing the fluorescence spot located in the end of the nanotube. SEM images from the CNT electrode samples, (h) and (j), and the corresponding fluorescence images during the DEP, (i) and (k). The gap sizes (from CNT end to another electrode) are (a) ∼1 μm (see text), (h) ∼115 nm and (j) ∼350 nm [3].

5.1.3 DEP using the CNT electrode

Trapping of the 1 kbp DNA using a CNT electrode

In contrast to Sec. 5.1.2, where two fingertip electrodes were used for DEP, here the MWCNT is used as one of the electrodes. The CNT electrode sample shown in Fig. 5.3(a) and (c) was used to trap 1 kbp DNA. The trapped DNA spots using different frequencies are shown in Fig. 5.3(d)-(g). It can be clearly observed from the Fig. 5.3(b), in which the SEM image (Fig. 5.3(a)) and the fluorescence image (Fig. 5.3(e)) are placed on top of each other, that DNA was collected to the end of the CNT, where the DEP force is in its maximum as shown by the simulation results in

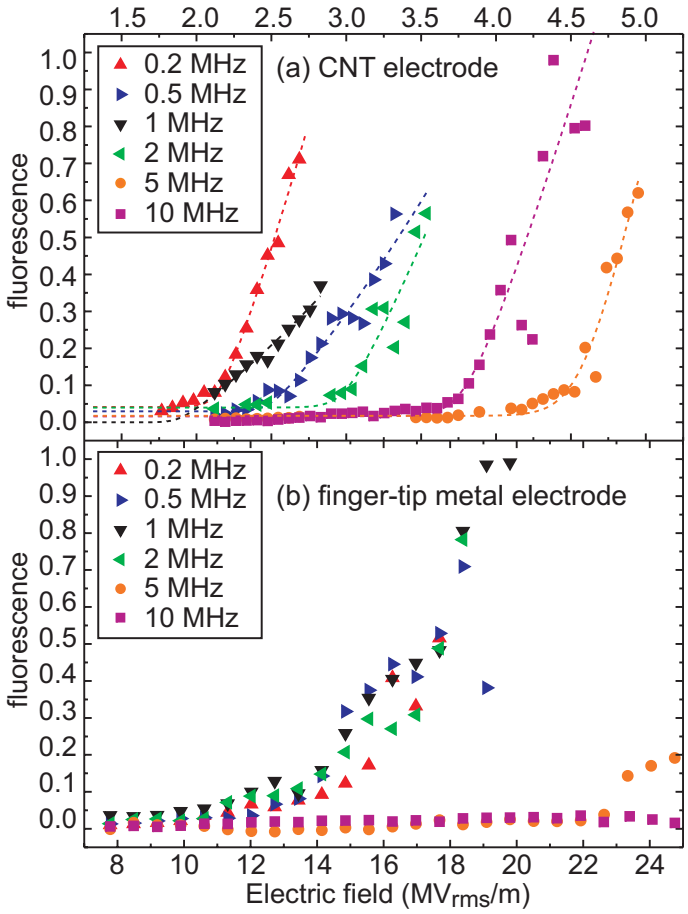

FIGURE 5.4 Comparison of the trapping efficiency of the CNT and the fingertip electrodes using the 1 kbp DNA. The fluorescence intensity (a) in the end of the CNT, when the separation from the metal electrode was $d \approx 1$ μm, and (b) in the gap between the fingertip electrodes, when the electrode separation was $d \approx 100$ nm, as a function of the electric field (i.e. an average electric field strength between the electrodes, $E = V/d$). Dotted lines in (a) are fits to the data using the function in Eq. 5.2. By comparing the field strength needed to trap the DNA in these cases, one can clearly see that CNT electrode shows better performance than lithographically fabricated nanoelectrodes [3].

Fig. 4.6 (and also the 'DEP potential' is in its minimum at the end of the CNT).

The gap between the metal electrode and the CNT seems to be ~400 nm when looking at the AFM image in Fig. 5.3(c). However, during DEP the fluorescence spot is rather located to ~1 μm distance from the metal electrode. One can see from the AFM image Fig. 5.3(c) that the nanotube gets narrower and clumpy near to its end and the conformation appears deformed, which suggests that the 'real end' of the MWCNT (in the sense of an electrical conductivity) is thereby at ~1 μm distance from the metal electrode. This suggests that the DEP can also be used for the characterization of the integrity of carbon nanotubes and other ultrathin nanowires.

The fluorescence intensity in the DEP trap, i.e., at the end of the CNT, for the sample in Fig. 5.3(a)-(g) is shown as a function of the average electric field strength

(the voltage divided by the gap size of 1 μm) using different trapping frequencies in Fig. 5.4(a).

Trapping of the 145 bp DNA using the CNT electrode

Two different CNT electrode samples, shown in Fig. 5.3(h) and Fig. 5.3(j), were used to trap the 145 bp DNA. In the both samples the expected behaviour, i.e., the DNA is collected around the CNT rather that to the metal electrodes, was observed as can be seen from the fluorescence images in Fig. 5.3(i) and Fig. 5.3(k). In contrast to the sample used in the case of 1 kbp DNA, where the DNA was clearly collected to the end of the CNT on the whole frequency range from 0.1 to 10 MHz, in the samples used for the 145 bp DNA the gathering to the CNT was not so clearly visible on the whole frequency range, but was most efficient at 5 MHz frequency. This is possibly due to the vicinity of the metal electrodes to the CNT end, which causes the gathering of some amount of the DNA also to the rough metal electrode edges (high field gradients) which decreases a fluorescence contrast. It also seems in Fig. 5.3(i) and Fig. 5.3(k) that the DNA is collected along the whole CNT and not only to the CNT end, which may also be due to the vicinity of the metal electrodes.

5.1.4 Fingertip vs. CNT electrode

The fluorescence intensity of the captured 1 kbp DNA as a function of the average electric field strength (i.e. the voltage divided by the electrode separation) in the cases of the CNT and the metal electrodes is shown in Fig. 5.4. By comparing the trapping efficiency, i.e., the minimum field strength needed to realize trapping, in Fig. 5.4(a) and Fig. 5.4(b), one can observe that the trapping occurs with lower average electric field in the case of the CNT electrode.

These experimental results are consistent with the simulation results shown in Fig. 4.6, from which one can see that a considerably higher DEP force can be achieved by using a carbon nanotube (diameter 2 nm) as an electrode when compared to the fingertip electrodes. In the CNT electrode sample used in the experiment the diameter of the MWCNT was $\sim$6 nm, which yields a bit lower DEP force than in the case of a CNT of 2 nm diameter used in the simulations. However, it was shown that the CNT works as an effective DEP trap, even if the CNT end is relatively far from the other electrode.

5.2 Polarizability of the DNA fragments

5.2.1 Calculation of the DNA polarizability

The fluorescence intensity - trapping voltage curves obtained from the DEP experiments *in situ* under the confocal microscope in Sec. 5.1 are accompanied with the

results of the electric field simulations in Sec. 4.5.1 to determine the polarizability of the DNA fragments. The results reveal information about the dependence of the polarizability on the frequency of the trapping signal and the length of the DNA fragment. The data from the DEP movies obtained using both electrode configurations, i.e., two fingertip electrodes [4] or one CNT and one fingertip electrode [3], has been used.

By determining the electric field on the edge of the trapping area, i.e., on the edge of the potential well in Fig. 4.7(b) (in the point where $U_{\mathrm{DEP}}+U_{\mathrm{thermal}}=0$), which is needed to trap a certain molecule, one can calculate its effective polarizability

$$\alpha = \frac{3k_BT}{E_{min}^2}. \tag{5.1}$$

In the experiments, the electric field was generated by applying the voltage to the nanoelectrodes. Thus, the task equates to determining of the minimum voltage V_{min} needed for trapping, using which one can resolve the electric field E_{min} in a certain point by the electric field simulations, e.g., E^2 obtained from the simulations using the dc voltage $V = 0.8V$ is shown in Fig. 4.7(a).

The minimum voltage V_{min} corresponds to the point when the observed fluorescence in the DEP trap exceeds the background noise level and thus, we can see that the trapping begins. The exact determination of V_{min} was done by fitting the fluorescence intensity-voltage curve to the formula

$$I = I_0 + A(V^b + V_{min}^b)^{2/b}, \tag{5.2}$$

which produces a V^2 dependence after the voltage V_{min} has been reached. The V^2 dependency is physically motivated by the DEP force, $F_{DEP} = \alpha\nabla(E^2)$, and has also been observed experimentally by Asbury and co-workers [13]. The parameter b determines the rate of the asymptotic change from a constant value, i.e., $I_0 + A \cdot V_{min}^2$, which is very small, to the V^2 dependency. The best fit to experimental data was found using the value b = 40. Note, that the absolute value of the fluorescence data only affects to the fitting parameter A, which is not used in the further analysis.

It would be possible to calculate the polarizability also using an experimentally determined minimum force F_{DEP} and the thermal drag force $F_{thermal}$ (see Sec. 3.1.2), but due to the more ambiguous description of the thermal drag force we used the DEP potential instead. The thermal drag force depends, e.g., on the size and shape of the molecule, which makes the treatment in the case of DNA harder to interpret. In the case of the thermal energy, which is (almost) the same in the cases of different size objects, we can neglect the size dependency in the calculations. However, the size dependency is still included in the obtained effective polarizability values.

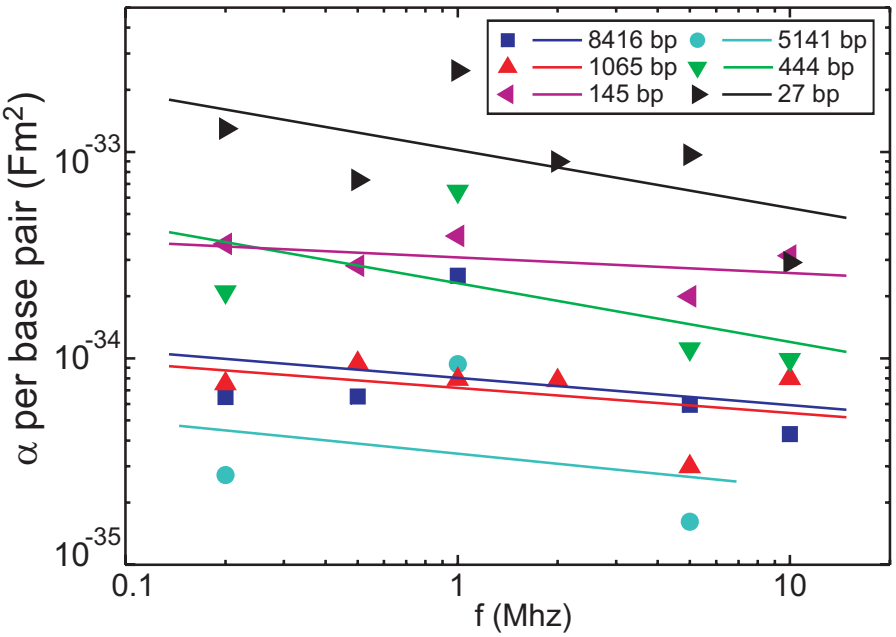

FIGURE 5.5 The experimentally obtained polarizabilities for the different size DNA fragments plotted as a function of the frequency. The polarizability per base pair is obtained by dividing the polarizability of the whole molecule by its length in base pairs [4].

5.2.2 Polarizability using the fingertip electrodes

In order to determine the DNA polarizability from the data obtained using the fingertip electrodes, the minimum voltages V_{min} were first determined by fitting the fluorescence - voltage curves to the function in Eq. 5.2. An example of the fitted curves in the case of 1 MHz frequency is shown in Fig. 5.1(b).

Next, the information obtained from the simulations was used to find out the electric field strength E_{min} on the edge of the observed fluorescence spot, i.e., on the edge of the DEP trap in Fig. 4.7(a), when the corresponding minimum voltage V_{min} is applied to the electrodes. E_{min} was read from simulated data at the distance $r = (0.5 \pm 0.1)$ (discussed below) from the end of the fingertip electrodes, perpendicular to them, in the plane 10 nm above and parallel to the substrate surface. After this, the polarizability was calculated by Eq. 5.1.

The radius of the smallest observable fluorescence spot, observed when the trapping begins and the fluorescence intensity starts to raise, was approximately $r = (0.5 \pm 0.1)$ μm for all the frequencies used. Note that even when the fluorescence spot size has a frequency dependence (resulting from the electrophoretic effects [45]), it cannot be resolved in the beginning of the trapping, but only later when the trapped spot is larger. However, the determination of the smallest resolved fluorescence spot size to $\sim$1 μm is not very accurate, since it is partially limited by the optical resolution of confocal microscope (i.e. $\sim$200 nm). Thus it can give a systematic error to the obtained polarizability values.

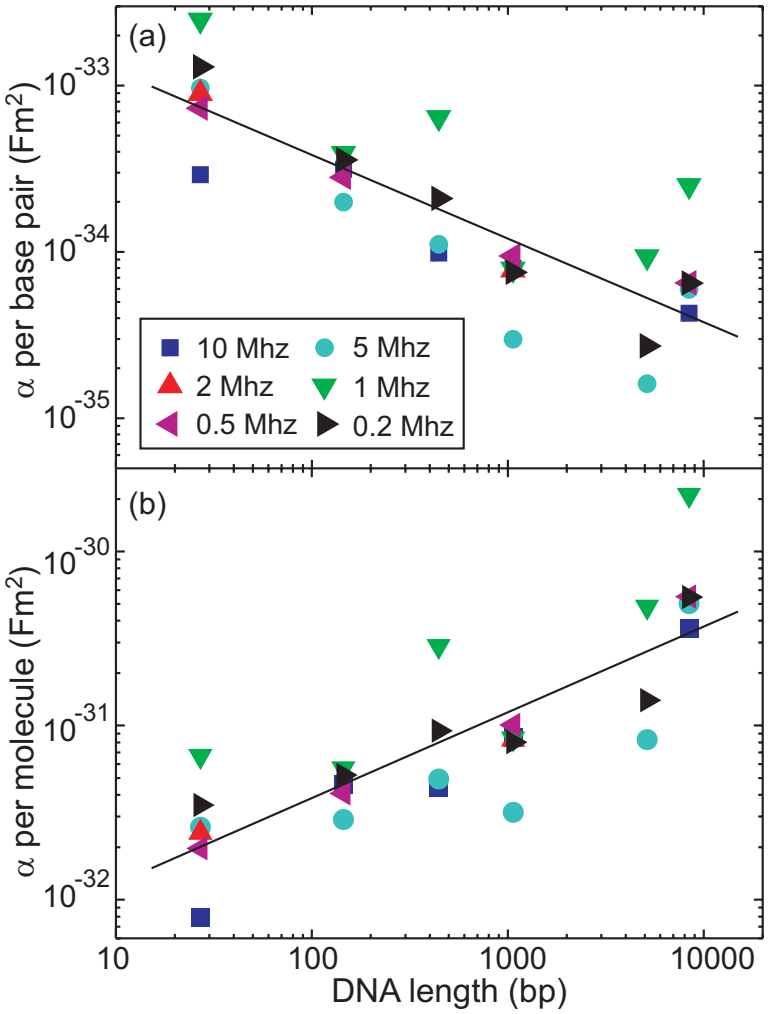

FIGURE 5.6 The experimentally obtained polarizabilities (a) per base pair and (b) per macromolecule plotted as a function of the length of the DNA fragment with different frequencies [4].

The calculated polarizabilities per base pair, i.e., the polarizability divided by the molecule length in base pairs, are plotted as a function of frequency in Fig. 5.5 and as a function of DNA length in Fig. 5.6(a). One can see that the polarizability per bp is larger in the case of the short DNA fragments, which is an indication of the polarization of the counter-ion cloud (discussed before in Sec. 5.1.2) [14, 15, 235]. The linear fits to the polarizability values of each fragment in Fig. 5.5 show that polarizability slightly decreases with the increase of the frequency. An exception to this is the 1 MHz frequency, which seems to yield the highest polarizability for almost all of the fragments. This is somewhat expected behaviour, since frequency of 1 MHz has been shown to work well for trapping of DNA in several studies [16, 26, 55, 183, 235, 281] and also in our experiments [1, 2, 3, 4]. The total polarizability of the DNA macromolecule, shown in Fig. 5.6(b), was observed to increase as a function of the molecule length as expected.

Long DNA fragments

In the case of long DNA molecules, i.e., substantially longer than the persistence length of DNA (∼150 bp) [215], the dependence of the polarizability on the DNA length can be understood via Manning's model [158]. In this model, the counterions move freely along the macromolecular 'DNA subunit', the length of which is roughly defined by the persistence length of DNA. Since each subunit adds almost similar contribution to the polarizability of the macromolecule, the total polarizability divided by the the length of the DNA remains approximately constant. This result is valid even the subunit length varies, e.g., as a function of DNA concentration [30].

The polarizability values found from the literature vary from $\sim 10^{-36}$ to $\sim 10^{-34}$ Fm^2/bp [15, 16, 220, 235]. For 2.7 kbp pUC18 plasmid DNA, Suzuki *et al* found the value $\sim 10^{-32}$ Fm^2 ($\sim 4 \cdot 10^{-36}$ Fm^2/bp) [235]. For 12 kbp pTA250 plasmid DNA, Bakewell *et al* measured the polarizability as a function of frequency, yielding values from $0.14 \cdot 10^{-30}$ Fm^2 ($\sim 2 \cdot 10^{-35}$ Fm^2/bp) for 5 MHz to $2.4 \cdot 10^{-30}$ Fm^2 ($\sim 2 \cdot 10^{-34}$ Fm^2/bp) for 0.1 MHz [15, 16]. Saif *et al* have found the polarizability $\sim 5 \cdot 10^{-33}$ Fm^2 ($\sim 6 \cdot 10^{-35}$ Fm^2/bp) for calf thymus DNA using a bit higher frequency (12.3 MHz) [220]. The polarizabilities per base pair we obtained in the case of relatively long DNA fragments (1, 5 and 8 kbp fragments in Fig. 5.5 and 5.6(a)) correspond to the range of values found from the literature. Observed differences between the experimentally obtained polarizability values may also be caused by the use of different buffer, e.g., viscosity [45], or the length and the shape of a DNA, e.g., the plasmid DNA has a circular conformation and also a globular shape secondary structure, which limits the unwinding and stretching of the plasmid DNA during DEP [235] and may result a weakening of the polarizability.

Short DNA fragments

In contrast, in the case of short DNA fragments (27, 145 and 444 bp fragments in Fig. 5.5 and 5.6(a)) it was observed that the polarizability per base pair does not remain constant but increases as a molecule gets shorter. There are two likely reasons causing this kind of behaviour. First, short DNA fragments, i.e., which have a contour length of the order of the DNA subunit length, behave more like a rigid rod (in contrast to a globular ball in the case of a long DNA), which enhances their polarizability in a longitudinal direction (a globular ball polarizes in many directions) [281]. Secondly, if the fragments are shorter or of the order of the thickness of the counter-ion cloud (∼10 nm), the polarizability per base pair is enhanced by the counter-ion cloud polarization (discussed before in section 5.2). This enhancement of the polarizability has not been observed in the earlier studies [15, 16, 220, 235], because the used DNA was long (2.7 - 12 kbp) compared to the fragments that were used in this study.

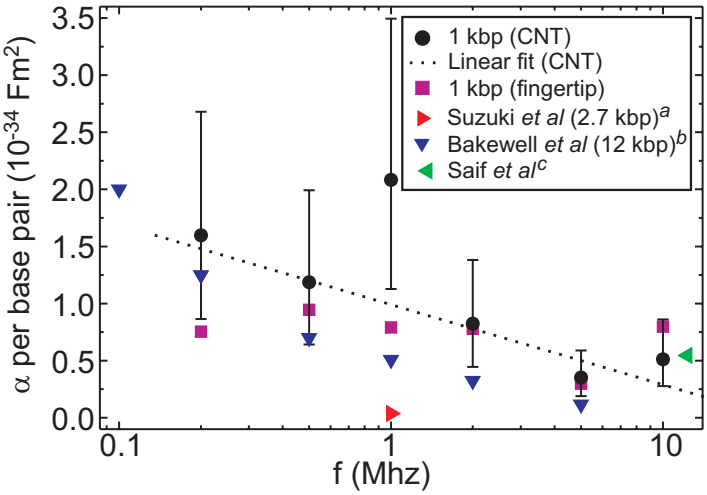

FIGURE 5.7 The polarizabilities of the 1 kbp DNA fragment calculated using the data obtained from the DEP using CNT electrode sample shown in Fig. 5.4(a) [3], plotted together with the values obtained using fingertip electrode samples (see Fig.5.5) [4]. The error bars originate from the uncertainty of the observed fluorescence spot radius $r = (0.5 \pm 0.1)\mu$m. Other values are from [a][235], [b][15], and [c][220].

5.2.3 Polarizability using CNT electrode

In addition to the polarisabilities calculated from the data obtained using the fingertip electrodes in Sec. 5.2.2, the polarizability of the 1 kbp DNA was also calculated from the data obtained using the CNT electrode sample shown in Fig. 5.3(a)-(g). The fluorescence - voltage curves shown in Fig. 5.4(a) were fitted to the function in Eq. 5.2 (the trapping voltage is obtained from the electric field strength by multiplying it with the gap size $d = 1\mu$m) and the polarizability was calculated from Eq. 5.1. The higher efficiency of the trapping in the case of the CNT electrode makes it more sensitive to the frequency used in the DEP process (higher trapping efficiency leads to a higher absolute variation of the trapped amounts) yielding more precise information (compared to fingertip electrode data) about the frequency dependency of the DNA polarizability. The normalized polarizability (polarizability divided by the molecule length in base pairs) as a function of frequency is shown in Fig. 5.7 together with values obtained using the fingertip electrodes (shown in Fig.5.5) and values from the literature for various size DNA molecules.

The polarizability values obtained for the 1 kbp DNA using the fingertip electrodes correspond well to the values obtained using the CNT electrode. In the latter case the average of the frequency dependent polarizability values was a bit higher: $\alpha_{\text{fingertip}} \approx 0.73 \cdot 10^{-34}$ Fm^2/bp and $\alpha_{\text{CNT}} \approx 1.1 \cdot 10^{-34}$ Fm^2/bp. The values for 2 and 5 MHz were very close to each other ($\Delta\alpha \approx 0.05 \cdot 10^{-34}$ Fm^2/bp), whereas in the case of 1 MHz the CNT electrode value was notably higher ($\Delta\alpha \approx 1.3 \cdot 10^{-34}$ Fm^2/bp).

From the data obtained using the CNT electrode sample one can more clearly observe (compared to the results from the fingertip electrode samples in Sec. 5.2.2)

that the polarizability of DNA decreases with the increase of the frequency, which has also been shown earlier for 12 kbp plasmid DNA by Bakewell *et al* [15, 16]. In addition, the polarizability of calf thymus DNA [220] corresponds well to our observed 10 MHz value even the DNA they used was much longer. However, the value ($\alpha = 10^{-32}$ Fm^2) obtained for a 2.7 kbp plasmid DNA [235] using the fluorescence anisotropy measurements is about one order of magnitude smaller than the other results. The similarity of the polarizability results in the case of different size DNAs can be understood by Manning's model [158] (discussed in Sec. 5.2.2).

5.3 Immobilization of DNA

DNA can be immobilized to the metal and insulator surfaces in several ways. For instance, DNA oligonucleotides can be immobilized to the silicon oxide surface using a silanization of the surface, which has been widely used in the fabrication of DNA microarrays used for genetic analysis. For the DNA immobilization on a metal surface, oligonucleotides modified with a thiol- or amino-group have been used. We have studied the immobilization of DNA on the gold electrodes through a sulphur-gold bonding (discussed in Sec. 2.3.4).

5.3.1 Comparison of hexanethiol- and DTPA-linkers

The immobilization of the 414 bp C6-DNA and the 415 bp DTPA-DNA to the fingertip gold electrodes using the DEP trapping was studied *in situ* under confocal microscope [4]. The immobilization of the modified DNA molecules was compared to the non-specific binding of the unmodified 444 bp DNA. The quantitative analysis was done by comparing the amount of the fluorescence that remained on the gap region after the trapping voltage was turned off. This indicates how well the molecules attach to the gold electrodes.

We observed that the molecules without linkers diffused away from the DEP trap very soon after the trapping voltage was turned off, whereas in the case of the hexanethiol- and DTPA-modified DNA a noticeable amount of the molecules remained on the gap. The amount of non-specific physisorption [237] of the unmodified DNA was quite small, which can be observed from the fluorescence quickly vanishing after the trapping voltage is turned off in Fig. 5.8(e). By comparing the amount of the immobilized DNA shown in Fig. 5.8(a-d), it seems that the hexanethiol-modified molecules attach better than the DTPA-modified molecules.

After the trapping voltage is turned off (on the right side of the dotted lines in Fig. 5.8(a, c, e)), especially in the case of the modified DNA , the fluorescence intensity curves have a bit negative slope. That can be related to the bleaching of the fluorescent dyes in the surface bound DNA molecules or the detachment of the molecules (and diffusion away from the gap). However, the bleaching tests (see bleaching

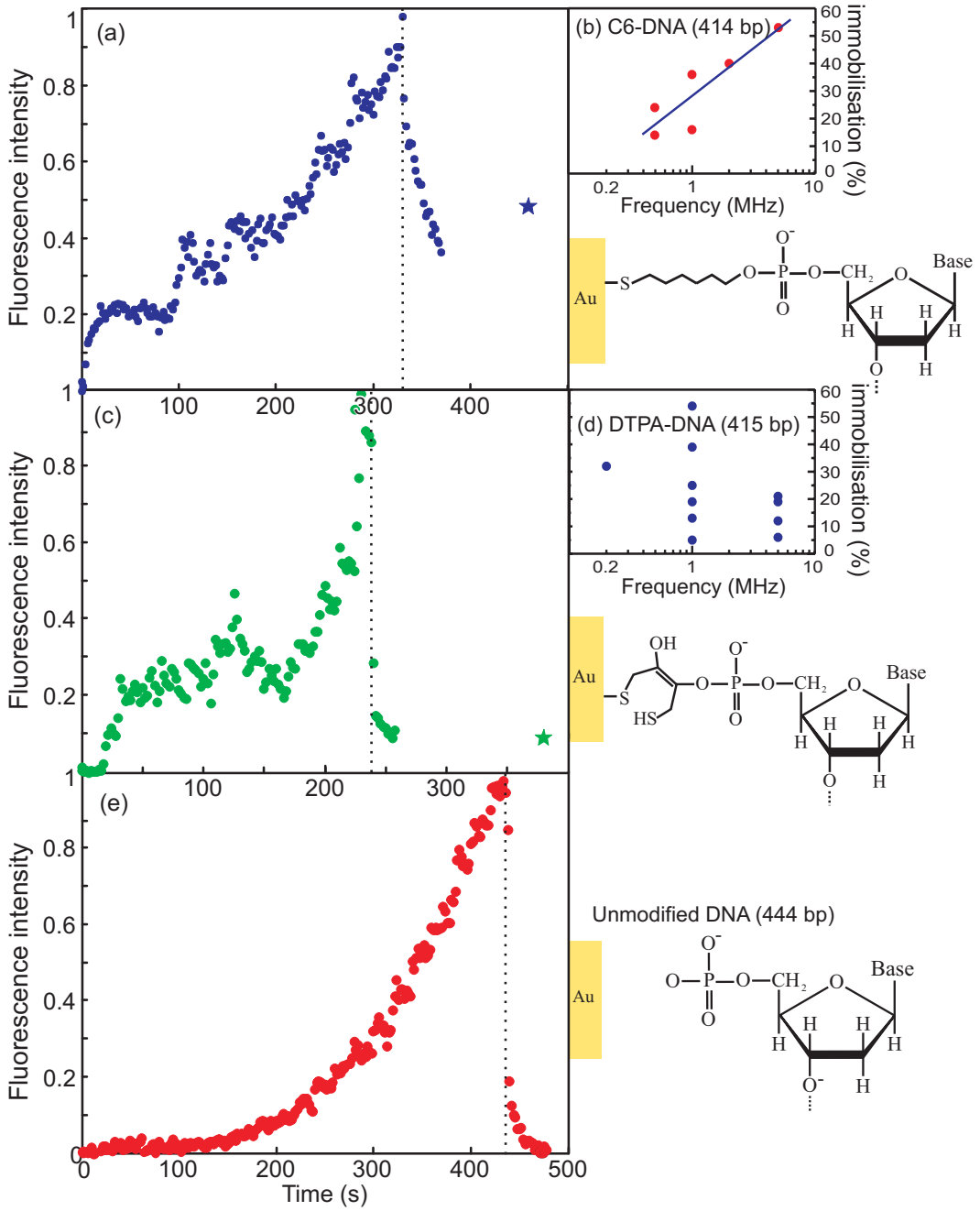

FIGURE 5.8 DEP trapping and immobilization of (a)-(b) the C6-DNA, (c)-(d) the DTPA-DNA and (e) the unmodified 444 bp DNA to the fingertip electrodes using a 5 MHz frequency (fluorescence data from three different samples) [4]. In (a), (c) and (e), the circles describe the data points obtained from the DEP movie and the stars represent the 'remained fluorescence' measured separately after the laser excitation had been turned off for a certain time (see time from x-axis). The dashed lines represent the times when the voltage was turned off. Effect of the trapping frequency on the immobilized amounts of (b) the C6-DNA and (d) the DTPA-DNA. The immobilized amounts are obtained by comparing the remained amount of the fluorescence with the maximum trapped fluorescence in the DEP trap in each sample. Schematic views of the binding of linkers suggested by DFT-calculations in Sec. 4.5.2 are shown under the immobilized amounts in (b) and (d).

tests in [4]) showed generally much smaller slope than this, which suggests that the fluorescence drop in this case is due to the diffusion of the excess (e.g. because of the Coulomb repulsion between the charged molecules) or the poorly attached (e.g. through a weak physical adsorption) DNA away from the gap. In the curves shown in Fig. 5.8(a, c, e), additional 0.5 mM TCEP-HCl was used in Hepes/NaOH buffer as a reduction agent. However, it was observed that the presence of the reduction agent ($\sim$0.5 mM TCEP-HCl or $\sim$2 mM $NaBH_4$) or the absence of it did not significantly affect to the amounts of the immobilized thiol-modified DNA in either case. However, the use of the reduction agent is essential to avoid formation of multimers through the sulphur-sulphur bonding between the separate molecules when aiming at the immobilization of individual molecules (discussed in Ch. 6).

The amount of the fluorescence remained on the gap divided by the maximum fluorescence observed in each sample during the DEP is plotted as a function of frequency in 5.8(b) and (d). The remained fluorescence was measured from the still image taken $\sim$1 minute after the capturing of the DEP movie was stopped. The C6-DNA seems to attach better by using the higher frequencies, which can be seen from the Fig. 5.8(b). A proposal for this kind of behaviour is that the hexanethiol-linker, in its reduced form, i.e., 5'-$(CH_2)_6$-SH, is highly reactive and can attach very fast when it gets near to the gold surface. Further, it was also observed that the DNA spot is better localized when using higher frequencies for DEP (see Sec. 5.1.2), which may ideally result in the larger amount of immobilized DNA in the case of a 'fast attaching' linker (in the case of a favourable reaction).

The immobilization results of the DTPA-DNA seem quite inconsistent as can be seen from Fig. 5.8(d) and have no observable regular behaviour, which indicates poor binding of the linker. The DFT-calculations (see Sec. 4.5.2) suggest that the DTPA-linker binds to the gold surface through (only) one of the sulphur atoms (see Fig. 5.8(d)) and that the binding takes place only if the original S-S bond is broken beforehand. This makes the attachment of the DTPA-linker less favourable reaction as compared to the attachment of -SH group in the hexanethiol-linker. This would result to a slower time-scale of the immobilization of the DTPA-linker leading to a better attachment in the case of lower frequencies (which is barely observed from Fig. 5.8(d)).

The DFT-calculations showed also a lower binding energy for DTPA-linker as compared to the hexanethiol-linker, which qualitatively agrees with the experimental observation of the weaker attachment of DTPA-linker as compared to hexanethiol-linker. In contrast to our observations, the manufacturer claims that the DTPA-linker can form two sulphur-gold bonds with the gold surface thus providing a better attachment than the monothiol-linkers (DNA-modifications are provided by Glen Reseach [8]). One possible explanation to this discrepancy is that the simultaneous applying of the DEP trapping in our experiments may reduce the immobilization yield of the DTPA-DNA.

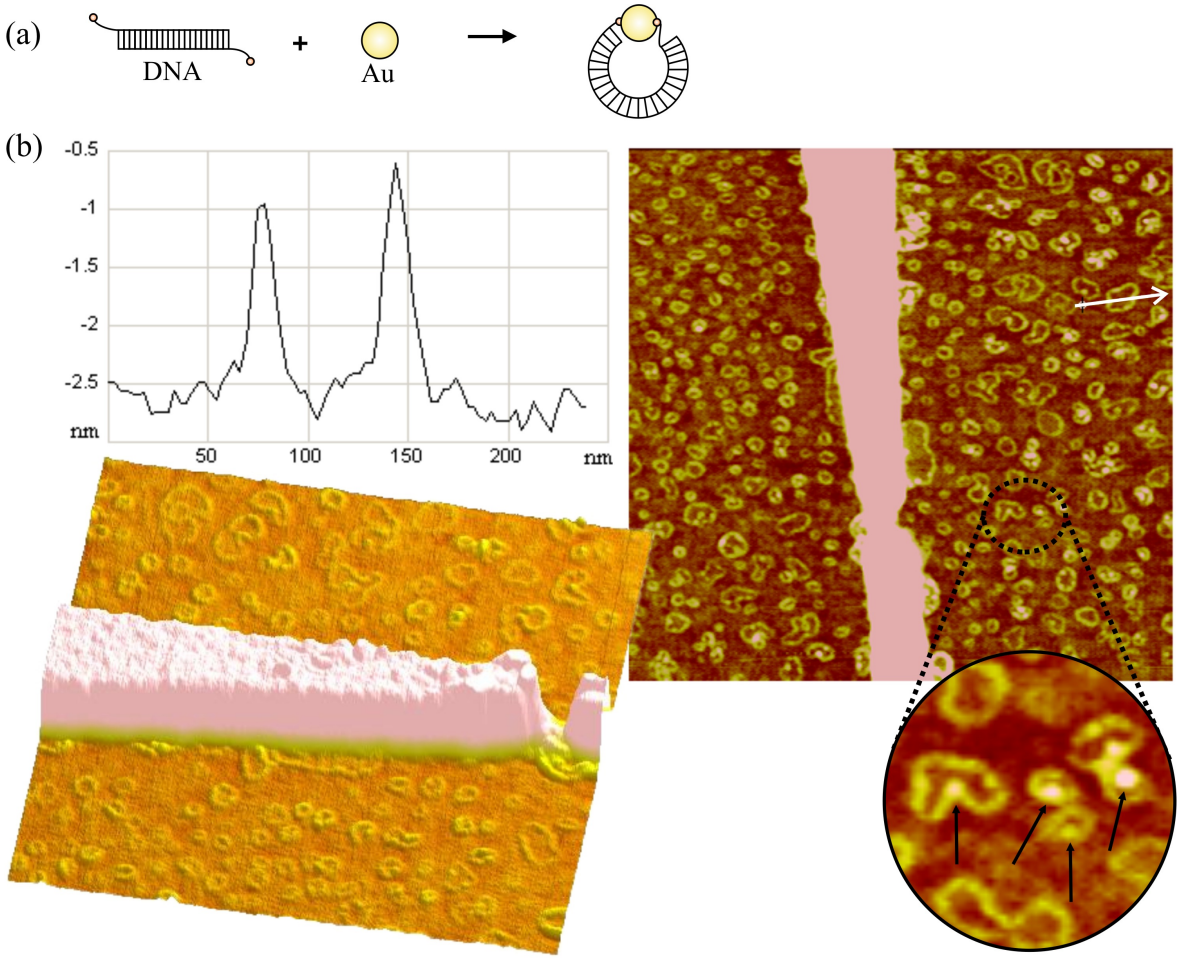

FIGURE 5.9 DNA rings structures observed after the single molecule immobilization experiments using the C6-DNA. (a) Suggested formation of the DNA ring. (b) An AFM image and the height profile (along white arrow) of one of the rings. Black arrows are pointing the 'diamonds in the rings', which are assumed to be gold nanoparticles. Figures are from [142].

5.3.2 DNA rings

Ring-like structures were observed near the fingertip electrode gap in three different samples. Two of the samples were used in the single molecule immobilization experiments with the C6-DNA (for the electrical measurements) and one was used in the immobilization studies of the DTPA-DNA *in situ* under the confocal microscope. An AFM image of the C6-DNA rings are shown in Fig. 5.9(b). It was suggested that this type of ring structures may be formed when both ends of the thiol-modified DNA are attached to a small gold nanoparticle (of diameter of $\sim$4 nm) as shown in Fig. 5.9(a). The gold nanoparticles may be detached from the gold electrodes, since the evaporated gold film is formed of small gold grains which can detach from the electrodes during the DEP (DEP has been widely used for the trapping of gold nanoparticles, see e.g. [37]).

6 Electrical measurements

6.1 Preliminary DEP experiments

In the preliminary DEP experiments, the parallel micro-electrodes with 12 μm separation were used to trap $\sim$16 μm long λ-DNA [1]. After applying 1 MHz signal for a certain time the sample was imaged with AFM and a large amount of λ-DNA networks was observed between the electrodes, which suggested that DEP works very well at least for long molecules.

In the first experiments aiming at the immobilization of a single 414 bp DNA molecule ($\sim$140 nm long) containing thiol-groups (5'-$(CH_2)_6$-SH) in the both ends (see Fig. 6.1), a number of molecules were gathered near the gap between fingertip electrodes [1] . After the optimization of the trapping parameters, samples containing a single or few DNA molecules bridging the electrodes were obtained [2] (discussed in next section).

6.2 Single molecule immobilization

The single molecule immobilization experiments were always performed right after the cleaning of the substrate by incubating a few microliter drop of the DNA solution (see Sec. 4.4.1) onto the substrate containing the nanoelectrodes and keeping the sample in a moist chamber (a closed box containing water in the bottom) to prevent the drop from drying, while applying a sinusoidal ac voltage to the elec-

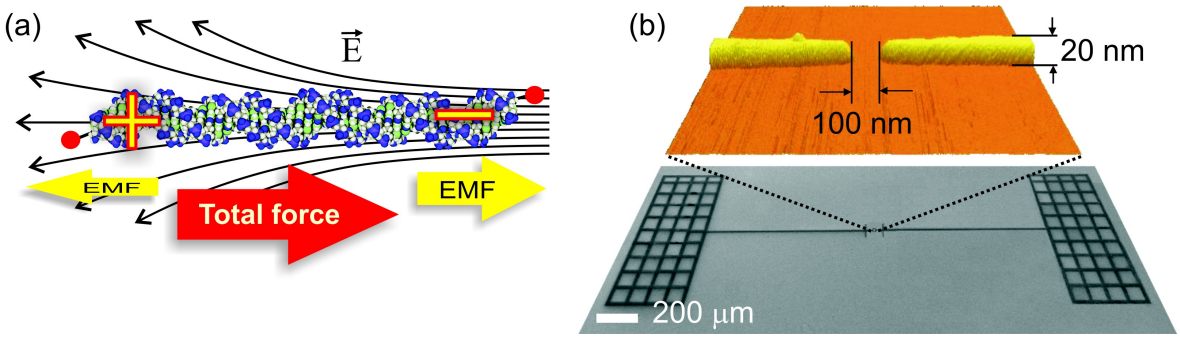

FIGURE 6.1 (a) The principle of DEP of DNA. (b) SEM (lower) and AFM (upper) image of the fingertip electrode structure.

trodes (Agilent 33120A waveform generator). The good parameters yielding single molecules between the electrodes were found to be around the frequency of 1 MHz and the voltage of 3 V_{p-p} (corresponding to the field strength of about 10^7 V/m in the gap). The voltage was applied for 20 min. After DEP, the substrate was rinsed several times with 6.5 mM Hepes and 2 mM NaOH (pH 7.0) buffer to remove excess salts and non-specifically bound DNA from the surface, and N_2 dried.

The excess increase of the electric field strength to strengthen DEP is not favorable, since too high voltage could break the formed sulphur-gold bonds and detach the DNA from the electrode [237]. A high voltage would also induce electrolysis, i.e., chemical oxidation-reduction reactions of the ions on the electrode surface, causing a finite current via the buffer, which further induces a lot of heat to the gap region and thus can cause denaturation of the immobilised DNA molecules. With the frequencies sufficiently lower than 1 MHz, the electrophoretic effects begin to overcome DEP thus reducing the trapping, as was observed in the confocal microscope studies (see Ch. 5). Whereas, when using frequencies higher than 1 MHz, the DEP force decreases, which can be understood by means of the frequency dependence of the polarizability of the DNA (relative to buffer components) [3, 4, 15, 16] due to the lower time-scale of the counter-ion polarisation (see Sec. 5.2). After the optimization of the DEP protocol, e.g., the use of low DNA concentration and a low conductivity buffer containing the reduction agent, the samples containing an individual DNA molecule bridging the electrodes were obtained (see Fig. 6.2) [2].

After the immobilization of DNA the samples were characterized using AFM imaging. AFM was used in tapping-mode in order to prevent the tip-induced damage on the DNA. In addition to a topographic image, the intermediate interactions between the tip and the surface in tapping-mode provide amplitude and phase images, which can be used to distinguish different features from the sample. The DNA as a soft material compared to the substrate and the electrodes is particularly distinguishable in the phase image (*phase-contrast imaging*, see e.g. [71]), which reveals the variations in material properties, such as adhesion, elasticity and viscoelasticity.

6.3 Hexanethiol-modified DNA

The AFM images of four samples containing different number of hexanethiol-modified DNA molecules, i.e., one, two or three individual molecules or a small DNA bundle, are shown in Fig. 6.2. Imaging took place in ambient conditions (RH ∼30 %). Thickness of the individual molecules on the dry SiO_2 substrate was measured to be about 1 nm (see Fig. 6.2(a)-(c)), while the thickness of a bundle was about 6 nm (see Fig. 6.2(d)). The sample with three individual molecules in Fig. 6.2(c) imaged after the electrical measurements showed the thickness of about 2 nm (see Fig. 6.2(e)). The increase of the height is most likely due to the gathering of contaminants from the air during the measurements.

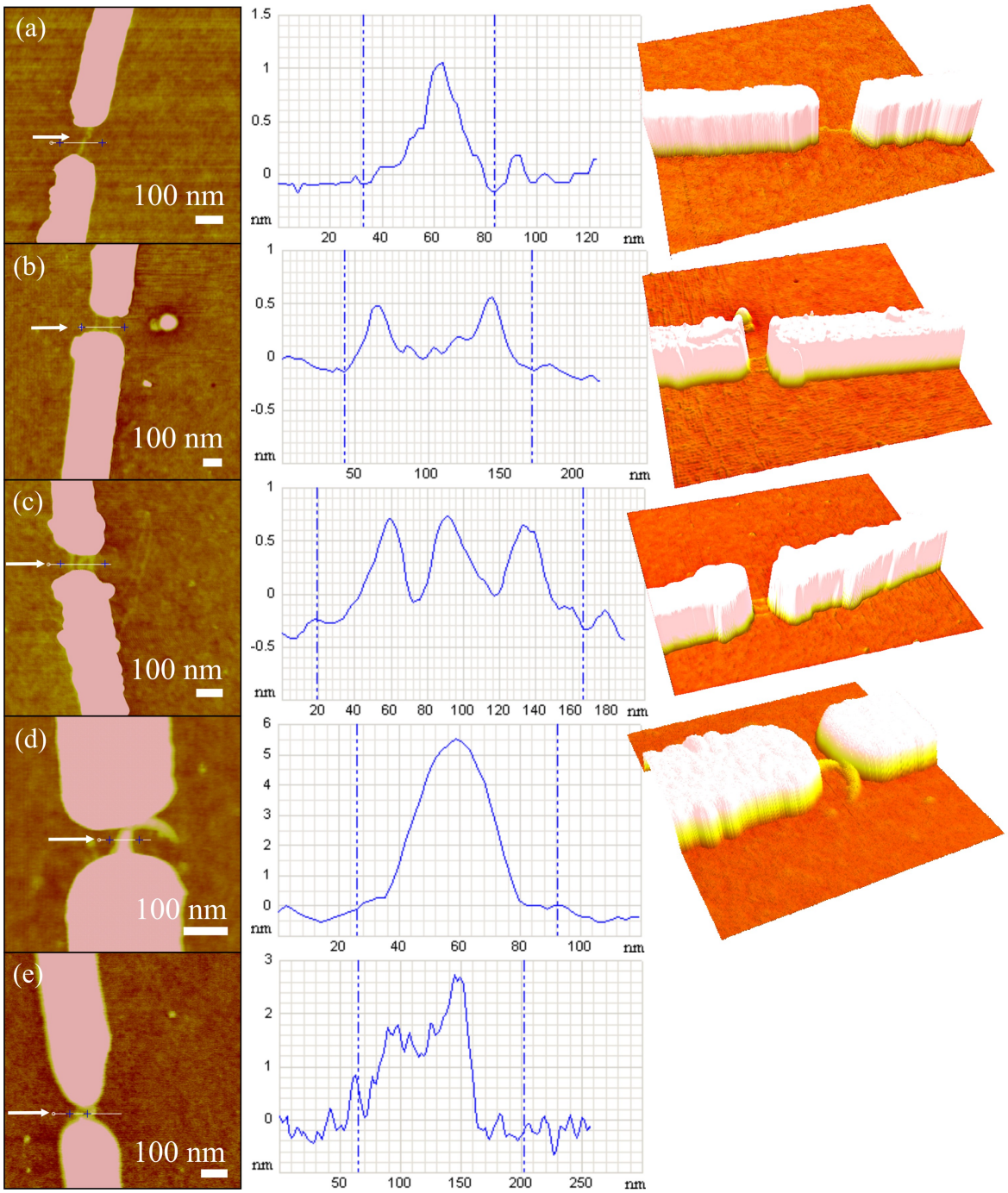

FIGURE 6.2 AFM images and height profiles of the DNA samples. (a) One, (b) two and (c) three individual DNA molecules and (d) a small DNA bundle attached between the fingertip electrodes. (e) The sample shown in (c) after the electrical measurements.

After the AFM characterization of the samples, the elecrical measurements were performed first in a 'dry' environment (relative humidity ∼30 %) and then in a 'moist' environment (relative humidity 80-90 %). The I-V characteristics of two of the samples (Fig. 6.2(c) and 6.2(d)) are shown in Fig. 6.3.

6.3.1 Dry DNA on the substrate

In the dry environment, all the samples showed insulating behaviour as seen from the Fig. 6.3(a)-(b). The I-V curves are linear with the resistance of tens of TΩ (except a few TΩ in the case of a DNA bundle). These results are in agreement with most of the results observed by other groups (see Sec. 2.3.3). Since the thickness of a dry DNA on the substrate was ∼1 nm (as observed in Fig. 6.2), its helical structure is strongly deformed deteriorating the π-orbital overlap between the bases. The deformation may be caused by the surface-molecule interactions [120] or the dehydration of a DNA in ambient conditions (RH ∼30 %). A dramatic dehydration of the DNA may also happen due to the nitrogen flow used for drying of the sample, which usually results only two or three water molecules per base pair [242].

6.3.2 The effect of humidity on the electrical conductivity

After the measurements in dry conditions, the sample was placed in the humid chamber. Several I-V curves were measured simultaneously with the slowly raising humidity. It was observed in five different samples, which contained a single or a few C6-DNA molecules bridging the electrodes, that the conductivity was clearly enhanced showing the resistance dropping to hundreds of MΩ, which is two orders of magnitude below the level of the reference samples in moist environment (the samples undergone the same procedure except that no DNA was used, see Sec. 6.4). However, some of the DNA samples behaved similarly to the reference samples, indicating that the DNA was not properly attached to the both electrodes or not conducting for some other reason, e.g., the structure of DNA was severely deformed.

The sample with three parallel molecules

As a detailed example, the sample with three molecules bridging the electrodes in Fig. 6.2(c) showed the minimum resistance of ∼250 MΩ after being 15 minutes in moisture (red filled circles in Fig. 6.3(a)). By using the approximate diameter of 2 nm and length of 140 nm, one can calculate the maximum conductance σ_{moist} ∼0.8 S/cm in the moist conditions (σ_{dry} ∼$1.6 \cdot 10^{-5}$ S/cm in the dry conditions). After this, the resistance of the sample slowly increased showing ∼700 MΩ after three hours in moisture (blue open circles in Fig. 6.3(a)). When the sample was dried with nitrogen and measured again in the dry environment, it showed again the resistance of tens

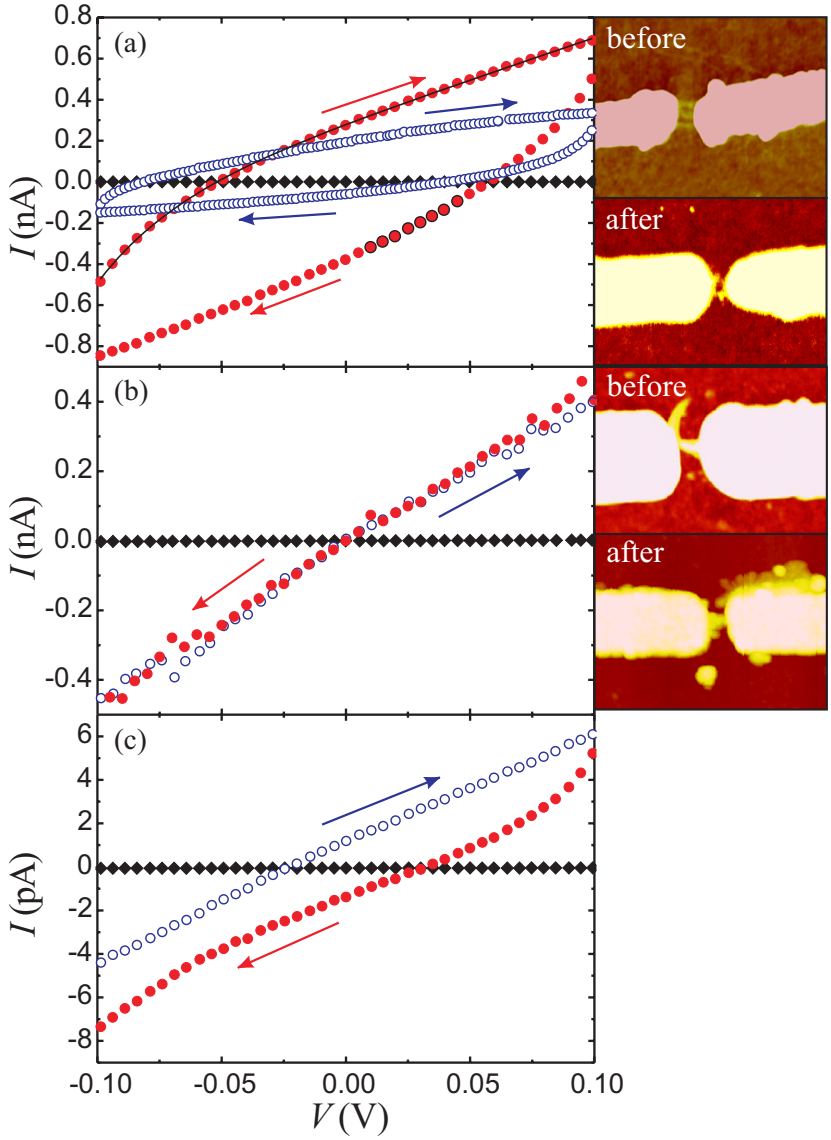

FIGURE 6.3 The I-V characteristics measured in the dry and the moist environment (a) for the sample shown in Fig. 6.2(c), and (b) for the sample shown in Fig. 6.2(d). The AFM images before and after the measurements are shown on the right side of I-V curves. (c) The I-V curves from the reference sample (without DNA). Black diamonds are measured in the dry conditions and circles in the moist conditions. In (a) the red filled (blue open) circles are measured after 15 minutes (3 hours) in moisture. Solid line in (a) is a fit to Eq. 6.1, which describes the charging effect.

of TΩ. In the AFM image taken after the measurements (see Fig.6.3(a)), one can see that at least two molecules are still bridging the electrodes.

After the intentional AFM imaging with a high tapping force, during which the DNA was 'scrathed' away from the gap, the sample showed in the moist conditions the minimum resistance of ∼7 GΩ, which is similar to the value observed in the reference samples. This indicates that it was the molecule itself where the low resistance originated from and not the environment.

The DNA bundle

Another sample, containing ∼6 nm high DNA bundle (see Fig. 6.2(d)), showed the resistance of ∼40 GΩ shortly after placing in the moist environment. After the sample was kept over ten hours in moisture, the resistance was dropped to ∼250 MΩ (circles in Fig. 6.3(b)), giving the conductance of σ_{moist} ∼0.1 S/cm in the moist conditions (σ_{dry} $\sim 0.6 \cdot 10^{-5}$ S/cm). After the sample was dried completely the resistance increased back to a few TΩ that was observed prior to the measurements in the moist environment. The AFM image after the measurements shows that the DNA bundle was still in place (see inset in Fig. 6.3(b)). It was observed that the conductivity enhancement in the moist environment in the case of the DNA bundle was much slower than in the case of the sample containing three individual molecules (discussed in Sec. 6.5).

6.4 Reliability checks

As can be concluded from the earlier DNA conductivity measurement discussed in Sec. 2.10 the performing of a reliable experiment on a single molecule level is very challenging. Due to this, the reliability of such experiments must be confirmed by performing careful control experiments.

During the immobilization of DNA using DEP, the contaminants and ions in the buffer can gather to the gap instead of DNA. These gathered substances may be misinterpreted as a DNA molecules when observed in the AFM image, particularly when characterizing the nanometer scale objects. Also, the contaminants are often gathered during the electrical measurements, especially in the moist conditions. However, these gathered substances are usually not of a regular shape, such as the DNA molecules, which have a rod-like shape and a certain length and height, and thus distinguishable quite easilly.

AFM imaging

To rule out the contribution of the possible contaminants to the observed conductivity, AFM images were taken right before and after the electrical measurements, in order to check that both the DNA and the electrodes were still in place and no major deformations were observed. In the AFM images taken after the DNA immobilization, only the objects of clearly regular shape are interpreted as a DNA molecule.

Normally, the gathering of the contaminants rather decreased the conductivity than increased it. However, it was observed in some cases that the electrodes were burned during the DEP immobilization or the electrical measurements, especially under the moist conditions. The burned residues on the substrate sometimes gave nice looking I-V curves, that were clean of noise, symmetric with respect to the

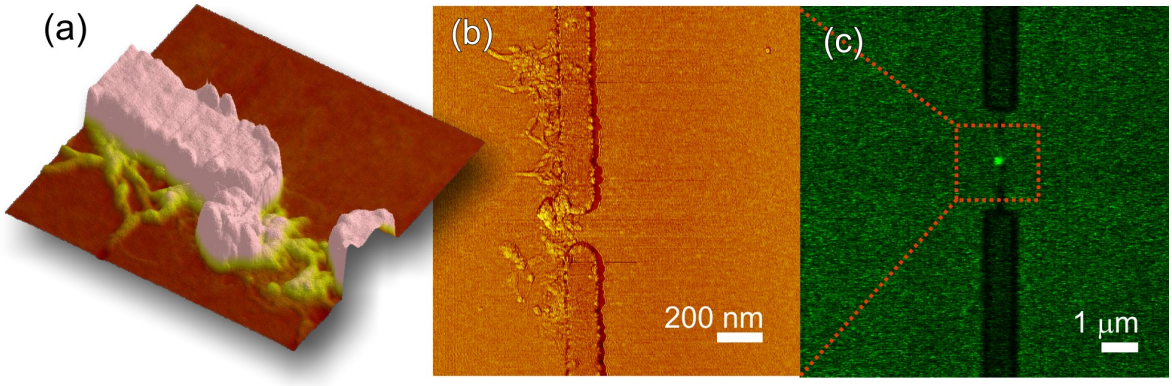

FIGURE 6.4 DNA labelling after immobilization. AFM (a) topography and (b) phase images. (c) Confocal microscope image of immobilized DNA near the electrodes. Green fluorescence is due to dsDNA specific dye attached to the immobilized DNA.

voltage and showed either insulating, semiconductive or conductive behaviour. To avoid this kind of misinterpretations, AFM imaging after each step is indispensable.

Confocal microscope imaging

To further check that the elongated, regular shaped objects observed in an AFM image are really DNA and not some contaminant, the confocal microscope and a double-stranded DNA specific fluorescent dye was used. When it was observed in the AFM image that there were several molecules immobilized near the gap (because the fluorescence of a single ∼140 nm dsDNA molecule cannot be distinguished in a confocal microscope image), the samples were labelled afterwards with PicoGreen dye and imaged with the confocal microscope. The AFM and the confocal microscope images from one of the samples are shown in Fig. 6.4, which verifies that the material in the gap indeed is DNA.

Reference samples

To exclude the contribution of the humid environment and the gathered buffer salts from giving rise to the observed conductivity, the control measurements were performed. For this purpose we used the 'reference samples', which were similar samples as used for DNA immobilization (i.e. contained a fingertip nanoelectrode structure) and were undergone the same procedure as the 'real' DNA samples, i.e., the DEP immobilization, the electrical measurements and the AFM imaging before and after the measurements, except that instead of DNA solution, only the buffer solution was used in the immobilization step.

I-V curves from a typical reference sample is shown in Fig. 6.3(c). The curves show a clear difference between the dry and the moist environment measurements. The resistance in dry environment was always around ∼10 TΩ as in the case of

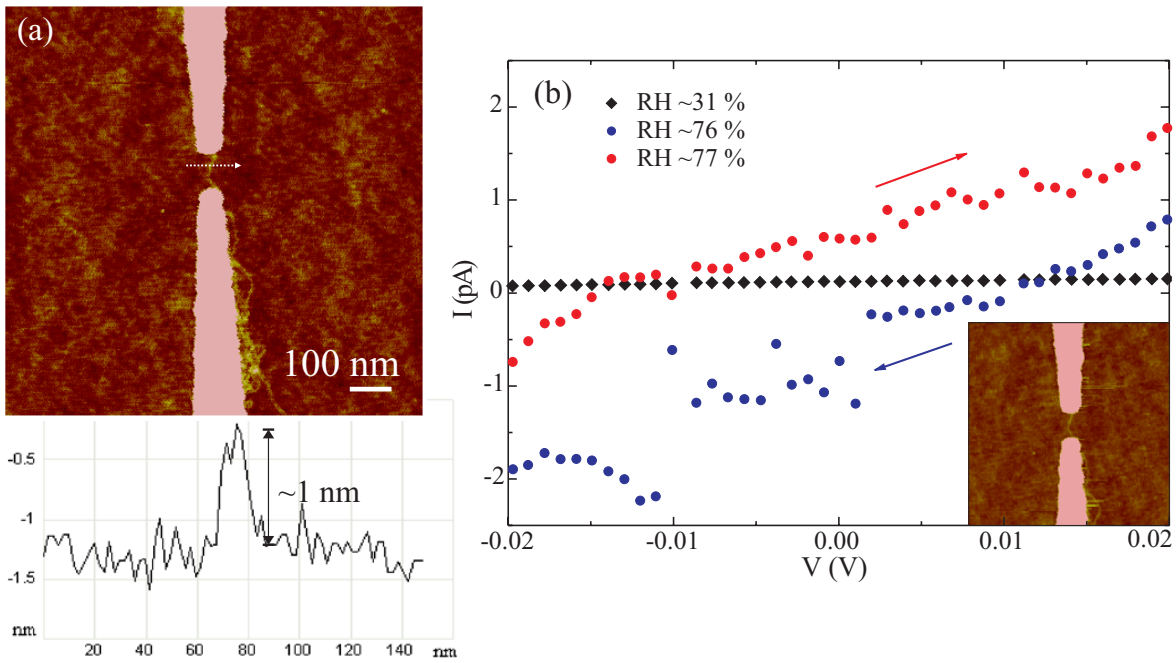

FIGURE 6.5 Reference measurement using the DNA shorter than the gap size. (a) An AFM image with height profile of the ~150 bp DNA and (b) the *I*-*V* curves (AFM image after measurement in the inset).

DNA samples. However, in the moist conditions, the minimum resistance observed for the reference samples was ~7 GΩ, i.e., about two orders of magnitude higher than in the case of conducting DNA sample.

Short DNA reference

Control measurements were also performed by using the DNA molecules which were much shorter than the gap between the electrodes, so that a single molecule cannot form a bridge between the electrodes. About 150 bp (~50 nm) PCR product was used in these measurements. Several fabricated samples containing DNA in the gap were measured but none of them showed conductivity enhancement with humidity. One of the samples, which have the resistance of ~16 GΩ in moist environment, is shown in Fig. 6.5. Sample looked the same after the electrical measurements.

6.5 Mechanism of the conductance

The number of samples, the AFM imaging before and after measurements, the confirmation of the presence of DNA using fluorescence confocal microscope, and the comparison to the reference samples using buffer without DNA, all together, provide strong evidence for the effect of moisture on the electrical conductivity of single

DNA molecules. Conductances calculated (approximately) for a small DNA network or a bundle were σ_{moist}0.1 - 0.2 S/cm and σ_{dry} $\sim$0.6 $\cdot 10^{-5}$ S/cm and for an individual DNA molecules σ_{moist}0.6 - 1.3 S/cm and σ_{dry} 1.6 - 2.5 $\cdot 10^{-5}$ S/cm. However, the nature of the conductivity cannot be unambiguously concluded.

Possible conduction through an absorbed water layer

The humidity enhanced conductivity of a DNA has been earlier explained by the contribution from an absorbed water layer around the DNA. The conduction by means of dipole relaxation losses of water molecules [34, 35] contributes only to ac currents and is not relevant in our case. Another option is proton transfer [86, 196], i.e., the dissociation of the water molecules in a hydrogen bonded water chain. Absorbed water layer may also provide a nano-scale conduction path for the ions (in the buffer) [239]. However, the last two proposed processes need reduction-oxidation reactions to occur at the electrodes, which is negligible in our experiments because of the low voltages used (also discussed in [265]).

Even if the conduction had an ionic origin, it might be incorporated into the helical conformation of DNA, which is strongly related to the amount of the absorbed water molecules, e.g., at least 13 water molecules per base pair are needed to preserve DNA in the B-form [250]. It has been shown that a single dsDNA on a graphite surface appears in its natural B-form at moist conditions, whereas it collapses to a form resembling A-DNA when dried to the surface [275]. In the dry conditions (RH $\sim$30 %) we also observed the reduced height of DNA corresponding to its deformed state (see Fig. 6.2). On the other hand, the absorbed water layer and counter-ions may have an important role in the conductivity of B-DNA, due to their possible doping effect [18, 64].

Hysteresis in I-V curves

The ions, i.e., the counter-ions, the buffer ions and the dissociated water ions, do not substantially contribute to the total steady-state dc current due to the lack of possible reduction-oxidation reactions, but they add an extra capacitive element to the equivalent circuit of the sample. The equivalent circuit of the sample consists of the resistances of the DNA (R_{DNA}) and the substrate ($R_{\mathrm{substrate}} \gg R_{\mathrm{DNA}}$, giving only a small leakage current and can be neglected) in parallel with the total capacitance of the sample (C_s), which includes the ions and the capacitance of the electrode structure. The resistance of wiring and the voltage source (R_s) is in series with the equivalent circuit of the sample shown in Fig. 6.6(a). The hysteresis caused by the diffusion of the ions to the surface of the electrodes, especially in the moist environment, was observed in the experiments and fitted to the theory [129]. In the case of a step-like dc bias voltage shown in Fig. 6.6(a), the behaviour can be described by

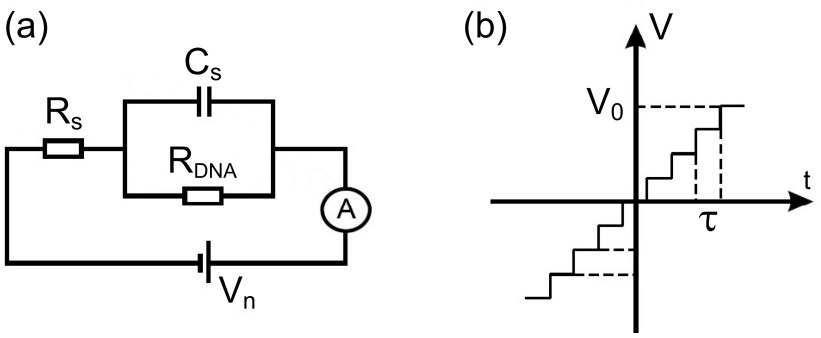

FIGURE 6.6 (a) An equivalent circuit of the measurement setup. (b) A step-like voltage bias sweep.

function

$$I = I_c + \frac{V_{\mathrm{n}}}{R_{\mathrm{DNA}}} + I_0 \alpha \frac{1-\alpha^n}{1-\alpha}, \tag{6.1}$$

where n is the number of performed voltage steps and V_n is the bias voltage corresponding to the present point. Other parameters are: I_c the device dependent constant leak current, I_0 the maximum charging current (depending on the voltage source used) and $\alpha = e^{-\tau/\tau_{\mathrm{c}}}$ is the exponential ratio between stabilization time τ, i.e., waiting time between a voltage change and the subsequent current measurement (see Fig. 6.6) and time constant of charging $\tau_{\mathrm{c}} \approx R_s C_s$. The derivation of the equation is performed in [135]. The fit of function in Eq. 6.1 to the experimental data is shown by black line in Fig. 6.3(a). The obtained time constant, τ_{c}, in that particular sample was of the order of 30 s in that case. However, in the case of DNA bundle the observed time constant was much less than the stabilization time (τ = 5 s) since it showed no hysteretic behaviour (see Fig. 6.3(b)). The source of a high variance in the hysteretic behaviour of the samples is somewhat unclear, but is most likely related to the different amounts of the salts dried on the substrate during sample preparation.

DNA conformation change

For a simple ionic conduction it would be enough to have a water layer present at the surface of the object, which contradicts with the slower time-scale of the humidity enhanced conductivity observed in the case of DNA bundle compared with a sample containing three individual molecules (see Sec. 6.3.2). One possibility is that the humidity enhanced increase in the conductivity may be related to the humidity enhanced conformational change, from a dehydrated form (i.e. A-DNA or denaturated DNA) back to the B-form, which provides improved π-stacking (discussed in Sec. 2.10). The slower time-scale of the humidity enhanced conductivity in the case of a bundle may be explained by the decelerated recovery of the helical conformation of the accumulated molecules inside the bundle, which may be also bonded

to each other by non-specific interactions. Also the increase of the conductance at the moist conditions only in some of the samples containing DNA suggests that a charge transfer/transport is highly sensitive to the conformation of DNA, which would not be the case in the ionic conduction possible also through the water layer on even deformed molecule.

Another indication of conductivity being due to the humidity enhanced conformational change is the increase of the resistance during the moist measurement of the sample containing individual molecules, which was not observed in the case of the bundle. This deterioration of conductivity may be due to the collecting of contaminants from the moist air, which can destroy the integrity of the helical conformation of individual DNA molecules very fast. However, in the case of the bundle, which is composed of several parallel helices, the outermost molecules help the inner molecules to keep the water inside and protect the inner molecules from the gathering of contaminants, thus making their helical conformation more stable and robust. The gathering of contaminants during the measurements can be observed as an increased height of the molecule in AFM image taken after the measurements (see Fig.6.2(e)).

Our results are consistent with the resistance values observed in buffer for λ-DNA by Tran *et al* (they obtained $\sigma_{\mathrm{inbuffer}}$ $\sim$2.4 S/cm and σ_{dry} $\sim$0.4 S/cm, where 15 % of the weight of dry DNA was due to water and counterions) [242] and for short synthetic 8-14 bp long duplexes by Xu *et al* (they obtained $\sigma_{\mathrm{inbuffer}}$ $\sim$0.9 S/cm) [265]. This suggests that the hydration layer around the dsDNA in a high humidity environment enables similar behaviour as the buffer environment, e.g., maintaining the double helical conformation of the B-DNA. DNA conductivity being sensitive to helical conformation of the DNA may also explain most of the results showing the highly insulating behaviour for the DNA (discussed in Sec. 2.3.4).

6.6 The molecule-electrode contact

To obtain more consistent information about the conductivity of DNA itself, a direct electrical contact between the molecule and the electrodes is needed. It has recently been shown that the molecule-electrode contacts have a dominant role on the electrical characteristics of the molecule (discussed e.g. in [100]).

Conductance of the hexanethiol-linker

The observed conductance in the measurements may be limited by the use of hexanethiol-linkers, which is supposed to be highly resistive. The resistances of alkanethiol (or alkanedithiol) molecules of different lengths have been measured by many groups using conducting AFM or STM either in a toluene solution [50, 264, 279] or in ambient conditions (which have a certain relative humidity, usually 30-50 %) [23, 263].

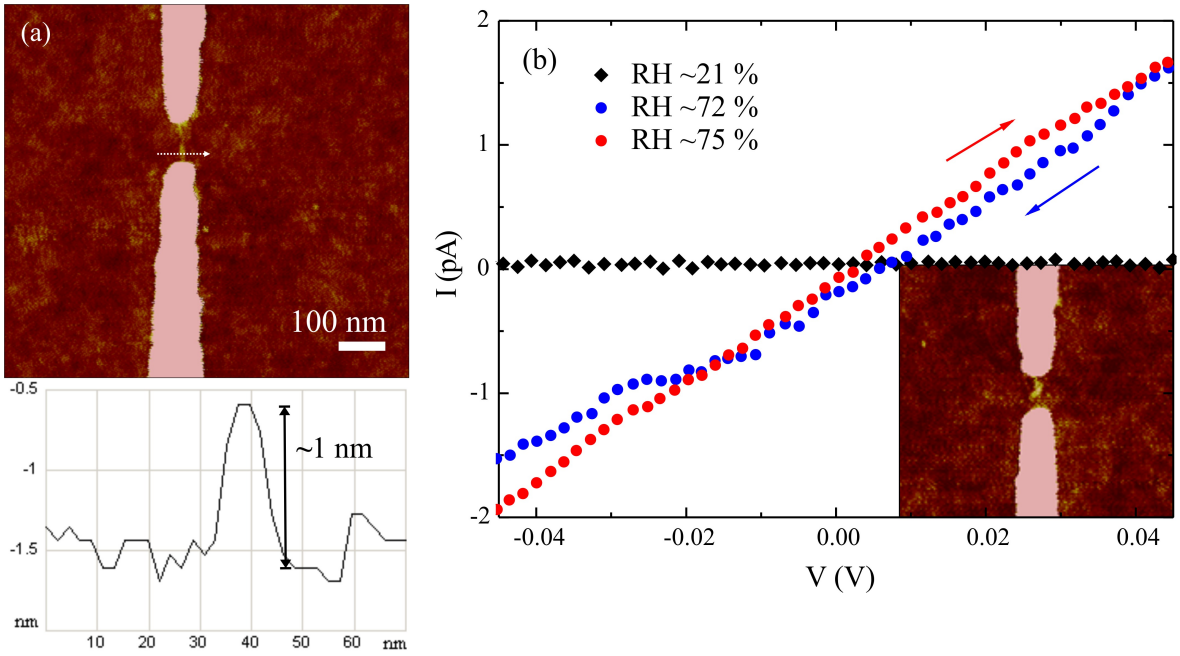

FIGURE 6.7 (a) An AFM image with height profile for the sample containing a single DTPA-DNA molecule and (b) the I-V curves obtained in different humidities (AFM image after measurement in the inset).

Toluene, which is an oxygen-free organic solvent, has higher resistivity than water, which minimizes the contribution of the leaking current through the solution.

The resistance values obtained for the hexanethiol-group vary from ∼10 MΩ [23, 263, 264] to ∼100MΩ [279], but do not change subject to the used environment. According to this, the possible leaking current through the humid air does not have a high contribution to these obtained resistance values, at least when using small dc voltages (maximum 100 mV dc voltage was used in our measurements). The contribution of the water vapor to the possible enhancement of a tunneling current through the hexane is negligible, since the alkane-chain is quite inert as such and the surrounding water vapor is not supposed to affect its conductivity much. The dc resistance of an individual hexanethiol-linker under the high humidity (RH ∼90 %) is not known, but it is most likely at least about 10 MΩ, which was found in a recent and the most reliable measurements by Xu *et al* [264]. Thus, the real conductivity of the DNA itself may be lower than the observed I-V curves show.

DTPA-modified DNA

We studied the contribution of the molecule-electrode contact on the observed conductivity of the ∼140 nm long DNA molecules by using a different type of 5′-modification as a linker instead of the hexanethiol discussed in Sec. 6.3. Since any of the commercially available 5′-modifications are not designed for the charge migration applications, we choose the most promising one by intuition. DTPA-modifi-

cation, shown in Fig. 4.2(b), contains two sulphur-atoms, in order to provide a better bonding to a gold electrode, and a shorter alkane-chain between the sulphur-atoms and the 5'-end phosphate group, which further would have a lower resistance. In addition, the DTPA-linker brings the DNA π-stack closer to the electrode surface, which could induce a direct contact between the molecular orbitals and gold surface states.

DEP immobilization and the electrical measurements were performed using DTPA-DNA similarly as in the case of C6-DNA and individual molecules bridging the electrodes were obtained in tens of samples. All the measured DTPA-DNA samples showed in the dry conditions again the resistance of order of 10 TΩ, whereas in the moist conditions the lowest observed resistance was as high as $\sim$4 GΩ, i.e., the behaviour is similar to the reference samples (see Sec. 6.4). AFM images and the I-V characteristics for one of the DTPA-DNA samples, showing the resistance of $\sim$25 GΩ in the moist conditions, is shown in Fig. 6.7.

The lower conductivity observed for the DTPA-DNA relative to the C6-DNA can be qualitatively explained by the results obtained from the DFT-calculations (see Sec. 4.8). A lower binding energy was obtained for the DTPA-linker (E_b = 1.2 eV) compared the case of the hexanethiol-linker (E_b = 1.8 eV), which may result in the worse electrical contact in the case of the DTPA-linker. It was also observed in the DEP immobilization studies performed under confocal microscope, that the C6-DNA is attached better than the DTPA-DNA (see Sec. 5.3).

Conducting DNA-linker

By using a shorter linker, e.g., the DTPA-linker, it is possible to bring the π-stack into the vicinity of the electrode surface. However, it is not clear how the molecular orbitals, e.g., the π-orbitals of the bases, bond with the gold surface states, which finally determines the nature of the contact. In order to form an electrical contact in this way, the distance between the gold atoms and the stacked bases should most probably be of less than $\sim$5 Å (the optimum distance for π-orbital overlap between aromatic bases is 3.4 Å). In the case of insulating linker, this is the only way to form an electrical contact.

A more reproducible approach towards the electrically conducting molecule-electrode contact is to utilize the chemical binding to electrodes, e.g., thiols [100], but use a conducting spacer, e.g., conjugated polymers, instead of the insulating alkane-chains, such as the hexanethiol. However, also the thiol-group may bound to the gold surface, i.e., Au(111), in several different ways, which can yield to a highly different electrical properties of the contact [20].

In the ongoing research (PhD. student Kaisa Helttunen, NanoScience Center, University of Jyväskylä) a new type of DNA-modifications are designed and fabricated using a chemical synthesis in order to investigate their electrical properties when used as a DNA-linker.

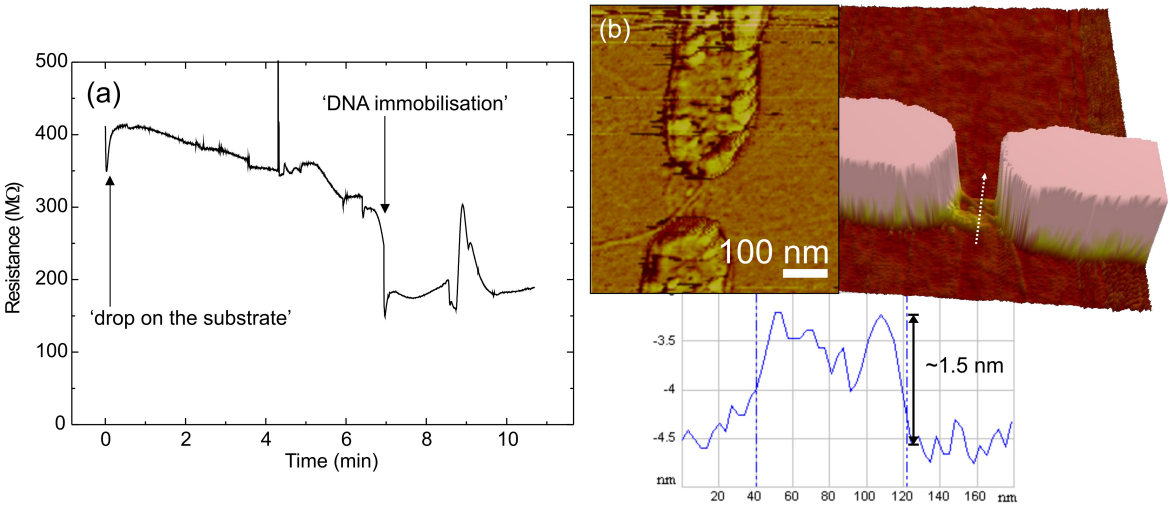

FIGURE 6.8 Monitoring of the C6-DNA immobilization by measuring the 0.1 Hz ac-current. (a) The ac-resistance of the sample during the DEP trapping. (b) AFM images (phase image and 3D height image) with a heigh profile after the DEP.

Since the conventional DNA-linker are attached to 5'-end, there is a phosphate and sugar groups between the linker and the nearest base which may not offer a sufficient contact to the π-stack. An optimal linker in order to study the electrical properties of DNA might have at least the following features: (1) The linker is composed of at least $\sim$1 nm long conductive polymer chain, which would function as a spacer in order to prevent the surface interactions from harming the stacking of the bases, and (2) the linker would be directly attached to the last base of the stack, which would preferably be a Guanine. The feature (2) has already been implemented in the work by Zhang *et al* [276, 277], where they incorporated a modified nucleotide, i.e., 4-thiothymidine-5'-trithiophosphate (S^4-dTTP), in the both ends of λ-DNA. They observed highly insulating behaviour, which is most likely due to use of $\sim$16 μm long molecule lying on the substrate and measurements performed in a high vacuum. Also the attachment of the base directly to the electrode may be disadvantageous in that case.

6.7 DEP monitoring results

The attachment of the DNA molecules during the DEP trapping can be monitored by measuring the current through the sample using one of the following methods: (1) low frequency ac and lock-in technique or (2) a small dc offset in the DEP signal as discussed in Sec. 4.4.3 (see Fig. 4.5).

As an example of the DEP monitoring by using method (1), a slow ac excitation of frequency, f_{AC} = 0.1 Hz, and voltage, V_{AC} = 140 $\mathrm{mV_{p-p}}$, was applied onto the DEP signal, i.e., frequency, f_{DEP} = 750 kHz, and voltage, V_{DEP} = 2 $\mathrm{V_{p-p}}$. Since the

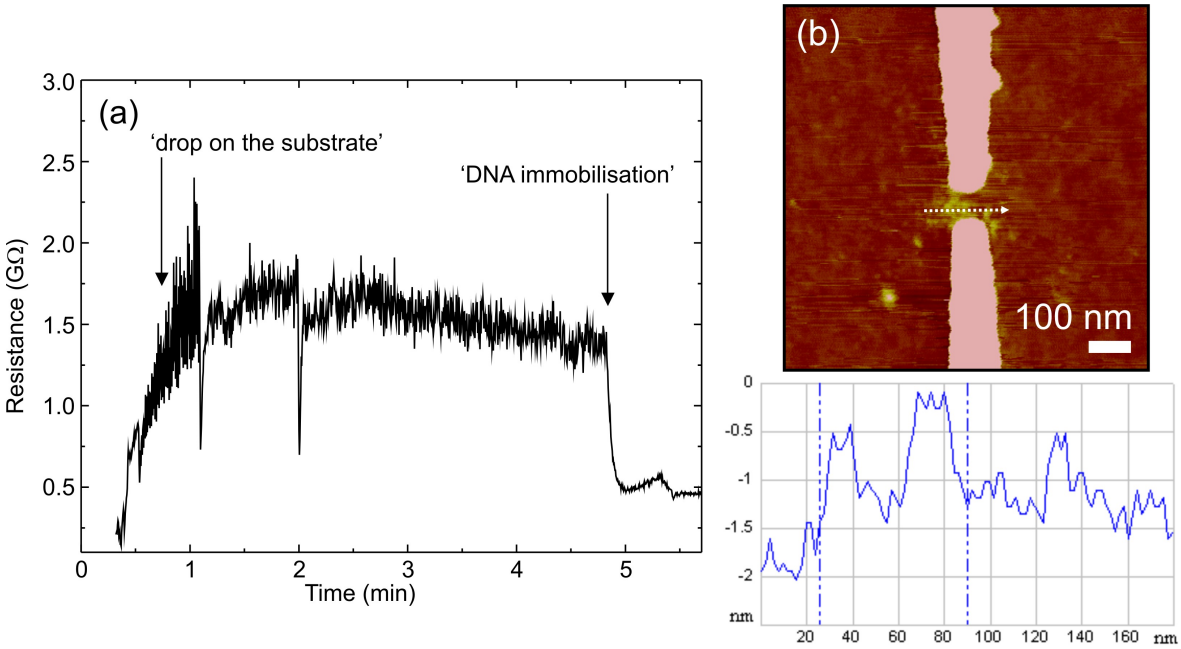

FIGURE 6.9 Monitoring of the DTPA-DNA immobilization by measuring the dc-current. (a) The dc resistance of the sample during DEP trapping. (b) An AFM image and heigh profile after DEP.

fingertip electrode sample containing a drop of DNA solution of the substrate is highly capacitive (due to the buffer ions), we desired to use as low ac frequency as possible in order to distinguish as high parallel dc resistances as possible. We observed that f = 0.1 Hz was the lowest frequency using which a stable response was obtained. The ac current observed during the DEP trapping of the C6-DNA is shown as a function of time in Fig. 6.8(a). In the beginning, the measured ac-resistance was ∼450 MΩ and after a jump, which was interpreted as a molecule attachment, the resistance was ∼185 MΩ. After the DEP, a few molecules were immobilised between the electrodes as observed in Fig. 6.9(b). In the subsequent I-V measurements, the sample showed resistances of ∼5 TΩ in the dry conditions and a minimum ∼4 GΩ in the moist conditions, and thus, did not exhibit a drop of resistance to hundreds of MΩ in moisture as some C6-DNA samples discussed in Sec. 6.3. Since the sample showed a resistance of ∼185 MΩ during DEP, the molecule may be deformed during drying of the drop and AFM imaging before the I-V measurements.

As an example of DEP monitoring using setup (2), a small dc-offset, V_{DC} = 140 mV, was applied onto the DEP signal, i.e., frequency, f_{DEP} = 1 MHz, and voltage,V_{DEP} = 3 V_{pp}. A series resistance, R_s = 10 MΩ, was used to limit the maximum current not to burn the molecules. The 1 MHz DEP signal was grounded after sample using a capasitance, C = 1 nF. The monitoring current during the DEP trapping of the DTPA-DNA is shown in Fig. 6.9(a). The resistance suddenly jumped from the original ∼1.5 GΩ to ∼500 MΩ, which may be interpreted as an immobilization of a DNA molecule between the electrodes. After the DEP, there were some molecules observed in the

AFM image shown in Fig. 6.9(b). However, several other samples showed the resistance of hundreds of MΩ in DEP monitoring already right after the drop of DNA solution was placed on the substrate (before the DEP voltage was turned on), which makes the observed jump in Fig. 6.9(a) not reliable. In the I-V measurements, the sample in Fig. 6.9(b) showed resistances of ∼20 TΩ in dry conditions and a minimum ∼13 GΩ in the moist conditions, like observed before for the DTPA-DNA (see Sec. 6.6).

One can conclude that the drop (from 1 to 8 μl) of buffer solution on the substrate yields too high contribution to the observed current and the attachment of single DNA molecules could not be unambiguously distinguished using either the low-frequency or the dc-offset as the monitoring signal. In addition, the monitoring current contains small fluctuations due to, e.g., the evaporation of the buffer, which makes the observation of a single DNA molecule immobilization very difficult. If the conductance of the molecules could be enhanced, e.g., by using DNA doping, or the measurement setup could be more stabilized it might be possible to observe a single DNA immobilization. However, the further optimization of DEP monitoring setup was not possible in the contents of this work.

6.8 PicoGreen enhanced conductivity

The AFM imaging and the electrical measurements were also performed for the samples already used in the DEP studies under the confocal microscope (discussed in Ch. 5). The essential difference in this case is that the DNA used in the confocal experiments is labelled with the PicoGreen fluorescent dye. The resistance in the dry environment (RH ∼30 %) was always order of tens of TΩ, as before in Sec. 6.3 and 6.6. However, in the moist environment the samples containing PicoGreen labelled DNA showed much lower resistance than the samples containing unlabelled DNA (observed for both the C6-DNA and the DTPA-DNA).

One of the samples obtained from the DTPA-DNA immobilization under the confocal microscope shown in Fig. 6.10(a) contained several individual (PicoGreen labelled) molecules in parallel (although there is also some contamination spot between the electrodes). The I-V curves were measured simultaneously with the increasing or decreasing humidity (see Fig. 6.10(b)). In the moist environment, the sample showed the minimum resistance of ∼95 MΩ. The resistances obtained in different humidities, shown in Fig. 6.10(c), almost fit to the exponential function (a line, when y-axis in logarithmic scale). The humidity in the chamber was decreased by purging the chamber with a low N_2 flow, which may cause a dramatic dehydration of the DNA [242] inducing a fast deterioration of conductivity.

The enhancement of the conductivity was also observed for several other samples, which were labelled with PicoGreen after the immobilization. For instance, for a sample containing DTPA-DNA (unlabelled) shown in Fig. 6.9, a minimum resis-

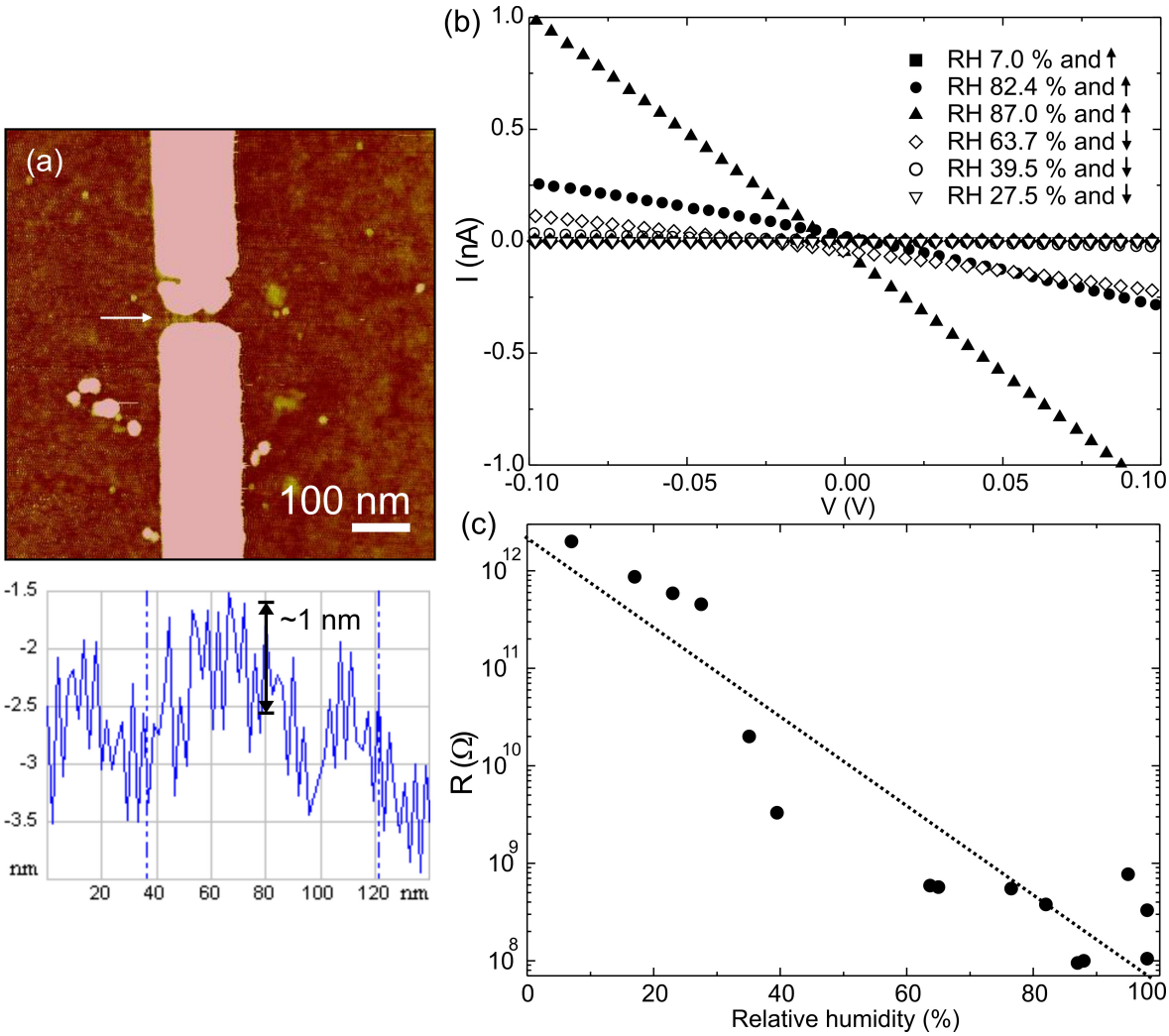

FIGURE 6.10 (c) An AFM image and a height profile from the sample containing several parallel DTPA-DNA immobilized under the confocal microscope. (b) I-V curves measured simultaneously with increasing or decreasing humidity (see arrows after humidity). (c) The resistances obtained from the I-V curves plotted as a function of the humidity and the linear fit showing approximately exponential decrease of the resistance as a function of the humidity.

tance in the moist conditions was ∼13 GΩ. After keeping the sample over night in the PicoGreen solution (1/100 diluted into Hepes/NaOH buffer) the minimum resistance in the moist environment had dropped to ∼200 MΩ. The resistance observed in this case was about the same as in the samples measured after the confocal microscope DEP experiments.

The PicoGreen enhanced conductivity was not observed in the reference samples, i.e., the clean fingertip electrode samples kept in Hepes/NaOH buffer which contained PicoGreen dye over night and then flushed with N_2. The resistance of these reference samples were a few TΩ in the dry environment and tens of GΩ in the moist environment. Since this effect of PicoGreen enhanced conductivity was

observed for both C6-DNA and DTPA-DNA, it may be that the dye molecules themselves form a contact between the electrodes and the DNA (not through the linker). The dye molecules contain aromatic ring structures (as described, e.g., in [231, 283]), which is one possible source of the enhanced conductivity. Observed conductivity enhancement may be due to PicoGreen dye acting as a molecular dopant for the DNA or to the formation of a conducting medium around the DNA from the PicoGreen molecules.

The photo-induced conductivity enhancement has been earlier observed in the films made of DNA modified with intercalated dyes, such as acridine orange (AO) [83, 84, 193] or ethidium bromide [194]. The group of Tomoji Kawai also observed that the conductivity of the films made of AO modified poly(dG)-poly(dC) DNA can be enhanced by increasing humidity [83]. They estimated that the conductivity value of the AO-DNA complex is of the order of 10^{-4} and 10^{-5} S/cm in $\sim$18 % humidity and in vacuum, respectively, but under a relatively high humidity ($\sim$70%) the conductivity was of the order of 10^{5} S/cm. One can estimate that the conductivity for the individual PicoGreen modified DNA molecules in our samples is σ_{moist} $\sim$1 S/cm in high humidity (RH 50-100 %) and σ_{dry} 10^{-5} S/cm in low humidity (RH $\sim$30 %). However, this is not directly comparable to the values obtained for the DNA films, since the films contain more hydration water, which increases the conductivity.

6.9 Observations from the experiments

There are several minor issues that need to be considered when performing experiments with single molecules. One critical point is the formation of the sulphur-gold bond between the molecule and the electrodes.

Cleaning of the gold electrodes

It was observed in the experiments that the cleaning step right before the immobilization of DNA is required, since the carbon residue which are collected from the ambient air prevents the formation of a specific suphur-gold bonding. A widely used efficient gold surface cleaning method is Piranha solution (70% H_2SO_4: 30% H_2O_2 at 60°C), which is used e.g. in [98]. However, this cleaning process was inappropriate in our case, since the nanoelectrodes containing titanium as an adhesion layer are stripped away in Piranha. Two more gentle (but effective) cleaning methods have been used in the cleaning of gold surface prior to DEP immobilization of DNA: (1) A short flash in an oxygen plasma RIE or (2) A consecutive acid-base cleaning with 1 M NaOH and 1 M HCl with a simultaneous sonication and a subsequent water flush and a drying with N_2. There was no clear difference in the amount of the immobilised DNA observed using these two cleaning procedures. However, the

RIE cleaning is more reproducible and convenient, and thus it was mostly used.

Aluminum residues in Gold

In addition to the cleanliness of the gold surface, the strength of a formed sulphur-gold bond is sensitive to the material impurities in the gold. It is known that the adding of impurity, such as aluminum, to gold film may change the work function of gold even as much as $\sim$1 eV, due to which thiols do not bind to gold surface anymore. It was observed in some stage of this research, that the DNA molecules detached from the electrodes during the electrical measurements. Before the measurements the molecules were (weakly) attached between the electrodes since they were observed in AFM images.

In order to find a reason for the detachment of the molecules, the material analysis of the gold electrodes were performed using a Laser-induced plasma spectroscopy (LIPS) (Analysis performed by Hannu Häkkänen, NanoScience Center, University of Jyväskylä). We found a small amount of aluminum impurities among the evaporated gold, which was the most probably reason for the detachment of the molecules during the measurements. The aluminum residue were tracked to originate from the aluminum oxide (Al_2O_3) cup used in the gold evaporation during the metallization step. (A change of the evaporation cup material from graphite to aluminum oxide was done for a purpose not related to our research.) The use of a graphite cup (used for most of the samples) did not cause any residues to gold. Even if there was some carbon residues in the gold after the evaporation, they were removed from the gold film (at least from the surface) through the formation of a carbon oxide (CO_2) during the oxygen plasma RIE cleaning, whereas the aluminum is not removed.

Properties of the surface

The interactions between the molecules and the substrate can strongly deform the double-helical structure of a DNA. This can cause the insulating behavior observed in the several experiments (see Ch. 2.3.4). It has been observed that the surface deformations can be diminished by using, e.g., pentylamine [120] or a silane treatment of the substrate [93] or a spermidine treatment of the DNA [94]. In this work, no chemical surface treatment has not been used, which resulted in the reduced thickness of the dry DNA molecules on the surface (i.e. 1 nm). However, the thickness of the molecules may be higher in the moist environment used during the measurements. AFM imaging under the moist conditions would reveal information about this subject, but was not available in contents of this work.

It has been observed that DNA on hydrophopic surfaces tend to form bundles, whereas on hydrophilic surfaces it remains as single molecules [238]. The oxygen plasma RIE cleaning that we used changed the originally hydrophobic SiO_2 sur-

face to hydrophilic, which was utilized to obtain the immobilization of individual molecules rather than DNA bundles, providing us a way to investigate DNA conductivity on a single molecule level.

7 Conclusions and future aspects

Conclusions

In this work it was observed that the efficiency of the DEP trapping depends in addition to the field strength also on the applied ac signal frequency and the length of the DNA used. By utilizing this, DEP can be used as a tool for a separation of DNA molecules by their different properties, as earlier demonstrated for proteins [178] and carbon nanotubes [134]. It was also demonstrated that the use of a CNT as an electrode for the DEP trapping of nanometer scale DNA molecules yields significantly better performance as compared to the lithographically fabricated 100 nm wide fingertip type nanoelectrodes, even when the electrode separation is much larger in the case of the CNT sample. This fulfills the scaling down of the dimensions of the DEP trap and thus indeed realizes the 'electrical nanotweezers' via DEP, as proposed by P. J. Burke [37]. Yet, a further challenge in the use of a CNT as an electrode for DEP is how to achieve an immobilization, i.e., how to obtain a reliable and reproducible contact between the CNT and the DNA.

In addition to the trapping and immobilization, the electrical conductivity of DNA was studied on a single molecule level. The sulphur-based DNA-modifications and the DEP trapping of DNA was efficiently used to immobilize individual $\sim$400 bp long DNA molecules as a bridge between the gold nanoelectrodes. The measured resistance of a single or few molecules was a few TΩ in dry environment (RH $\sim$30 %), but was substantially enhanced in the moist environment (RH 80-90 %) showing the resistance of the order of hundreds of MΩ. We suggest that the conductivity enhancement observed in the humid environment originates from the change of the helical conformation of the DNA from a dehydrated form (i.e. denaturated or A-form) to its natural B-form. It was also observed that the PicoGreen fluorescent labelling of the DNA before the immobilization further enhanced the conductivity observed in humid environment. These observations increase the general understanding of the nanometer scale DNA molecules and can thus be exploited in designing of electronic DNA-based devices.

We further showed that the simultaneous conductance measurement using a low frequency ac or a small dc-offset signal during the DEP trapping can be used as an efficient tool for tracking the electrical properties of the small molecules. However, the resistance of a single over 100 nm long DNA molecule used in conductivity studies was too high to be reliably observed in this way.

In summary, the novel results here as compared to what has been done in the literature before are: 1) realization of the dielectrophoretic trapping of as short as 27 bp long DNA using *in situ* confocal microscopy and production of single molecule samples, 2) use of a multi-walled carbon nanotube (MWCNT) as an electrode for a more efficient dielectrophoretic trapping of DNA, 3) observation of a humidity induced conductivity change in the individual 414 bp long thiol-anchored DNA molecules, 4) the DNA polarizability dependency on the length of the molecule.

Future prospects

From the perspective of this thesis, I would divide the future research into two different issues: 1) investigation of the electrical properties of short DNA dublexes by using a highly conducting DNA-linker, in order to lower the total resistance of the immobilized molecule and 2) utilization of DEP as a tool for an advanced positioning of the nanoscale DNA-based components.

To preserve the integrity of DNA, which is a prerequisite for reliable transport measurements, suspended electrodes or a 'bio-compatible' substrate treatment should be used. In order to obtain even more detailed information about the conformation of the molecules when embedded in the prefabricated nanostructure, atomic resolution characterization of the sample using, e.g., scanning tunneling microscopy (STM) or transmission electron microscopy (TEM), is required. The TEM imaging requires a low pressure environment, which is a limitation for biomolecules, but the conformation in the dry state could be accurately studied. Using STM the molecules can be characterized in different humidities, revealing information about the humidity dependence of the DNA conformation [275].

The above mentioned new experiments would provide important basic scientific information about DNA. Considering potential applications, it may well be that the DNA turns out to be not conducting enough as such. There are several ways to improve its conductivity, e.g., using the M-DNA or a generation of charge carriers into the DNA using an oxygen or iodine doping.

However, the most promising application for DNA is its use as a self-assembling scaffold for the positioning of more robust components. The complex DNA constructs, such as DNA origami [217], may be used as 'DNA circuit boards' for organizing the components of the molecular electronics, such as carbon nanotubes or gold nanoparticles, into a highly ordered circuits. Interfacing of this type of assemblies with the top-down fabrication techniques opens a new era of DNA nanotechnology. In addition to single DNA molecules DEP may be used as an effective tool to guide the self-assembled DNA-based components, such as DNA templated FET [127] or DNA circuit boards, to a desired location as a part of the final molecular electronics circuit.

Bibliography

[1] Article **A.I** in this thesis.

[2] Article **A.II** in this thesis.

[3] Article **A.III** in this thesis.

[4] Article **A.IV** in this thesis.

[5] PyMOL-program (http://pymol.sourceforge.net/) have been used to make sterescopic images. Coordinates obtained from ndb atlas gallery for A-DNA: PDB 2D47, NDB ADL025 and for B-DNA: PDB 425D, NDB BD0003 (http://ndbserver.rutgers.edu/atlas/xray/index.html).

[6] *User Guide to Modification and Labelling*, (Glen Research, Sterling, VA, 1999). http://www.glenres.com.

[7] *International Technology Roadmap for Semiconductors.* http://public.itrs.net/ ((accessed May 2006)).

[8] *DTPA–immobilize oligos to gold surfaces by multiple thiol anchorages,* (The Glen Report, Sterling, VA, 2003). http://www.glenres.com/GlenReports/GR16-12.html.

[9] ADLEMAN, L. M., *Molecular computation of solutions to combinatorial problems*. Science **266** (1994) 1021.

[10] AICH, P., LABIUK, S. L., TARI, L. W., DELBAERE, L. J. T., ROESLER, W. J., FALK, K. J., STEER, R. P., AND LEE, J. S., *M-DNA: A Complex Between Divalent Metal Ions and DNA which Behaves as a Molecular Wire*. J. Mol. Biol. **294** (1999) 477.

[11] ALIVISATOS, A. P., JOHNSSON, K. P., PENG, X., WILSON, T. E., LOWETH, C. J., JR, M. P. B., AND SCHULTZ, P. G., *Organization of 'nanocrystal molecules' using DNA*. Nature **382** (1996) 609.

[12] ARKIN, M. A., STEMP, E. D. A., HOLMLIN, R. E., BARTON, J. K., HÖRMANN, A., OLSON, E. J., AND BARBARA, P. F., *Rates of DNA-Mediated Electron Transfer Between Metallointercalators*. Science **273** (1996) 475.

[13] ASBURY, C. L., DIERCKS, A. H., AND VAN DEN ENGH, G., *Trapping of DNA by dielectrophoresis*. Electrophoresis **23** (2002) 2658.

[14] ASBURY, C. L. AND VAN DEN ENGH, G., *Trapping of DNA in nonuniform oscillating electric fields*. Biophys. J. **74** (1998) 1024.

[15] BAKEWELL, D., ERMOLINA, I., MORGAN, H., MILNER, J., AND FELDMAN, Y., *Dielectric relaxation measurements of 12 kbp plasmid DNA*. Biochem. Biophys. Acta **1493** (2000) 151.

[16] BAKEWELL, D. J. AND MORGAN, H., *Dielectrophoresis of DNA: Time- and Frequency-Dependent Collections on Microelectrodes*. IEEE Trans. NanoBiosci. **5** (2006) 1.

[17] BAKEWELL, D. J. G., HUGHES, M. P., MILNER, J. J., AND MORGAN, H., *Dielectrophoretic Manipulation of Avidin And DNA*. Proc. 20^{th} Ann. Int. Conf. of the IEEE Engineering in Medicine and Biology Society **20** (1998).

[18] BARNETT, R. N., CLEVELAND, C. L., JOY, A., LANDMAN, U., AND SCHUSTER, G. B., *Charge Migration in DNA: Ion-Gated Transport*. Science **294** (2001) 567.

[19] BARTH, J. V., COSTANTINI, G., AND KERN, K., *Engineering atomic and molecular nanostructures at surfaces*. Nature **437** (2005) 671.

[20] BASCH, H., COHEN, R., AND RATNER, M. A., *Interface Geometry and Molecular Junction Conductance: Geometric Fluctuation and Stochastic Switching*. Nano Lett. **5** (2005) 1668.

[21] BATCHELDER, J. S., *Dielectrophoretic manipulator*. Rev. Sci. Instrum. **54** (1983) 300.

[22] BECKER, F. F., WANG, X.-B., HUANG, Y., PETHIG, R., VYKOUKAL, J., AND GASCOYNE, P. R. C., *The Removal of Human Leukaemia Cells from Blood Using Interdigitated Microelectrode*. J. Phys. D: Appl. Phys. **27** (1994) 2659.

[23] BEEBE, J. M., ENGELKES, V. B., MILLER, L. L., AND FRISBIE, C. D., *Contact Resistance in Metal-Molecule-Metal Junctions Based on Aliphatic SAMs: Effects of Surface Linker and Metal Work Function*. J. Am. Chem. Soc. **124** (2002) 11268.

[24] BERLIN, Y. A., BURIN, A. L., AND RATNER, M. A., *Charge Hopping in DNA*. J. Am. Chem. Soc. **123** (2001) 260.

[25] BERLIN, Y. A., BURIN, A. L., AND RATNER, M. A., *Elementary steps for charge transport in DNA: thermal activation vs. tunneling*. Chem. Phys. **275** (2002) 61.

[26] BEZRYADIN, A., DEKKER, C., AND SCHMID, G., *Electrostatic trapping of single conducting nanoparticles between nanoelectrodes*. Appl. Phys. Lett. **71** (1997) 1273.

[27] BIXON, M., GIESE, B., WESSELY, S., LANGENBACHER, T., MICHEL-BEYERLE, M. E., AND JORTNER, J., *Long-range charge hopping in DNA*. Proc. Natl Acad. Sci. **96** (1999) 11713.

[28] BIXON, M. AND JORTNER, J., *Long-range and very long-range charge transport in DNA*. Chem. Phys. **281** (2002) 393.

[29] BOCKRATH, M., MARKOVIC, N., SHEPARD, A., M.TINKHAM, GUREVICH, L., KOUWENHOVEN, L. P., WU, M. W., AND SOHN, L. L., *Scanned Conductance Microscopy of Carbon Nanotubes and λ-DNA*. Nano Lett. **2** (2002) 187.

[30] BONE, S., LEE, R. S., AND HODGSON, C. E., *Dielectric studies of intermolecular interactions in native DNA*. Biochim. Biophys. Acta **1306** (1996) 93.

[31] BOON, E. M. AND BARTON, J. K., *Charge transport in DNA*. Curr. Opin. Struct. Biol. **12** (2002) 320.

[32] BRAUN, E., EICHEN, Y., SIVAN, U., AND BEN-YOSEPH, G., *DNA-templated assembly and electrode attachment of a conducting silver wire*. Nature **391** (1998) 775.

[33] BRAUN, G., INAGAKI, K., ESTABROOK, R. A., WOOD, D. K., LEVY, E., CLELAND, A. N., STROUSE, G. F., AND REICH, N. O., *Gold Nanoparticle Decoration of DNA on Silicon*. Langmuir **21** (2005) 10699.

[34] BRIMAN, M., ARMITAGE, N. P., HELGREN, E., AND GRÜNER, G., *Dipole Relaxation Losses in DNA*. Nano Lett. **4** (2004) 733.

[35] BRIMAN, N. P. A. M., , AND GRÜNER, G., *Charge transfer and charge transport on the double helix*. Phys. Stat. Sol. **241** (2004) 69.

[36] BRUN, A. M. AND HARRIMAN, A., *Dynamics of Electron Transfer between Intercalated Polycyclic Molecules: Effect of Interspersed Bases*. J. Am. Chem. Soc. **114** (1992) 3656.

[37] BURKE, P. J., *Nanodielectrophoresis: Electronic Nanotweezers*. Encycl. Nanosci. Nanotechnol. **6** (2004) 623.

[38] BURNS, J. A., BUTLER, J. C., MORAN, J., AND WHITESIDES, G. M., *Selective Reduction of Disulfides by Tris(2-carboxyethy1)phosphine*. J. Org. Chem. **56** (1991) 2648.

[39] CAI, L., TABATA, H., AND KAWAI, T., *Self-assembled DNA networks and their electrical conductivity*. Appl. Phys. Lett. **77** (2000) 3105.

[40] CALZOLARI, A., FELICE, R. D., MOLINARI, E., AND GARBESI, A. Appl. Phys. Lett. **80** (2002) 3331.

[41] CARPENA, P., BERNAOLA-GALVÁN, P., IVANOV, P. C., AND STANLEY, H. E., *Metal-insulator transition in chains with correlated disorder*. Nature **418** (2002) 955.

[42] CASTELLANOS, A., RAMOS, A., GONZÁLEZ, A., GREEN, N. G., AND MORGAN, H., *Electrohydrodynamics and dielectrophoresis in microsystems: scaling laws*. J. Phys. D: Appl. Phys. **36** (2003) 2584.

[43] CHEN, J. AND SEEMAN, N. C., *Synthesis from DNA of a molecule with the connectivity of a cube*. Nature **350** (1991) 631.

[44] CHEN, X. Q., SAITO, T., YAMADA, H., AND MATSUSHIGE, K., *Aligning single-wall carbon nanotubes with an alternating-current electric field.* Appl. Phys. Lett. **78** (2001) 3714.

[45] CHOU, C.-F., TEGENFELDT, J., BAKAJIN, O., CHAN, S. S., COX, E. C., DARNTON, N., DUKE, T., AND AUSTIN, R. H., *Electrodeless Dielectrophoresis of Single- and Double-Stranded DNA*. Biophys. J. **83** (2002) 2170.

[46] CHOU, C.-F. AND ZENHAUSERN, F., *Electrodeless Dielectrophoresis for Micro Total Analysis Systems*. IEEE Engineering in Medicine and Biology Magazine **22** (2003) 62.

[47] COFFER, J. L., BIGHAM, S. R., LI, X., PINIZZOTTO, R. F., RHO, Y. G., PIRTLE, R. M., AND PIRTLE, I. L., *Dictation of the shape of mesoscale semiconductor nanoparticle assemblies by plasmid DNA*. Appl. Phys. Lett. **69** (1996) 3851.

[48] COHEN, H., NOGUES, C., NAAMAN, R., AND PORATH, D., *Direct measurement of electrical transport through single DNA molecules of complex sequence*. Proc. Natl. Acad. Sci. **102** (2005) 11589.

[49] CONWELL, E. M., *Charge transport in DNA in solution: The role of polarons*. Proc. Natl Acad. Sci. **102** (2005) 8795.

[50] CUI, X. D., PRIMAK, A., ZARATE, X., TOMFOHR, J., SANKEY, O. F., MOORE, A. L., MOORE, T. A., GUST, D., HARRIS, G., AND LINDSAY, S. M., *Reproducible Measurement of Single-Molecule Conductivity*. Science **294** (2001) 571.

[51] DANDLIKER, P. J., HOLMLIN, R. E., AND BARTON, J. K., *Oxidative Thymine Dimer Repair in the DNA Helix*. Science **275** (1997) 1465.

[52] DAVIS, J. T., *G-Quartets 40 Years Later: From 5'-GMP to Molecular Biology and Supramolecular Chemistry*. Angew. Chem. Int. Ed. **43** (2004) 668.

[53] DEKKER, C. AND RATNER, M. A., *Electronic properties of DNA*. Physics World **14** (2001) 29.

[54] DEMATTEI, C. R., HUANG, B., AND TOMALIA, D. A., *Designed Dendrimer Syntheses by Self-Assembly of Single-Site, ssDNA Functionalized Dendrons*. Nano Lett. **4** (2004) 771.

[55] DEWARRAT, F., CALAME, M., AND SCHÖNENBERGER, C., *Orientation and Positioning of DNA Molecules with an Electric Field Technique*. Single Mol. **3** (2002) 189.

[56] DING, B. Q., SHA, R. J., AND SEEMAN, N. C., *Pseudohexagonal 2D DNA Crystals from Double Crossover Cohesion*. J. Am. Chem. Soc. **126** (2004) 10230.

[57] DITTMER, W. U. AND SIMMEL, F. C., *Chains of semiconductor nanoparticles templated on DNA*. Appl. Phys. Lett. **85** (2004) 633.

[58] DONHAUSER, Z. J., MANTOOTH, B. A., KELLY, K. F., BUMM, L. A., MONNELL, J. D., STAPLETON, J. J., JR., D. W. P., RAWLETT, A. M., ALLARA, D. L., TOUR, J. M., AND WEISS, P. S., *Conductance Switching in Single Molecules Through Conformational Changes*. Science **292** (2001) 2303.

[59] DUCHESNE, J., DEPIREUX, J., BERTINCHAMPS, A., CORNET, N., AND VAN DER KAA, J. M., *Thermal and Electrical Properties of Nucleic Acids and Proteins*. Nature **188** (1960) 405.

[60] DUJARDIN, E., HSIN, L.-B., WANG, C. R. C., AND MANN, S., *DNA-driven self-assembly of gold nanorods*. Chem. Commun. (2001) 1264.

[61] EICHEN, Y., BRAUN, E., SIVAN, U., AND BEN-YOSEPH, G., *Self-assembly of nanoelectronic components and circuits using biological templates*. Acta Polym. **49** (1998) 663.

[62] ELEY, D. D. AND SPIVEY, D. I., *Semiconductivity of organic substances. Nucleic acid in the dry state*. Trans. Faraday. Soc. **58** (1962) 411.

[63] ELGHANIAN, R., STORHOFF, J. J., MUCIC, R. C., LETSINGER, R. L., AND MIRKIN, C. A., *Selective Colorimetric Detection of Polynucleotides Based on the Distance-Dependent Optical Properties of Gold Nanoparticles*. Science **277** (1997) 1078.

[64] ENDRES, R. G., COX, D. L., AND SINGH, R. R. P., *The quest for high-conductance DNA*. Rev. Mod. Phys. **76** (2004) 195.

[65] FAHLMAN, R. P., HSING, M., SPORER-TUHTEN, C. S., AND SEN, D., *Duplex Pinching: A Structural Switch Suitable for Contractile DNA Nanoconstructions*. Nano Lett. **3** (2003) 1073.

[66] FELDKAMP, U. AND NIEMEYER, C. M., *Rational Design of DNA Nanoarchitectures*. Angew. Chem. Int. Ed. **45** (2006) 1856.

[67] FINK, H.-W. AND SCHÖNENBERGER, C., *Electrical conduction through DNA molecules*. Nature **398** (1999) 407.

[68] FORD, W. E., HARNACK, O., YASUDA, A., AND WESSELS, J. M., *Platinated DNA as Precursors to Templated Chains of Metal Nanoparticles*. Adv. Mater. **13** (2001) 1793.

[69] FRANK-KAMENETSKII, M. D. AND MIRKIN, S. M., *Triplex DNA structures*. Annu. Rev. Biochem. **64** (1995) 65.

[70] FUKUI, K. AND TANAKA, K., *Distance dependence of photoinduced electron transfer in DNA*. Angew. Chem. Int. Ed. **37** (1998) 158.

[71] GARCÍA, R. AND PÉREZ, R., *Dynamic atomic force microscopy methods*. Surf. Sci. Rep. **47** (2002) 197.

[72] GARZON, M. H. AND DEATON, R. J., *Biomolecular computing and programming*. IEEE Trans. Evol. Comput. **3** (1999) 236.

[73] GERMISHUIZEN, W. A., TOSCH, P., MIDDELBERG, A. P. J., WÄLTI, C., DAVIES, A. G., WIRTZ, R., AND PEPPER, M., *Influence of alternating current electrokinetic forces and torque on the elongation of immobilized DNA*. J. Appl. Phys. **97** (2005) 014702.

[74] GERMISHUIZEN, W. A., WÄLTI, C., WIRTZ, R., JOHNSTON, M. B., PEPPER, M., DAVIES, A. G., AND MIDDELBERG, A. P. J., *Selective dielectrophoretic manipulation of surface-immobilized DNA molecules*. Nanotechnology **14** (2003) 896.

[75] GIESE, B., *Long-Distance Charge Transport in DNA: The Hopping Mechanism*. Acc. Chem. Res. **33** (2000) 631.

[76] GIESE, B., AMAUDRUT, J., KÖHLER, A.-K., SPORMANN, M., AND WESSELY, S., *Direct observation of hole transfer through DNA by hopping between adenine bases and by tunnelling*. Nature **412** (2001) 318.

[77] GÓMEZ-NAVARRO, C., MORENO-HERRERO, F., DE PABLO, P. J., COLCHERO, J., GÓMEZ-HERRERO, J., AND BARÓ, A. M., *Contactless experiments on individual DNA molecules show no evidence for molecular wire behavior*. Proc. Natl. Acad. Sci. **99** (2002) 8484.

[78] GOODMAN, R. P., BERRY, R. M., AND TURBERFIELD, A. J., *The single-step synthesis of a DNA tetrahedron*. Chem. Commun. (2004) 1372.

[79] GOODMAN, R. P., SCHAAP, I. A. T., TARDIN, C. F., ERBEN, C. M., BERRY, R. M., SCHMIDT, C. F., AND TURBERFIELD, A. J., *Rapid Chiral Assembly of Rigid DNA Building Blocks for Molecular Nanofabrication*. Science **310** (2005) 1661.

[80] GOPE, M. L., KEINÄNEN, R. A., P. A. KRISTO, CONNEELY, O. M., BEATTIE, W. G., ZARUCKI-SCHULZ, T. O., O'MALLEY, B. W., AND KULOMAA, M. S., *Molecular cloning of the chicken avidin cDNA*. Nucleic Acids Res. **15** (1987) 3595.

[81] GOTHELF, K. V. AND LABEAN, T. H., *DNA-programmed assembly of nanostructures*. Org. Biolom. Chem. **3** (2005) 4023.

[82] GREEN, N. G., MORGAN, H., AND MILNER, J. J., *Manipulation and trapping of sub-micron bioparticles using dielectrophoresis*. J. Biochem. Biophys. Methods **35** (1997) 89.

[83] GU, J., CAI, L., TANAKA, S., OTSUKA, Y., TABATA, H., AND KAWAI, T., *Electric conductivity of dye modified DNA films with and without light irradiation in various humidities*. J. Appl. Phys. **92** (2002) 2816.

[84] GU, J., TANAKA, S., OTSUKA, Y., TABATA, H., AND KAWAI, T., *Self-assembled dye-DNA network and its photoinduced electrical conductivity*. Appl. Phys. Lett. **80** (2002) 688.

[85] GU, Q., CHENG, C., AND HAYNIE, D. T., *Cobalt metallization of DNA: toward magnetic nanowires*. Nanotechnology **16** (2005) 1358.

[86] HA, D. H., NHAM, H., YO, K.-H., SO, H.-M., LEE, H. Y., AND KAWAI, T., *Humidity effects on the conductance of the assembly of DNA molecules*. Chem. Phys. Lett. **355** (2002) 405.

[87] HALL, D. B., HOLMLIN, R. E., AND BARTON, J. K., *Oxidative DNA damage through long-range electron transfer*. Nature **382** (1996) 731.

[88] HARTZELL, B., MCCORD, B., ASARE, D., CHEN, H., HEREMANS, J. J., AND SOGHOMONIAN, V., *Comparative current-voltage characteristics of nicked and repaired λ-DNA*. Appl. Phys. Lett. **82** (2003) 4800.

[89] HARTZELL, B., MCCORD, B., ASARE, D., CHEN, H., HEREMANS, J. J., AND SOGHOMONIAN, V., *Current-voltage characteristics of diversely disulfide terminated λ-deoxyribonucleic acid molecules*. J. Appl. Phys. **94** (2003) 2764.

[90] HAZANI, M., HENNRICH, F., KAPPES, M., NAAMAN, R., PELED, D., SIDOROV, V., AND SHVARTS, D., *DNA-mediated self-assembly of carbon nanotube-based electronic devices*. Chem. Phys. Lett. **391** (2004) 389.

[91] HEATH, J. R. AND RATNER, M. A., *Molecular Electronics*. Physics Today **56** (2003) 43.

[92] HEGNER, M., WAGNER, P., AND SEMENZA, G., *Immobilizing DNA on gold via thiol modification for atomic force microscopy imaging in buffer solutions*. FEBS Lett. **336** (1993) 452.

[93] HEIM, T., DERESMES, D., AND VUILLAUMEA, D., *Conductivity of DNA probed by conducting-atomic force microscopy: Effects of contact electrode, DNA structure, and surface interactions*. J. Appl. Phys. **96** (2004) 2927.

[94] HEIM, T., MÉLIN, T., DERESMES, D., AND VUILLAUME, D., *Localization and delocalization of charges injected in DNA*. Appl. Phys. Lett. **85** (2004) 2637.

[95] HELLER, A., *Spiers Memorial Lecture. On the hypothesis of cathodic protection of genes*. Faraday Discuss. **116** (2000) 1.

[96] HENDERSON, P. T., JONES, D., HAMPIKIAN, G., KAN, Y., AND SCHUSTER, G. B., *Long-distance charge transport in duplex DNA: The phonon-assisted polaron-like hopping mechanism*. Proc. Natl. Acad. Sci. **96** (1999) 8353.

[97] HERMON, Z., CASPI, S., AND BEN-JACOB, E., *Prediction of charge and dipole solitons in DNA molecules based on the behaviour of phosphate bridges as tunnel elements*. Europhys. Lett. **43** (1998) 482.

[98] HERNE, T. M. AND TARLOV, M. J., *Characterization of DNA Probes Immobilized on Gold Surfaces*. J. Am. Chem. Soc. **119** (1997) 8916.

[99] HIHATH, J., XU, B., ZHANG, P., AND TAO, N., *Study of single-nucleotide polymorphisms by means of electrical conductance measurements*. Proc. Natl. Acad. Sci. **102** (2005) 16981.

[100] HIPPS, K. W., *Its all about contacts*. Science **294** (2001) 536.

[101] HIRVINIEMI, L., *Hiilinanoputket elektrodeina dielektroforeesissa*, Master's thesis (pro gradu), University of Jyväskylä, NanoScience Center (2006).

[102] HÄKKINEN, H., WALTER, M., AND GRÖNBECK, H., *Divide and Protect: Capping Gold Nanoclusters with Molecular Gold-Thiolate rings*. J. Phys. Chem. B **110** (2006) 9927.

[103] HÖLZEL, R. AND BIER, F. F., *Dielectrophoretic manipulation of DNA*. IEE Proc.-Nanobiotechnol. **150** (2003) 47.

[104] HÖLZEL, R., CALANDER, N., CHIRAGWANDI, Z., WILLANDER, M., AND BIER, F. F., *Trapping Single Molecules by Dielectrophoresis*. Phys. Rev. Lett. **95** (2005) 128102.

[105] HOOGSTEEN, K., *The crystal and molecular structure of a hydrogen-bonded complex between 1-methylthymine and 9-methyladenine*. Acta Crystallogr. **16** (1963) 907.

[106] HOPKINS, D. S., PEKKER, D., GOLDBART, P. M., AND BEZRYADIN, A., *Quantum Interference Device Made by DNA Templating of Superconducting Nanowires*. Science **308** (2005) 1762–1765.

[107] HUGHES, M. P., *AC electrokinetics: applications for nanotechnology*. Nanotechnology **11** (2000) 124.

[108] HUGHES, M. P. AND MORGAN, H., *Dielectrophoretic trapping of single submicrometre scale bioparticles*. J. Phys. D: Appl. Phys. **31** (1998) 2205.

[109] HUGHES, M. P., MORGAN, H., AND RIXON, F. G., *Dielectrophoretic manipulation and characterization of herpes simplex virus-1 capsids*. Euro. Biophys. J. **30** (2001) 268.

[110] HWANG, J. S., HWANG, S. W., AND AHN, D., *Electrical conduction measurement of thiol modified DNA molecules*. Superlattices and Microstructures **34** (2003) 433.

[111] HWANG, J. S., HWANG, S. W., AND AHN, D., *Formation of Electrical Interconnects by Self-Trapping of Deoxyribonucleic Acid Molecules*. Jpn. J. Appl. Phys. **43** (2004) 3803.

[112] HWANG, J. S., KONG, K. J., AHN, D., LEE, G. S., AHN, D. J., AND HWANG, S. W., *Electrical transport through 60 base pairs of poly(dG)-poly(dC) DNA molecules*. Appl. Phys. Lett. **81** (2002) 1134.

[113] HWANG, J. S., LEE, G. S., KONG, K. J., AHN, D. J., HWANG, S. W., AND AHN, D., *Electrical transport through poly(G)-poly(C) DNA molecules*. Microelectronic Engineering **63** (2002) 161.

[114] HYTÖNEN, V. P., HÖRHÄ, J., AIRENNE, T. T., NISKANEN, E. A., HELTTUNEN, K. J., JOHNSON, M. S., SALMINEN, T. A., KULOMAA, M. S., AND NORDLUND, H. R., *Controlling quaternary structure assembly: subunit interface engineering and crystal structure of dual chain avidin*. J. Mol. Biol. **359** (2006) 1352.

[115] HYTÖNEN, V. P., MÄÄTTÄ, J. A. E., NYHOLM, T. K. M., LIVNAH, O., EISENBERG-DOMOVICH, Y., HYRE, D., NORDLUND, H. R., HÖRHÄ, J., NISKANEN, E. A., PALDANIUS, T., KULOMAA, T., PORKKA, E. J., STAYTON, P. S., LAITINEN, O. H., AND KULOMAA, M. S., *Design and Construction of Highly Stable, Protease-resistant Chimeric Avidins*. J. Biol. Chem. **280** (2005) 10228.

[116] IQBAL, S. M., BALASUNDARAMA, G., GHOSH, S., BERGSTROMB, D. E., AND BASHIRC, R., *Direct current electrical characterization of ds-DNA in nanogap junctions*. Appl. Phys. Lett. **86** (2005) 153901.

[117] JONES, T. B., *Basic theory of dielectrophoresis and electrorotation*. IEEE EMBS Magazine **22** (2003) 33.

[118] JORTNER, J., BIXON, M., LANGENBACHER, T., AND MICHEL-BEYERLE, M. E., *Charge transfer and transport in DNA*. Proc. Natl. Acad. Sci. **95** (1998) 12759.

[119] KABATA, H., KUROSAWA, O., ARAI, I., WASHIZU, M., MARGARSON, S., GLASS, R., AND SHIMAMOTO, N., *Visualization of single molecules of RNA polymerase sliding along DNA*. Science **262** (1993) 1561.

[120] KASUMOV, A. Y., KLINOV, D. V., ROCHE, P.-E., GUÉRON, S., AND BOUCHIAT, H., *Thickness and low-temperature conductivity of DNA molecules.* Appl. Phys. Lett. **84** (2004) 1007.

[121] KASUMOV, A. Y., KOCIAK, M., GUÉRON, S., REULET, B., VOLKOV, V. T., KLINOV, D. V., AND BOUCHIAT, H., *Proximity-Induced Superconductivity in DNA*. Science **291** (2001) 280.

[122] KAWABATA, T. AND WASHIZU, M., *Dielectrophoretic detection of molecular bindings*. IEEE Trans. Indust. Appl. **37** (2001) 1625.

[123] KELLEY, S. O. AND BARTON, J. K., *Electron Transfer Between Bases in Double Helical DNA*. Science **283** (1999) 375.

[124] KELLEY, S. O., BOON, E. M., BARTON, J. K., JACKSON, N. M., AND HILL, M. G., *Single-base mismatch detection based on charge transduction through DNA*. Nucleic Acids Res. **27** (1999) 4830.

[125] KELLEY, S. O., HOLMLIN, R. E., STEMP, E. D. A., AND BARTON, J. K., *Photoinduced Electron Transfer in Ethidium-Modified DNA Duplexes: Dependence on Distance and Base Stacking*. J. Am. Chem. Soc. **119** (1997) 9861.

[126] KELLEY, S. O., JACKSON, N. M., HILL, M. G., AND BARTON, J. K., *Long-Range Electron Transfer through DNA Films*. Angew. Chem. Int. Ed. **38** (1999) 941.

[127] KEREN, K., BERMAN, R. S., BUCHSTAB, E., SIVAN, U., AND BRAUN, E., *DNA-Templated Carbon Nanotube Field-Effect Transistor*. Science **302** (2003) 1380.

[128] KEREN, K., KRUEGER, M., GILAD, R., BEN-YOSEPH, G., SIVAN, U., AND BRAUN, E., *Sequence-Specific Molecular Lithography on Single DNA Molecules*. Science **297** (2002) 72.

[129] KLEINE, H., WILKEA, R., PELARGUS, C., ROTT, K., PÜHLER, A., REISS, G., ROSA, R., AND ANSELMETTI, D., *Absence of intrinsic electric conductivity in single dsDNA molecules*. J. Biotechnology **112** (2004) 91.

[130] KLEINE-OSTMANN, T., JÖRDENS, C., BAASKE, K., WEIMANN, T., DE ANGELIS, M. H., AND KOCH, M., *Conductivity of single-stranded and double-stranded deoxyribose nucleic acid under ambient conditions: The dominance of water*. Appl. Phys. Lett. **88** (2006) 102102.

[131] KOBAYASHI, N., UEMURA, S., KUSABUKA, K., NAKAHIRA, T., AND TAKAHASHI, H., *An organic red-emitting diode with a water-soluble DNA-polyaniline complex containing Ru(bpy)$_3^{2+}$*. J. Mater. Chem. **11** (2001) 1766.

[132] KOSHIO, A., YUDASAKA, M., AND IIJIMA, S., *Metal-free production of high-quality multi-wall carbon nanotubes, in which the innermost nanotubes have a diameter of 0.4 nm*. Chem. Phys. Lett. **356** (2002) 595.

[133] KOTLYAR, A. B., BOROVOK, N., MOLOTSKY, T., COHEN, H., SHAPIR, E., AND PORATH, D., *Long, Monomolecular Guanine-Based Nanowires*. Adv. Mater. **17** (2005) 1901.

[134] KRUPKE, R., HENNRICH, F., V. LÖHNEYSEN, H., AND KAPPES, M. M., *Separation of Metallic from Semiconducting Single-Walled Carbon Nanotubes*. Science **301** (2003) 344.

[135] KUZYK, A., *Dielectrophoresis of nanoscale dsDNA and its electrical conductivity*, Master's thesis (pro gradu), University of Jyväskylä, NanoScience Center (2005).

[136] LABEAN, T. H., YAN, H., KOPATSCH, J., LIU, F., WINFREE, E., REIF, J. H., AND SEEMAN, N. C., *Construction, Analysis, Ligation, and Self-Assembly of DNA Triple Crossover Complexes*. J. Am. Chem. Soc. **122** (2000) 1848.

[137] LAITINEN, O. H., AIRENNE, K. J., HYTÖNEN, V. P., PELTOMAA, E., MÄHÖNEN, A. J., WIRTH, T., LIND, M. M., MÄKELÄ, K. A., TOIVANEN, P. I., SCHENKWEIN, D., HEIKURA, T., NORDLUND, H. R., KULOMAA, M. S., AND YLÄ-HERTTUALA, S., *A multipurpose vector system for the screening of libraries in bacteria, insect and mammalian cells and expression in vivo*. Nucleic Acids Res. **33** (2005) e42.

[138] LE, J. D., PINTO, Y., SEEMAN, N. C., MUSIER-FORSYTH, K., TATON, T. A., AND KIEHL, R. A., *Metallic Nanocomponent Arrays on a Surface*. Nano Lett. **4** (2004) 2343.

[139] LEE, H. Y., TANAKA, H., OTSUKA, Y., YOO, K.-H., LEE, J.-O., AND KAWAI, T., *Control of electrical conduction in DNA using oxygen hole doping*. Appl. Phys. Lett. **80** (2002) 1670.

[140] LEGRAND, O., CÔTE, D., AND BOCKELMANN, U., *Single molecule study of DNA conductivity in aqueous environment*. Phys. Rev. E **73** (2006) 031925.

[141] LEHN, J.-M., *Toward Self-Organization and Complex Matter*. Science **295** (2002) 2400.

[142] LEHTIVUORI, H., *Nanometriluokan DNA-molekyylien ohjaus- ja kiinnittämiskokeet sekä kytkentäryhmän vaikutus elektrodi-DNA-elektrodi rakenteen sähkönjohtavuuteen*, Master's thesis (pro gradu), University of Jyväskylä, NanoScience Center (2006).

[143] LEI, C. H., DAS, A., ELLIOTT, M., AND MACDONALD, J. E., *Conductivity of macromolecular networks measured by electrostatic force microscopy*. Appl. Phys. Lett. **83** (2003) 482.

[144] LEWIS, F., WU, T., GREENFIELD, Y. Z. R. L. S., AND WASIELEWSKI, M., *Distance-dependent electron transfer in DNA hairpins*. Science **277** (1997) 673.

[145] LEWIS, F. D., LIU, X., LIU, J., MILLER, S. E., HAYES, R. T., AND WASIELEWSKI, M. R., *Direct measurement of hole transport dynamics in DNA*. Nature **406** (2000) 51.

[146] LI, S., HE, P., DONG, J., GUO, Z., AND DAI, L., *DNA-Directed Self-Assembling of Carbon Nanotubes*. J. Am. Chem. Soc. **127** (2005) 14.

[147] LI, X., YANG, X., QI, J., AND SEEMAN, N. C., *Antiparallel DNA double crossover molecules as components for nanoconstruction*. J. Am. Chem. Soc. **118** (1996) 6131.

[148] LIANG, C. Y. AND SCALCO, E. G., *Electrical Conduction of a High Polymerized Sample of Sodium Salt of Deoxyribonucleic Acid*. J. Chem. Phys. **40** (1964) 919.

[149] LIU, D. AND BALASUBRAMANIAN, S., *A Proton-Fuelled DNA Nanomachine*. Angew. Chem. Int. Ed. **42** (2003) 5734.

[150] LIU, D., PARK, S. H., REIF, J. H., AND LABEAN, T. H., *DNA nanotubes self-assembled from triple-crossover tiles as templates for conductive nanowires*. Proc. Nat. Acad. Sci. **101** (2004) 717.

[151] LIU, D., WANG, M. S., DENG, Z. X., WALULU, R., AND MAO, C. D., *Tensegrity: Construction of Rigid DNA Triangles with Flexible Four-Arm DNA Junctions*. J. Am. Chem. Soc. **126** (2004) 2324.

[152] LIU, Q., WANG, L., FRUTOS, A. G., CONDON, A. E., CORN, R. M., AND SMITH, L. M., *DNA computing on surfaces*. Nature **403** (2000) 175.

[153] LONG, Y.-T., KRAATZ, C.-Z. L. H.-B., AND LEEY, J. S., *AC Impedance Spectroscopy of Native DNA and M-DNA*. Biophysical J. **84** (2003) 3218.

[154] LUO, Y., COLLIER, C. P., JEPPESEN, J. O., NIELSEN, K. A., DEIONNO, E., HO, G., PERKINS, J., TSENG, H.-R., YAMAMOTO, T., STODDART, J. F., AND HEATH, J. R., *Two-Dimensional Molecular Electronics Circuits*. Chem. Phys. Chem. **3** (2002) 519.

[155] LÖWDIN, P.-O., *Proton Tunneling in DNA and its Biological Implications*. Rev. Mod. Phys. **35** (1963) 724.

[156] MA, Y. F., ZHANG, J. M., ZHANG, G. J., AND HE, H. X., *Polyaniline Nanowires on Si Surfaces Fabricated with DNA Templates*. J. Am. Chem. Soc. **126** (2004) 7097.

[157] MALO, J., MITCHELL, J. C., VÉNIEN-BRYAN, C., HARRIS, J. R., WILLE, H., SHERRATT, D. J., AND TURBERFIELD, A. J., *Engineering a 2D Protein-DNA Crystal*. Angew. Chem. Int. Ed. **44** (2005) 3057.

[158] MANNING, G. S. Q., *The molecular theory of polyelectrolyte solutions with applications to the electrostatic properties of polynucleotides*. Rev. Biophys. **11** (1978) 179.

[159] MAO, C., LABEAN, T. H., REIF, J. H., AND SEEMAN, N. C., *Logical computation using algorithmic self-assembly of DNA triple-crossovermolecules*. Nature **407** (2000) 493.

[160] MAO, C., SUN, W., SHEN, Z., AND SEEMAN, N. C., *A nanomechanical device based on the B-Z transition of DNA*. Nature **397** (1999) 144.

[161] MARCUS, R. A. AND SUTIN, N., *Electron transfers in chemistry and biology*. BioChim. BioPhys. Acta **811** (1985) 265.

[162] MARKX, G. H., HUANG, Y., ZHOU, X.-F., AND PETHIG, R., *Dielectrophoretic characterization and separation of micro-organisms*. Microbiology **140** (1994) 585.

[163] MARKX, G. H. AND PETHIG, R., *Dielectrophoretic Separation of Cells: Continuous Separation*. Biotechnol. Bioeng. **45** (1995) 337.

[164] MARSH, T. C. AND HENDERSON, E., *G- Wires: Self-Assembly of a Telomeric Oligonucleotide, d(GGGGTTGGGG), into Large Superstructures*. Biochemistry **33** (1994) 10718.

[165] MARSH, T. C., VESENKA, J., AND HENDERSON, E., *A new DNA nanostructure, the G-wire, imaged by scanning probe microscopy*. Nucl. Acids Res. **23** (1995) 696.

[166] MASUDA, S., WASHIZU, M., AND KAWABATA, I., *Movement of blood cells in liquid by nonuniform traveling field*. IEEE Trans. Indust. Appl. **24** (1988) 217.

[167] MASUDA, S., WASHIZU, M., AND NANBA, T., *Novel method of cell fusion in field constriction area in fluid integrated circuit*. IEEE Trans. Indust. Appl. **25** (1989) 732.

[168] MATHIEU, F., LIAO, S., KOPATSCH, J., WANG, T., MAO, C., AND SEEMAN, N. C., *Six-Helix Bundles Designed from DNA*. Nano Lett. **5** (2005) 661.

[169] MEADE, T. J. AND KAYYEM, J. F., *Electron transfer through DNA: site-specific modification of duplex DNA with ruthenium donors and acceptors*. Angew. Chem. Int. Ed. **34** (1995) 352.

[170] MEGGERS, E., KUSCH, D., SPICHTY, M., WILLE, U., AND GIESE, B., *Electron Transfer through DNA in the Course of Radical-Induced Strand Cleavage*. Angew. Chem. Int. Ed. **37** (1998) 460.

[171] MEGGERS, E., MICHEL-BEYERLE, M. E., AND GIESE, B., *Sequence Dependent Long-Range Hole Transport in DNA*. J. Am. Chem. Soc. **120** (1998) 12950.

[172] MIRKHALAF, F., PAPROTNY, J., AND SCHIFFRIN, D. J., *Synthesis of Metal Nanoparticles Stabilized by Metal-Carbon Bonds*. J. Am. Chem. Soc. **128** (2006) 7400.

[173] MIRKIN, C. A., LETSINGER, R. L., MUCIC, R. C., AND STORHOFF, J. J., *A DNA-based method for rationally assembling nanoparticles into macroscopic materials*. Nature **382** (1996) 607.

[174] MIRKIN, S. M. AND FRANK-KAMENETSKII, M. D., *H-DNA and related structures*. Annu. Rev. Biophys. Biomol. Struct. **23** (1994) 541.

[175] MITCHELL, G. P., MIRKIN, C. A., AND LETSINGER, R. L., *Programmed Assembly of DNA Functionalized Quantum Dots*. J. Am. Chem. Soc. **121** (1999) 8122.

[176] MÜLLER, T., GERARDINO, A. M., SCHNELLE, T., SHIRLEY, S. C., BORGODONI, F., DE GASPERIS, G., LEONI, R., AND FUHR, G., *Trapping of micrometre and sub-micrometre particles by high-frequency electric fields and hydrodynamic forces*. J. Phys. D: Appl. Phys. **29** (1996) 340.

[177] MONSON, C. F. AND WOOLLEY, A. T., *DNA-Templated Construction of Copper Nanowires*. Nano Lett. **3** (2003) 359.

[178] MORGAN, H., HUGHES, M. P., AND GREEN, N. G., *Separation of Submicron Bioparticles by Dielectrophoresis*. Biophysical J. **77** (1999) 516.

[179] MURPHY, C., ARKIN, M., JENKINS, Y., GHATLIA, N., BOSSMANN, S., TURRO, N., AND BARTON, J., *Long-range photoinduced electron transfer through a DNA helix*. Science **262** (1993) 1025.

[180] NAGARAJAN, R., LIU, W., KUMAR, J., TRIPATHY, S. K., BRUNO, F. F., AND SAMUELSON, L. A., *Manipulating DNA Conformation Using Intertwined Conducting Polymer Chains*. Macromolecules **34** (2001) 3921.

[181] NAKAMAE, S., CAZAYOUS, M., SACUTO, A., MONOD, P., AND BOUCHIAT, H., *Intrinsic Low Temperature Paramagnetism in B-DNA*. Phys. Rev. Lett. **94** (2005) 248102.

[182] NAKAYAMA, H., OHNO, H., AND OKAHATA, Y., *Intramolecular electron conduction along DNA strands and their temperature dependency in a DNA-aligned cast film*. Chem. Commun. (2001) 2300.

[183] NAMASIVAYAM, V., LARSON, R. G., BURKE, D. T., AND BURNS, M. A., *Electrostretching DNA molecules using polymer-enhanced media within microfabricated devices*. Anal. Chem. **74** (2002) 3378.

[184] NEDELCU, S. AND WATSON, J. H. P., *Size separation of DNA molecules by pulsed electric field dielectrophoresis*. J. Phys. D: Appl. Phys. **37** (2004) 2197.

[185] NIEMEYER, C. M., *Progress in "engineering up" nanotechnology devices utilizing DNA as a construction material*. Appl. Phys. A **68** (1999) 119.

[186] NIEMEYER, C. M., *Self-assembled nanostructures based on DNA: towards the development of nanobiotechnology*. Curr. Opin. Chem. Biol. **4** (2000) 609.

[187] NIEMEYER, C. M., *Nanoparticles, Proteins, and Nucleic Acids: Biotechnology Meets Materials Science*. Angew. Chem. Int. Ed. **40** (2001) 4128.

[188] NIEMEYER, C. M., ADLER, M., GAO, S., AND CHI, L. F., *Supramolecular Nanocircles Consisting of Streptavidin and DNA*. Angew. Chem. Int. Ed. **39** (2000) 3055.

[189] NIEMEYER, C. M., ADLER, M., LENHERT, S., GAO, S., FUCHS, H., AND CHI, L. F., *Nucleic Acid Supercoiling as a Means for Ionic Switching of DNA - Nanoparticle Networks*. ChemBioChem **2** (2001) 260.

[190] NIEMEYER, C. M. AND SIMON, U., *DNA-Based Assembly of Metal Nanoparticles*. European Journal of Inorganic Chemistry **2005** (2005) 3641.

[191] NOGUES, C., COHEN, S. R., DAUBE, S. S., AND NAAMAN, R., *Electrical properties of short DNA oligomers characterized by conducting atomic force microscopy*. Phys. Chem. Chem. Phys. **6** (2004) 4459.

[192] NYAMJAV, D., KINSELLA, J. M., AND IVANISEVIC, A., *Magnetic wires with DNA cores: A magnetic force microscopy study*. Appl. Phys. Lett. **86** (2005) 093107.

[193] OKAHATA, Y., KOBATASHI, T., TANAKA, K., AND SHIMOMURA, M., *Anisotropic Electric Conductivity in an Aligned DNA Cast Film*. J. Am. Chem. Soc. **120** (1998) 6165.

[194] OKAHATA, Y., KOBAYASHI, T., NAKAYAMA, H., AND TANAKA, K., *DNA aligned cast film and its anisotropic electron conductivity*. Supramolecular Science **5** (1998) 317.

[195] O'NEILL, P., ROTHEMUND, P. W. K., KUMAR, A., AND FYGENSON, D. K., *Sturdier DNA Nanotubes via Ligation*. Nano Lett. **6** (2006) 1379.

[196] OTSUKA, Y., LEE, H.-Y., GU, J.-H., LEE, J.-O., YOO, K.-H., H. TANAKA, H. T., AND KAWAI, T., *Influence of Humidity on the Electrical Conductivity of Synthesized DNA Film on Nanogap Electrode*. Jpn. J. Appl. Phys. **41** (2002) 891.

[197] DE PABLO, P. J., MORENO-HERRERO, F., COLCHERO, J., HERRERO, J. G., HERRERO, P., BARÓ, A. M., ORDEJÓN, P., SOLER, J. M., AND ARTACHO, E., *Absence of dc-Conductivity in λ-DNA*. Phys. Rev. Lett. **85** (2000) 4992.

[198] PARK, S.-H., BARISH, R., LI, H., REIF, J. H., FINKELSTEIN, G., YAN, H., AND LABEAN, T. H., *Three-Helix Bundle DNA Tiles Self-Assemble into 2D Lattice or 1D Templates for Silver Nanowires*. Nano Lett. **5** (2005) 693.

[199] PARK, S. H., PISTOL, C., AHN, S. J., REIF, J. H., LEBECK, A. R., DWYER, C., AND LABEAN, T. H., *Finite-Size, Fully Addressable DNA Tile Lattices Formed by Hierarchical Assembly Procedures*. Angew. Chem. Int. Ed. **45** (2006) 735.

[200] PARK, S. H., YIN, P., LIU, Y., REIF, J. H., LABEAN, T. H., AND YAN, H., *Programmable DNA Self-Assemblies for Nanoscale Organization of Ligands and Proteins*. Nano Lett. **5** (2005) 729.

[201] PARK, S.-J., LAZARIDES, A. A., MIRKIN, C. A., AND LETSINGER, R. L., *Directed Assembly of Periodic Materials from Protein and Oligonucleotide-Modified Nanoparticle Building Blocks*. Angew. Chem. Int. Ed. **40** (2001) 2909.

[202] PARK, S.-J., TATON, T. A., AND MIRKIN, C. A., *Array-Based Electrical Detection of DNA with Nanoparticle Probes*. Science **295** (2002) 1503.

[203] PAUKSTELIS, P. J., NOWAKOWSKI, J., BIRKTOFT, J. J., AND SEEMAN, N. C., *Crystal Structure of a Continuous Three-Dimensional DNA Lattice*. Chem. Biol. **11** (2004) 1119.

[204] PERKINS, T. T., SMITH, D. E., LARSON, R. G., AND CHU, S., *Stretching of a single tethered polymer in a uniform flow*. Science **268** (1995) 83.

[205] PINTO, Y. Y., LE, J. D., MUSIER-FORSYTH, N. C. S. K., TATON, T. A., AND KIEHL, R. A., *Sequence-Encoded Self-Assembly of Multiple-Nanocomponent Arrays by 2D DNA Scaffolding*. Nano Lett. **5** (2005) 2399.

[206] POHL, H. A., *Dielectrophoresis: The Behavior of Neutral Matter in Nonuniform Electric Fields* (Cambridge University Press: Cambridge, U.K., 1978).

[207] PORATH, D., A. BEZRYADIN, S. D. V., AND DEKKER, C., *Direct measurement of electrical transport through DNA molecules*. Nature **403** (2000) 635.

[208] PORATH, D., CUNIBERTI, G., AND FELICE, R. D., *Charge Transport in DNA-Based Devices*. Top. Curr. Chem. **237** (2004) 183.

[209] RADHAKRISHNAN, I. AND PATEL, D. J., *DNA triplexes: solution structures, hydration sites, energetics, interactions, and function*. Biochemistry **33** (1994) 11405.

[210] RAJSKI, S. R., JACKSON, B. A., AND BARTON, J. K., *DNA repair: models for damage and mismatch recognition*. Mutat Res. **447** (2000) 49.

[211] RAKITIN, A., AICH, P., PAPADOPOULOS, C., KOBZAR, Y., VEDENEEV, A. S., LEE, J. S., AND XU, J. M., *Metallic Conduction through Engineered DNA: DNA Nanoelectronic Building Blocks*. Phys. Rev. Lett. **86** (2001) 3670.

[212] REPP, J., MEYER, G., PAAVILAINEN, S., OLSSON, F. E., AND PERSSON, M., *Imaging Bond Formation Between a Gold Atom and Pentacene on an Insulating Surface*. Science **312** (2006) 1196.

[213] RICHTER, J., MERTIG, M., POMPE, W., MÖNCHAND, I., AND SCHACKERT, H. K., *Construction of highly conductive nanowires on a DNA template*. Appl. Phys. Lett. **78** (2001) 536.

[214] RICHTER, J., SEIDEL, R., KIRSCH, R., MERTIG, M., POMPE, W., PLASCHKE, J., AND SCHACKERT, H. K., *Nanoscale Palladium Metallization of DNA*. Adv. Mater. **12** (2000) 507.

[215] RIZZO, V. AND SCHELLMAN, J. A., *Flow dichroism of T7 DNA as a function of salt concentration*. Biopolymers **20** (1981) 2143.

[216] ROTH, S., *One-Dimensional Metals* (VCH Verlagsgesellschaft, Weinheim, Germany, 1995).

[217] ROTHEMUND, P. W. K., *Folding DNA to create nanoscale shapes and patterns*. Nature **440** (2006) 297.

[218] ROTHEMUND, P. W. K., EKANI-NKODO, A., PAPADAKIS, N., KUMAR, A., FYGENSON, D. K., AND WINFREE, E., *Design and Characterization of Programmable DNA Nanotubes*. J. Am. Chem. Soc. **126** (2004) 16344.

[219] ROTHEMUND, P. W. K., PAPADAKIS, N., AND WINFREE, E., *Algorithmic Self-Assembly of DNA Sierpinski Triangles*. PLoS Biol. **2** (2004) 2041.

[220] SAIF, B., MOHR, R. K., MONTROSE, C. J., AND LITOVITZ, T. A., *On the Mechanism of Dielectric Relaxation in Aqueous DNA Solutions*. Biopolymers **31** (1991) 1171.

[221] SCHNELLE, T., MÜLLER, T., FIEDLER, S., SHIRLEY, S. G., LUDWIG, K., HERRMAN, A., FUHR, G., WAGNER, B., AND ZIMMERMANN, U., *Trapping of viruses in high-frequency electric field cages*. Naturwissenschaften **83** (1996) 172.

[222] SEEMAN, N. C., *Nucleic acid junctions and lattices*. J. Theor. Biol. **99** (1982) 237.

[223] SEEMAN, N. C., *Nucleic Acid Nanostructures and Topology*. Angew. Chem. Int. Ed. **37** (1998) 3220.

[224] SEEMAN, N. C., *DNA in a material world*. Nature **421** (2003) 427.

[225] SHI, J. AND BERGSTROM, D. E., *Assembly of novel DNA cycles with rigid tetrahedral linkers*. Angew Chem. Int. Ed. **36** (1997) 111.

[226] SHIGEMATSU, T., SHIMOTANI, K., MANABE, C., WATANABE, H., AND SHIMIZU, M., *Transport properties of carrier-injected DNA*. J. Chem. Phys. **118** (2003) 4245.

[227] SHIH, W. M., QUISPE, J. D., AND JOYCE, G. F., *A 1.7-kilobase single-stranded DNA that folds into a nanoscale octahedron*. Nature **427** (2004) 618.

[228] SHIMAMOTO, N., *One-dimensional diffusion of proteins along DNA. Its biological and chemical significance revealed by single molecule measurements*. J. Biol. Chem. **274** (1999) 15293.

[229] SHIN, J. S. AND PIERCE, N. A., *A Synthetic DNA Walker for Molecular Transport*. J. Am. Chem. Soc. **126** (2004) 10834.

[230] SIMMEL, F. C. AND YURKE, B., *A DNA-based molecular device switchable between three distinct mechanical states*. Appl. Phys. Lett. **80** (2002) 883.

[231] SINGER, V. L., JONES, L. J., YUE, S. T., AND HAUGLAND, R. P., *Characterization of PicoGreen Reagent and Development of a Fluorescence-Based Solution Assay for Double-Stranded DNA Quantitation*. 1997 Anal. Biochem. **249** (1997) 228.

[232] SNART, R. S., *Photoelectric effects of deoxyribonucleic acid*. Biopolymers **6** (1968) 293.

[233] SOGHOMONIAN, V., HEREMANS, J. J., CHEN, H., AND HARTZELL, B., *Experimental Current-Voltage Characteristics of DNA and Modified DNA Molecules*. TMS Letters **1** (2004) 139.

[234] STORM, A. J., VAN NOORT, J., DE VRIES, S., AND DEKKER, C., *Insulating behavior for DNA molecules between nanoelectrodes at the 100 nm length scale*. Appl. Phys. Lett. **79** (2001) 3881.

[235] SUZUKI, S., YAMANASHI, T., TAZAWA, S., KUROSAWA, O., AND WASHIZU, M., *Quantitative Analysis of DNA Orientation in Stationary AC Electric Fields Using Fluorescence Anisotropy*. IEEE Trans. Ind. Appl. **34** (1998) 75.

[236] SWAROOP, B. AND SCHAFFER, P. S., *Conduction in silicon nitride and silicon nitride-oxide films*. J. Phys. D.: Appl. Phys. **3** (1970) 803.

[237] TAKEISHI, S., RANT, U., T.FUJIWARA, BUCHHOLZ, K., USUKI, T., ARINAGA, K., TAKEMOTO, K., YAMAGUCHI, Y., TORNOW, M., FUJITA, S., ABSTREITER, G., AND YOKOYAMA, N., *Observation of electrostatically released DNA from gold electrodes with controlled threshold voltages*. J. Chem. Phys. **120** (2004) 5501.

[238] TANAKA, S., CAI, L.-T., TABATA, H., AND KAWAI, T., *Formation of two-dimensional network structure of DNA molecules on Si substrate*. Jpn. J. Appl. Phys. **40** (2001) L407.

[239] TANIGUCHI, M. AND KAWAI, T., *DNA electronics*. Physica E **33** (2006) 1.

[240] TANIGUCHI, M., LEE, H. Y., TANAKA, H., AND KAWAI, T., *Electrical Properties of Poly(dA)·Poly(dT) and Poly(dG)·Poly(dC) DNA Doped with Iodine Molecules*. Jpn. J. Appl. Phys. **42** (2003) L215.

[241] TERAWAKI, A., OTSUKA, Y., LEE, H. Y., MATSUMOTO, T., TANAKA, H., AND KAWAI, T., *Conductance measurement of a DNA network in nanoscale by point contact current imaging atomic force microscopy*. Appl. Phys. Lett. **86** (2005) 113901.

[242] TRAN, P., ALAVI, B., AND GRUNER, G., *Charge Transport along the λ-DNA Double Helix*. Phys. Rev. Lett. **85** (2000) 1564.

[243] TSUKAHARA, S., YAMANAKA, K., AND WATARAI, H., *Dielectrophoretic behavior of single DNA in planar and capillary quadrupole microelectrodes*. Chem. Lett. **3** (2001) 250.

[244] TUUKKANEN, S., *Compensation of Capasitive Crosscoupling in the Cooper Pair Pump*, Master's thesis (pro gradu), University of Jyväskylä, Department of Physics (2002).

[245] TUUKKANEN, S., VIRTANEN, J., HYTÖNEN, V. P., KULOMAA, M. S., AND TÖRMÄ, P., *Fabrication of DNA monolayers on gold substrates and guiding of DNA with electric field*. Rev. Adv. Mater. Sci. **5** (2003) 228.

[246] UEDA, M., YOSHIKAWA, K., AND DOI, M., *Stretching of long DNA under alternating current electric fields in a concentrated polymer solution*. Polym. J. **29** (1997) 1040.

[247] WACKERBARTH, H., MARIE, R., GRUBB, M., ZHANG, J., HANSEN, A. G., CHORKENDORFF, I., CHRISTENSEN, C. B. V., BOISEN, A., AND ULSTRUP, J., *Thiol- and disulfide-modified oligonucleotide monolayer structures on polycrystalline and single-crystal Au(111) surfaces*. J. Solid State Eletrochem. **8** (2004) 474.

[248] WAN, C., FIEBIG, T., KELLEY, S. O., TREADWAY, C. R., BARTONDAGGER, J. K., AND ZEWAIL, A. H., *Femtosecond dynamics of DNA-mediated electron transfer*. Proc. Natl. Acad. Sci. **96** (1999) 6014.

[249] WAN, C., FIEBIG, T., SCHIEMANN, O., BARTON, J. K., AND ZEWAILDAGGER, A. H., *Femtosecond direct observation of charge transfer between bases in DNA*. Proc. Natl. Acad. Sci. **97** (2000) 14052.

[250] WARMAN, J. M., DE HAAS, M. P., AND RUPPRECHT, A., *DNA: A Molecular Wire?* Chem. Phys. Lett. **249** (1996) 319.

[251] WASHIZU, M., *Equivalent multipole-moment theory for dielectrophoresis and electrorotation in electromagnetic field*. J. Electrostat. **62** (2004) 15.

[252] WASHIZU, M. AND KUROSAWA, O., *Electrostatic Manipulation of DNA in Microfabricated Structures*. IEEE Trans. Ind. Appl. **26** (1990) 1165.

[253] WASHIZU, M., KUROSAWA, O., ARAI, I., SUZUKI, S., AND SHIMAMOTO, N., *Applications of Electrostatic Stretch-and-Positioning of DNA*. IEEE Trans. Ind. Appl. **31** (1995) 447.

[254] WASHIZU, M., SUZUKI, S., KUROSAWA, O., NISHIZAKA, T., AND SHINOHARA, T., *Molecular Dielectrophoresis of Biopolymers*. IEEE Trans. Ind. Appl. **30** (1994) 835.

[255] WASHIZU, N., NANBA, T., AND MASUDA, S., *Handling of biological cells using fluid integrated circuit*. IEEE Trans. Indust. Appl. **26** (1990) 352.

[256] WATANABE, H., MANABE, C., SHIGEMATSU, T., SHIMOTANI, K., AND SHIMIZU, M., *Single molecule DNA device measured with triple-probe atomic force microscope*. Appl. Phys. Lett. **79** (2001) 2462.

[257] WATSON, J. D. AND CRICK, F. H. C., *A Structure for Deoxyribose Nucleic Acid*. Nature **171** (1953) 737.

[258] WHITESIDES, G. M., MATHIAS, J. P., AND SETO, C. T., *Molecular self-assembly and nanochemistry: a chemical strategy for the synthesis of nanostructures*. Science **254** (1991) 1312.

[259] WILLIAMS, K. A., VEENHUIZEN, P. T. M., DE LA TORRE, B. G., ERITJA, R., AND DEKKER, C., *Nanotechnology: Carbon nanotubes with DNA recognition*. Nature **420** (2002) 761.

[260] WILLIAMS, T. T., ODOM, D. T., AND BARTON, J. K., *Variations in DNA Charge Transport with Nucleotide Composition and Sequence*. J. Am. Chem. Soc. **122** (2000) 9048.

[261] WINFREE, E., LIU, F., WENZLER, L. A., AND SEEMAN, N. C., *Design and self-assembly of two-dimensional DNA crystals*. Nature **394** (1998) 539.

[262] WÄLTI, C., TOSCH, P., DAVIES, A. G., GERMISHUIZEN, W. A., AND KAMINSKI, C. F., *Establishment of the ac electrokinetic elongation mechanism of DNA by three-dimensional fluorescent imaging*. Appl. Phys. Lett. (2006) 153901.

[263] WOLD, D. J. AND FRISBIE, C. D., *Fabrication and Characterization of Metal-Molecule-Metal Junctions by Conducting Probe Atomic Force Microscopy*. J. Am. Chem. Soc. **123** (2001) 5549.

[264] XU, B. AND TAO, N. J., *Measurement of Single-Molecule Resistance by Repeated Formation of Molecular Junctions*. Science **301** (2003) 1221.

[265] XU, B., ZHANG, P., LI, X., , AND TAO, N., *Direct Conductance Measurement of Single DNA Molecules in Aqueous Solution*. Nano Lett. **4** (2004) 1105.

[266] XU, M. S., TSUKAMOTO, S., ISHIDA, S., KITAMURA, M., ARAKAWA, Y., ENDRES, R. G., AND SHIMODA, M., *Conductance of single thiolated poly(GC)-poly(GC) DNA molecules*. Appl. Phys. Lett. **87** (2005) 083902.

[267] YAMAMOTO, K., AKITA, A., AND NAKAYAMA, Y., *Orientation and purification of carbon nanotubes using ac electrophoresis*. J. Phys. D: Appl. Phys. **31** (1998) L34.

[268] YAN, H., PARK, S. H., FINKELSTEIN, G., REIF, J. H., AND LABEAN, T. H., *DNA-Templated Self-Assembly of Protein Arrays and Highly Conductive Nanowires*. Science **301** (2003) 1882.

[269] YAN, H., ZHANG, X., SHEN, Z., AND SEEMAN, N. C., *A robust DNA mechanical device controlled by hybridization topology*. Nature **415** (2002) 62.

[270] YIN, P., YAN, H., DANIELL, X. G., TURBERFIELD, A. J., AND REIF, J. H., *A Unidirectional DNAWalker That Moves Autonomously Along a Track*. Angew. Chem. Int. Ed. **43** (2004) 4906.

[271] YING, L., WHITE, S. S., BRUCKBAUER, A., MEADOWS, L., KORCHEV, Y. E., AND KLENERMAN, D., *Frequency and Voltage Dependence of the Dielectrophoretic Trapping of Short Lengths of DNA and dCTP in a Nanopipette*. Biophys. J. **86** (2004) 1018.

[272] YOO, K.-H., HA, D. H., LEE, J.-O., PARK, J. W., KIM, J., LEE, J. J. K. H.-Y., KAWAI, T., AND CHOI, H. Y., *Electrical Conduction through Poly(dA)-Poly(dT) and Poly(dG)-Poly(dC) DNA Molecules*. Phys. Rev. Lett. **87** (2001) 198102.

[273] YUN, Y. J., PARK, G., JUNG, S., AND HAA, D. H., *Anomalous temperature dependence of electrical conductance of DNA-linked Au nanoparticle aggregates*. Appl. Phys. Lett. **88** (2006) 063902.

[274] YURKE, B., TURBERFIELD, A. J., JR, A. P. M., SIMMEL, F. C., AND NEUMANN, J. L., *A DNA-fuelled molecular machine made of DNA*. Nature **406** (2000) 605.

[275] ZAREIE, M. H. AND LUKINS, P. B., *Atomic-resolution STM structure of DNA and localization of the retinoic acid binding site*. Biochem. Biophys. Res. Commun. **303** (2003) 153.

[276] ZHANG, Y., *Experimental transport studies of $YBa_2Cu_3O_{7-\delta}$ and λ-DNA*, Ph.D. thesis, Department of Physics, Princeton university (2003).

[277] ZHANG, Y., AUSTIN, R. H., KRAEFT, J., COX, E. C., AND ONG, N. P., *Insulating Behavior of λ-DNA on the Micron Scale*. Phys. Rev. Lett. **89** (2002) 198102.

[278] ZHANG, Y. AND SEEMAN, N. C., *Construction of a DNA-Truncated Octahedron*. J. Am. Chem. Soc. **116** (1994) 1661.

[279] ZHAO, J. AND UOSAKI, K., *Formation of Nanopatterns of a Self-Assembled Monolayer (SAM) within a SAM of Different Molecules Using a Current Sensing Atomic Force Microscope*. Nano Lett. **2** (2002) 137.

[280] ZHENG, J., CONSTANTINOU, P. E., MICHEEL, C., KIEHL, A. P. A. R. A., AND SEEMAN, N. C., *Two-Dimensional Nanoparticle Arrays Show the Organizational Power of Robust DNA Motifs*. Nano Lett. **6** (2006) 1502.

[281] ZHENG, L., BRODY, J. P., AND BURKE, P. J., *Electronic manipulation of DNA, proteins, and nanoparticles for potential circuit assembly*. Biosensors and Bioelectronics **20** (2004) 606.

[282] ZHENG, L., LI, S., BRODY, J. P., AND BURKE, P. J., *Manipulating Nanoparticles in Solution with Electrically Contacted Nanotubes Using Dielectrophoresis*. Langmuir **20** (2004) 8612.

[283] ZIPPER, H., BRUNNER, H., BERNHAGEN, J., AND VITZTHUM, F., *Investigations on DNA intercalation and surface binding by SYBR Green I, its structure determination and methodological implications*. Nucleic Acids Res. **32** (2004) e103.